12-2007

PROPERTY MEASUREMENTS AND EVALUATION OF HEAT LEAK

Nathan Race
Clemson University, nrace@clemson.edu

PROPERTY MEASUREMENTS AND EVALUATION OF HEAT LEAK IN SINTERED STAINLESS WICKS

A Thesis
Presented to
the Graduate School of
Clemson University

In Partial Fulfillment
of the Requirements for the Degree
Master of Science
Mechanical Engineering

---

by
Nathan S. Race
December 2007

Accepted by:
Dr. Jay M. Ochterbeck, Committee Chair
Dr. David A. Zumbrunnen
Dr. Chenning Tong

ABSTRACT

Heat transport in capillary wick structures is an important parameter in loop heat pipe (LHP) design. The purpose of this study was to investigate the conductive heat leak in operating capillary wick structures. The heat leak is the portion of applied heat load conducted through the wick in spite of the convection of working fluid. Four sintered 316 stainless steel wicks were tested for porosity, effective thermal conductivity, pore size, and heat leak. Pore sizes were found to correlate well with the nominal pore size and pores were very narrowly distributed within a size range of approximately 1-10μm. Effective thermal conductivity was found to vary linearly with temperature over the range of 300-400K for all samples within the range of 0.7 W/m-K to 3.7 W/m-K in vacuum. Using a correlation for truncated packed spheres, the conductivity of the samples saturated in methanol was determined. These values ranged from 1.1 W/m-K to 4.1 W/m-K. Other models in the literature predicted the effective thermal conductivity to within an order of magnitude for all samples; however, the models did not capture the temperature dependence of conductivity and errors of 100% or more were found in some cases. The samples were tested in a vertical orientation for heat leak in operation as a capillary wick with methanol as a working fluid. Evaporative heat fluxes between 5,000 and 65,000 W/m^2 were measured. Heat leak was found to vary linearly with the power dissipated by evaporation. The heat leak fraction of the total dissipated power decreased monotonically in a power-law relationship with total dissipated power. For each sample, this fractional heat leak approached a limit proportional to the sample effective conductivity. This limit was on the order of 1% of the total dissipated power.

ACKNOWLEDGMENTS

I would like to thank my advisor Dr. Jay Ochterbeck for his assistance and support of this research, as well as my committee members Drs. David Zumbrunnen and Chenning Tong. I'm also grateful to my colleagues Brandon Hathaway and Brian d'Entremont for their humor, intelligence, and openness to rambling political discussions.

I would also like sincerely thank and acknowledge my parents, without whom none of this would have been possible, and Casey Rice for her understanding and patience during difficult times.

TABLE OF CONTENTS

Page

LIST OF TABLES

LIST OF FIGURES

NOMENCLATURE

A	Area (m^2)
C	Unit Correction Constant (0.58402 psi-cm/dyne-m)
C_p	Specific Heat (kJ/kg-K)
d	Diameter (m)
F	Filter Flow Percentage (%)
G	Lumped Conductance Parameter
h_{fg}	Latent Heat (kJ/kg)
k	Thermal Conductivity (W/m-K)
K	Permeability (m^2)
L	Characteristic Length (m)
m	Mass (g)
$\dot{m}$	Mass Flow Rate (kg/s)
Nu	Nusselt Number
P	Pressure (kPa)
Q	Flow Rate (l/min)
$\dot{Q}$	Power (W)
q''	Heat Flux (W/m^2)
r	Radius (m)
R	Electrical Resistance (Ω)
T	Temperature (K)

t	Thickness (m)
V	Volume (m^3)
x	Distance (m)
Δ	Difference
λ	Tortuosity Factor
μ	Dynamic Viscosity (Pa-s)
ρ	Density (kg/m^3)
ς	Ratio of advection and conduction
σ	Surface Tension (dynes/cm)
φ	Porosity
φ'	Modified Porosity Parameter

Subscripts

a	Axial
avg	Average
c	Capillary
cc	Compensation Chamber
dry	Unsaturated
e	Evaporator
eff	Effective
evap	Evaporative
f	Fluid

high	High or Top
i	Inner
leak	Heat Leak
liq	Liquid
loss	Loss calibration
low	Low or Bottom
max	Maximum
meter	Flux Meter
meth	Saturated in methanol
min	Minimum
n	Index
NIST	NIST Reference Sample
o	Outer
pore	Pore
r	Radial
s	Sphere
samp	Sample
sat	Saturation
tot	Total
up	Upper or Top
w	Wick
wet	Saturated sample

CHAPTER ONE
INTRODUCTION

A Loop Heat Pipe (LHP) is a highly efficient heat transfer device which utilizes the latent heat of a working fluid to transport large amounts of heat through evaporation and condensation. The thermal conductance of these devices is typically orders of magnitude greater than a solid conductor of equivalent size [1]. While this statement may be true for traditional heat pipes as well, LHPs derive significant advantages from a few key features: 1) the use of smooth-walled tubes for liquid and vapor lines, 2) the ability to design for optimal heat exchange in the evaporator and condenser, and 3) the reduced distance that liquid must travel in the wick [1].

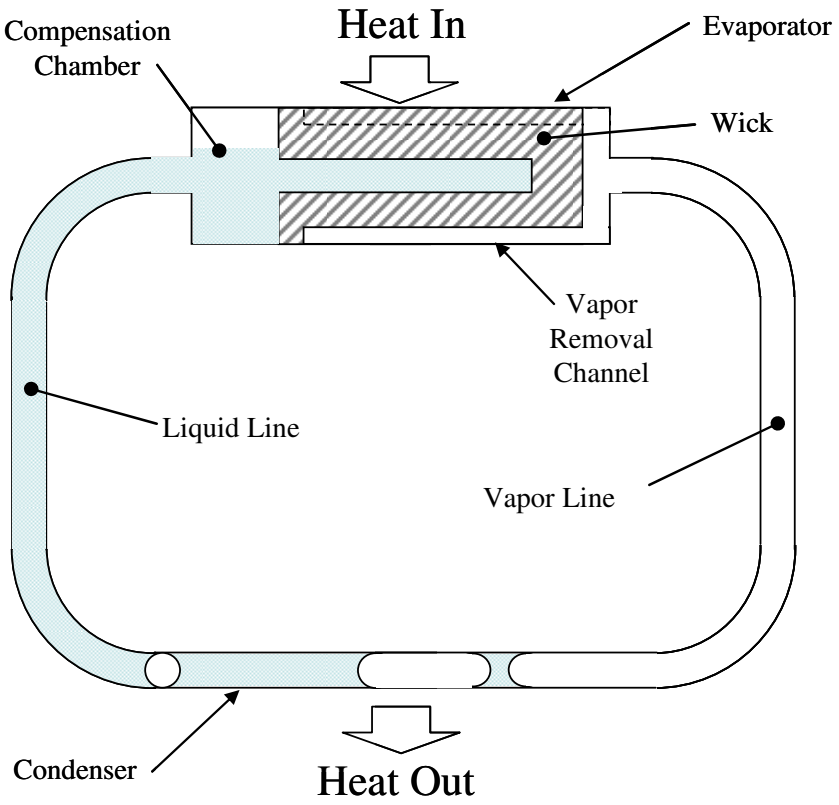

Figure 1-1: Schematic of a Loop Heat Pipe, adapted from [1].

These features allow for reduced pressure losses in the adiabatic section, enhanced heat exchange in crucial areas, and increased pumping pressure, thereby increasing the distance and/or height over which the device can operate. Another feature of LHPs is the compensation chamber – also called the hydroaccumulator or reservoir – which is attached to the evaporator and serves as a reservoir for excess liquid in the loop. A wick connects the compensation chamber and the evaporator ensuring a continuous supply of liquid for the evaporator. The physical coupling of these two components causes a portion of the applied heat load to "leak" into the compensation chamber.

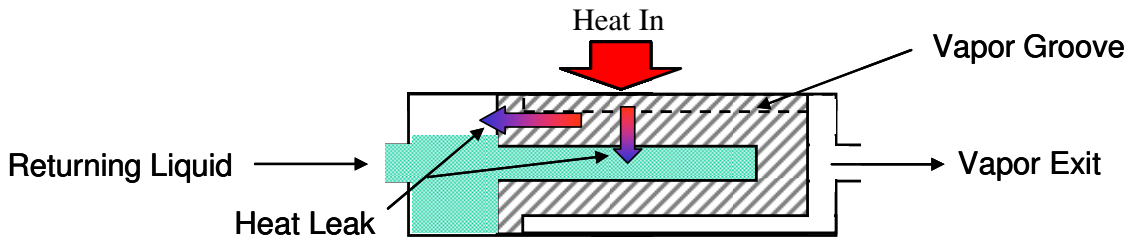

Figure 1-2: Heat leak in a LHP evaporator

The result, depending on the ambient conditions and properties of the loop, is a rise in operating temperature due to loss of liquid sub-cooling in the compensation chamber [2, 3]. Figure 1-3 represents a "V" shaped operating temperature profile typical of a LHP operating with an ambient temperature greater than the sink temperature. At low power, the heat leak to the compensation chamber both through the wick and from the returning fluid causes the temperature to increase thus raising the saturation temperature of the fluid in the evaporator. As power increases, so does the mass flow rate within the pipe and likewise the condenser utilization. This increases the subcooling

of the liquid returning to the compensation chamber and causes a reduction in operating temperature. Once the condenser is fully utilized, the loop is at its minimum operating temperature; additional power results in warmer fluid exiting the condenser as no additional heat can be removed with the existing operating temperature. This in turn leads to a reduction in liquid subcooling in the compensation chamber and a rise in operating temperature. As the operating temperature reaches a level where the condenser can reject all applied power, the loop will stabilize. Increasing the heat leak between the evaporator and compensation chamber leads to a rise in the operating temperature of the loop [4].

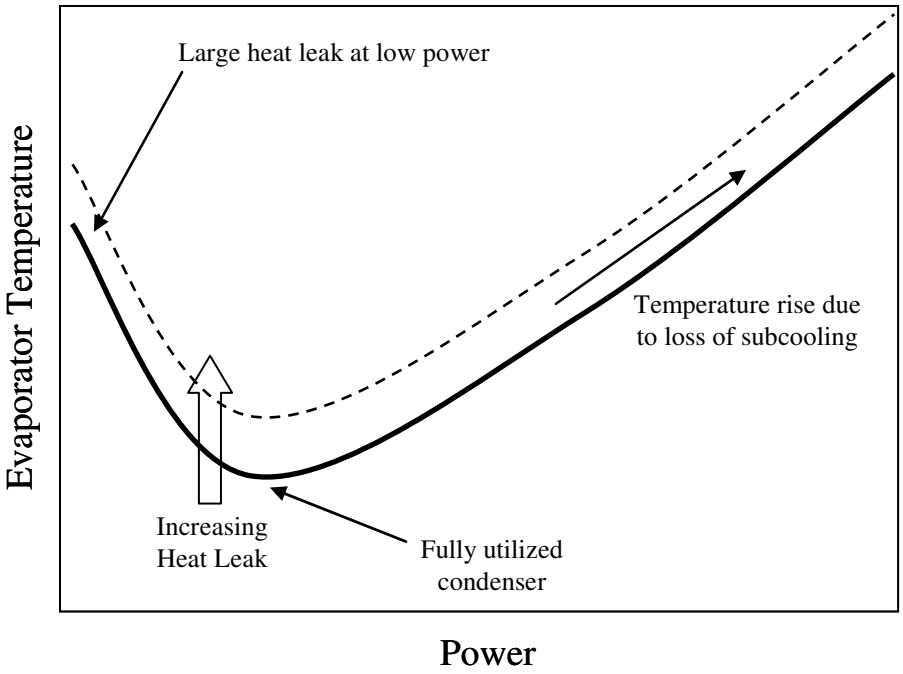

Figure 1-3: Typical operating temperature of LHP v. applied power.

While the conduction of heat through the outer walls of the LHP is straightforward, the heat transfer within the porous structures of the wick is quite complex. This work will determine the heat leak through porous sintered 316L stainless steel wick samples by measuring the temperature gradients in operating wick structures under varying evaporative heat loads. In addition, the following wick properties will be measured: effective thermal conductivity, porosity, bubble point, mean flow pore size, pore size distribution, and permeability.

Literature Review

Effective Thermal Conductivity

Bonnefoy et al. [5] studied the effective conductivity of sintered nickel LHP wicks under vacuum as well as saturated in air, water, and methanol. For the vacuum case, a porous sample was inserted between calibrated stainless steel flux meters and placed in a vacuum chamber surrounded by a radiation shield. Power was applied to the top portion of the column while the bottom portion was maintained at a specified temperature by a recirculating bath. Temperature gradients in the flux meters were recorded to determine the heat flux through the column. The effective conductivity was then found as

$$k_{eff} = q'' \Big/ \left(\frac{T_{up} - T_{low}}{t_{samp}} \right) \tag{1}$$

For the saturated tests, a small Delrin™ fixture was used to retain fluid within the wick. The Delrin™ cylinder was sealed against the flux meters with o-rings. The results of these tests were compared with models in the literature. The model given by Chi [6] yielded excellent agreement with the average measured data as shown in Figure 1-4.

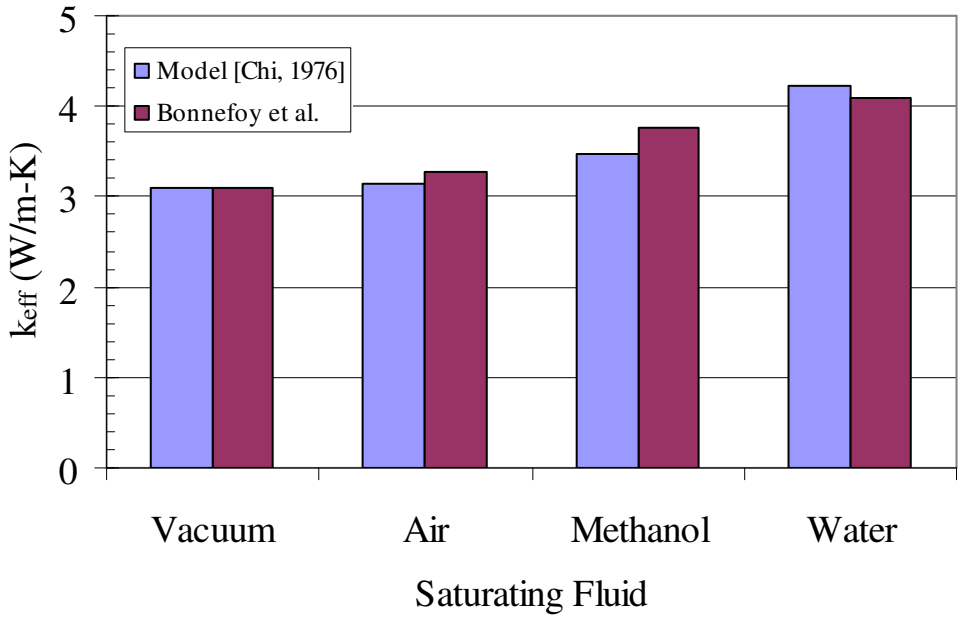

Figure 1-4: Experimental data and values predicted by Chi correlation.

Chi's model assumes a case of truncated packed spheres for calculating particle contact areas and gives the effective conductivity as

$$k_{eff} = \frac{\pi}{8}\left(\frac{r_c}{r_s}\right)^2 k_s + \left[1 - \frac{\pi}{8}\left(\frac{r_c}{r_s}\right)^2\right]\left[\frac{k_f k_s}{\phi' k_s + k_f\left(1-\phi'\right)}\right] \tag{2}$$

Where: $$\phi' = \frac{\phi}{1 - \frac{\pi}{8}\left(\frac{r_c}{r_s}\right)^2}$$

Chi [6] presented a model for non-truncated packed spheres, given as

$$k_{eff} = \frac{k_f \left[\left(2k_f + k_s\right) - 2\left(1-\phi\right)\left(k_f - k_s\right) \right]}{\left[\left(2k_f + k_s\right) + \left(1-\phi\right)\left(k_f - k_s\right) \right]} \tag{3}$$

Peterson [7] provided an alternate model for packed spheres as

$$k_{eff} = \frac{k_f \left[2k_f + k_s - 2\phi\left(k_f - k_s\right) \right]}{2k_f + k_s + \phi\left(k_f - k_s\right)} \tag{4}$$

Mo et al. [8] studied the effective thermal conductivity of sintered nickel samples at various fill ratios with different wetting fluids. The samples consisted of sintered carbonyl nickel powder with a mean particle size of 2 μm. Both specimens had a porosity of approximately 55%. The conductivity was measured by means of a hot disk thermal constant analyzer; this method involves placing an electric heater/sensor between two identical samples. The heater and samples are allowed to reach thermal equilibrium before power is applied. Once equilibrium is achieved, power is applied and the change in electrical resistivity of the heater is recorded and analyzed to yield effective thermal conductivity measurements. Their results were compared to models in the literature with generally poor agreement. One model, that of Chaudhary and Bhandari [9], yielded reasonable values with 100% fill ratio. The model is a useful combination of the two simplest effective conductivity expressions, the series and parallel models [6, 7].

This model gives

$$k_{eff} = k_{\max}^{n} k_{\min}^{1-n} \tag{5}$$

Where: $0.42 < n < 0.51$

$$k_{\max} = \phi k_f + (1-\phi) k_s$$

$$k_{\min} = \frac{k_f k_s}{\left[\phi k_s + (1-\phi) k_f\right]}$$

Permeability and Pore Size

Holley and Faghri [10] outlined methods for permeability and effective pore radius measurements based on the rate-of-rise test. Typically, the rate-of-rise test requires observing the liquid front as it rises in a dry wick partially immersed in a liquid pool. As the precise location of this front can be difficult to detect, the authors devised a method using mass uptake rather than the meniscus front to determine the rate of rise of liquid in the wick. By analyzing the climbing meniscus, the authors developed a series of equations which could be used to numerically reduce the mass uptake data to yield permeability and pore size results.

Several relationships for permeability can be found, the most common is the Blake-Kozeny equation [6], which gives the permeability of a bed of packed spheres as

$$K = \frac{r_p^2 \phi^3}{37.5(1-\phi)^2} \tag{6}$$

Williams and Harris [11] investigated the in-plane and cross-plane properties of step-graded metal felt wicks for heat pipe applications. Porosity, effective pore radius, and liquid permeability were determined using imbibition, capillary flow porometery, and pressure-flow rate data, respectively. The authors determined that many of the correlations in the literature for pore size and permeability are too general in nature, echoing the conclusions of Bonnefoy et al. [5] in regard to effective thermal conductivity. Typically, the correlations use porosity as the defining characteristic of the pore structure. While significant, it is by no means the only relevant characteristic of porous media structure. Owing to the variable nature of sintered media fabrication and the interrelated thermophysical properties of the resulting structure, the problem of developing a broadly applicable prediction for effective thermal conductivity and other properties remains unsolved. Measurement remains the most effective method of accurately determining properties of porous media.

Evaporative Heat Transfer in Porous Media

Several studies conducted in recent years examine evaporative heat transfer from porous media. Ren and Wu [12] modeled the effect of wick effective thermal conductivity in LHP evaporators; a two-dimensional axisymmetric model was developed yielding results in agreement with the literature in some respects, namely the position of the liquid front in relation to a heated fin [13, 14]. Ultimately the authors found that increased wick conductivity resulted in an increase in the heat transfer coefficient and an elimination of heat leak to the liquid line through more efficient heat transfer to the working fluid at low heat fluxes where convection dominates conduction. For higher

heat flux ($q" = 20{,}000\ W/m^2$), the same trends were observed however the effect of conduction was comparable to the effect of convection and the heat leak to the evaporator core was reduced but not eliminated. Figure 1-6 and shows the temperature gradients at the boundary of the wick. Notice the slope at the boundary from *e-a* and *c-b* indicating a reduction of heat leak into the evaporator core with increasing k_{eff}.

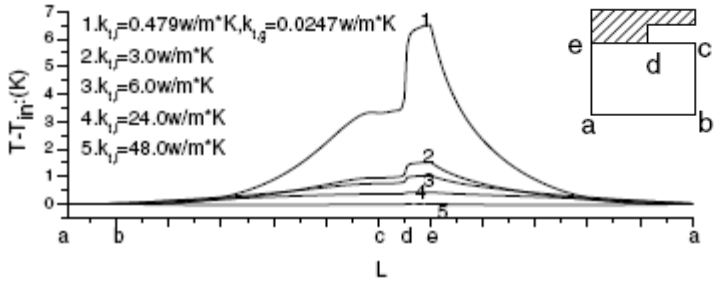

Figure 1-5: Boundary temperatures for $q" = 2000\ W/m^2$, adapted from [12]

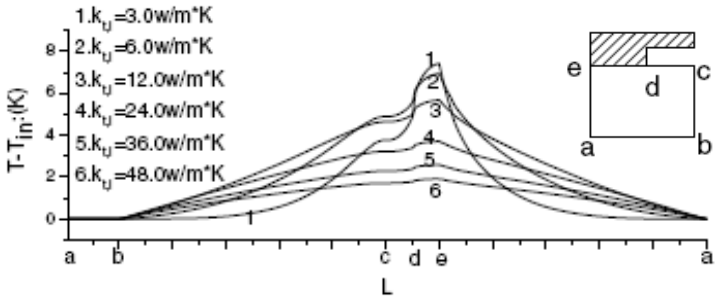

Figure 1-6: Boundary temperatures for $q" = 20{,}000\ W/m^2$, adapted from [12].

This result is in contrast to those of Zhao and Liao [14] who present temperature profiles indicating decreasing heat leak for increasing heat flux in a bed of packed spheres (r_s = 5.45E-04 m). Heat was applied to the top of the bed through a finned copper block. The packed bed was fed by an adjustable reservoir and spillway system that allowed adjustment of the hydrostatic head that the wick was required to overcome.

Due to the low thermal conductivity of the glass beads (k = 0.706 W/m-K), combined with the small temperature gradients measured, the authors neglected the heat leak from the lower portion of the packed bed; nevertheless, the temperature profiles clearly show the trend in heat leak.

Iverson et al. [15] studied heat and mass transport in sintered copper wick structures. Wick samples were mounted vertically with the lower section immersed in a pool of water. A heater mounted to the back face of the wick applied power to the sample and the resulting temperature gradients were measured along with the mass flow rate of working fluid. The apparatus consisted of a double-walled glass chamber and lid with a clamping mechanism for the wick sample as well as a vacuum pump connection and thermocouple pass-throughs. The annulus between the glass walls was graduated for use as a condensation and mass flow rate measurement chamber. Based on an assumed effective thermal conductivity value of 40 W/m-K, the amount of heat leaked into the liquid pool was estimated. It was found that the heat leak as a percentage of input power decreased with increasing power from a maximum of about 4% to a minimum of about 1%, as seen in Figure 1-7. The trend was towards a leveling off near 1% of the input power at higher power levels. Heat fluxes up to 20 W/cm^2 were measured without dryout.

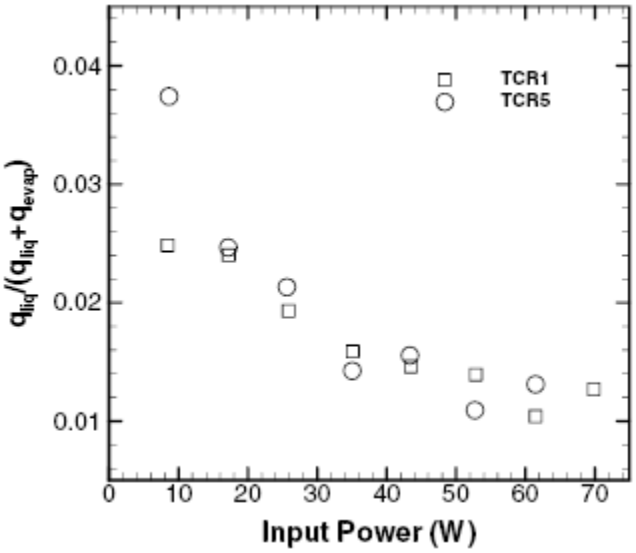

Figure 1-7: Heat leak fraction of total dissipated power, adapted from [15].

LHP Heat Leak Models

Heat leak is the term given to the portion of the applied heat load that is transferred to the compensation chamber rather than dissipated by phase change in the evaporator. Numerous models have been developed to represent this heat leak, the simplest of these utilizes a lumped conductance parameter, $G_{e,cc}$ and the temperature difference between the evaporator and compensation chamber. This conductance parameter varies with geometry and operating conditions. For example, the model given by Ku [4] and similarly by Furukawa [16] is

$$\dot{Q}_{e,cc} = G_{e,cc}\left(T_e - T_{cc}\right) \tag{7}$$

In steady state operation, the heat leak to the compensation chamber must be offset by the liquid returning from the condenser; Eq. (8) results, where ΔT represents the subcooling of the returning fluid

$$\dot{Q}_{e,cc} = \dot{m} c_p \Delta T \tag{8}$$

Chuang [17] developed a steady state LHP model which breaks the overall heat leak into two separate components: axially from the evaporator to the compensation chamber and radially from the heat source to the evaporator core. These two effects are related in that the formation of vapor bubbles in the evaporator core due to radial leak reduces the overall heat flow path back to the compensation chamber, increasing axial leak [4]. Chuang derived the following expressions for the axial and radial heat leak, respectively

$$\dot{Q}_{leak,a} = k_{eff} A \left(\frac{T_e - T_{cc}}{L} \right) + \left(Nu k_f \pi L \right) \left(\frac{T_e - T_{cc}}{2} \right) \tag{9}$$

$$\dot{Q}_{leak,r} = \frac{2\pi k_{eff} L \varsigma}{\left(r_o / r_i \right)^{\varsigma} - 1} \Delta T_w \tag{10}$$

where, ς represents a non-dimensional ratio of advection and conduction given by

$$\varsigma = \frac{\dot{m} c_p}{2\pi k_{eff} L} \tag{11}$$

In his analysis and experiment, Chuang assumed this parameter to be zero, i.e., pure conduction. For the low power cases studied this assumption was valid and resulted in low error, however for high power levels or low wick conductivity, this assumption loses validity.

The overarching simplification made in these models is that of a linear temperature profile within the wick structure. Even in situations where there exists a $\left.\frac{dT}{dr}\right|_{r_i}$ term, for simplicity the value of the radial or axial temperature derivative is typically taken as an overall temperature delta divided by a characteristic length. According to the results of Ren and Wu [12] this assumption is only valid for low power and/or high effective thermal conductivities. Iverson et al. [15] and Zhao and Liao [14] showed experimental results that demonstrated this as well.

Objectives

For this work, four samples of sintered stainless steel wicks manufactured by Mott Corporation (Farmington, CT) were evaluated to determine relevant wick properties before testing in a heat leak apparatus. Specifically, the objectives of this study were to:

- Measure sample porosity, permeability, and pore size distribution.
- Measure effective thermal conductivity of the samples in vacuum.
- Apply a correlation to determine saturated effective thermal conductivity.
- Determine the ratio of heat leak to evaporative heat dissipation for wick operation in a vertical orientation with methanol as the working fluid.

The resulting conductivity and permeability values were compared with models in the literature. Additionally, an apparatus was constructed to measure the heat leak through an operating wick sample as well as the evaporative power dissipated by the sample. The samples consisted of 25.4 mm diameter disks for property testing and rectangular samples 64 x 101 mm for heat leak testing. Each set of samples was cut from a single larger sample using wire EDM. Sample thickness ranged from 1.6 mm to 2.0 mm. A summary of sample thickness and manufacturer specified pore size is presented in Table 1-1.

Table 1-1: Summary of sample thickness and nominal pore size.

Sample ID:	**S03**	**S04**	**S06**	**S07**
Thickness (mm)	2.00	1.63	1.62	1.68
Nominal Pore Size (μm)	100-125	10	5	2

CHAPTER TWO
EXPERIMENTAL APPARATUS AND PROCEDURE

Porosity

The volumetric porosity of the samples was determined using the measured geometric properties of the samples as well as the measured mass, dry and saturated in methanol. An Ohaus VO4130 balance with 0.001 g resolution was used to determine mass values. Each measurement was repeated four times and the average of each was used in calculating sample porosity. For each sample, the dry mass measurement was repeated 4 times before the sample was saturated in a beaker of methanol. Each saturated mass measurement was taken immediately after removing the sample from the beaker; the sample was then placed back in the beaker for several minutes before each subsequent mass measurement. The fluid film held on the surface of the sample by surface tension was allowed to drip off but no effort was made to dry the surface as this could cause the surface pores to be cleared. It is estimated that this contributed as much as 5% error to these mass measurements.

Effective Thermal Conductivity

Effective thermal conductivity of the wick samples was determined using the temperature profile in a cylindrical column. The samples were cut into disks with 25.4 mm diameter and inserted between a pair of calibrated 304 stainless steel heat flux meters. A schematic of the apparatus is presented in Figure 2-1.

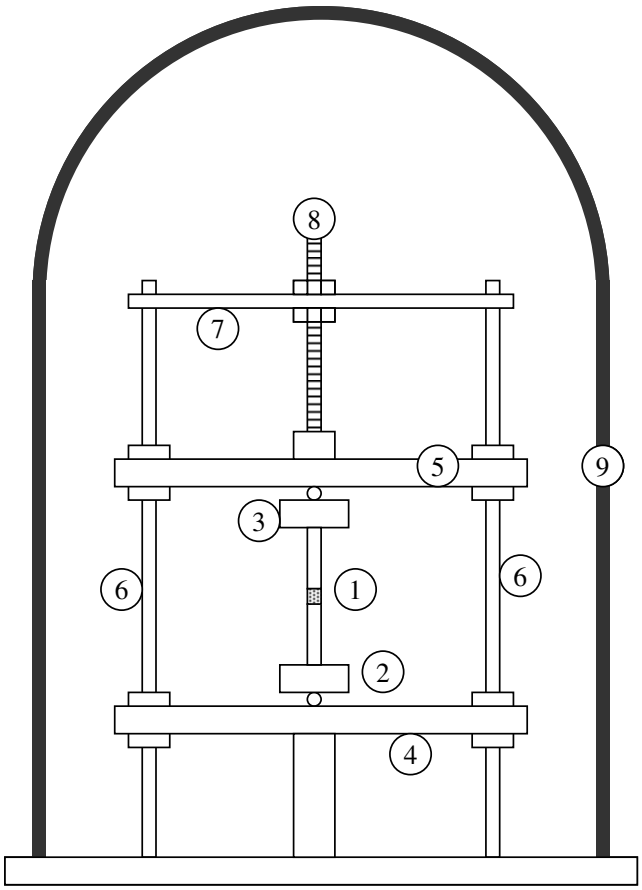

Item	Description
1	Sample Column
2	Sink Holder
3	Source Holder
4	Lower PE Plate
5	Upper PE Plate
6	Support Column
7	Top Plate
8	Threaded Adjusting Rod
9	Vacuum Bell

Figure 2-1: Effective thermal conductivity experimental apparatus.

Each heat flux meter was instrumented with three Omega 30-gauge SLE T-type thermocouples spaced in 9.53 mm increments from the sample surface. The resulting effective conductivity was calculated using Eq. (1) The thermocouples were monitored using a National Instruments data acquisition system and LabView™ software. The upper flux meter was mounted in a brass source holder heated by a 500 W band heater. The lower meter was mounted in the sink holder which was cooled by a VWR Scientific Model 1180A recirculating bath and an ethylene glycol-water mixture. Both the source and sink holders were mounted to polyethylene plates which were in turn mounted on linear bearings rolling on steel support rods. This assembly was placed under a vacuum

bell allowing the internal pressure to be reduced to approximately 0.06 kPa. The heater power was controlled using a Variac with 120 V input. Mean sample temperature could then be adjusted by setting the heater power and chiller temperature.

During testing, the sample column was surrounded by reflective insulation (Reflectix™). This was essentially bubble wrap faced with polished aluminum foil on both sides. Two flat pieces with a cutout for the flux meters were placed on either end of the column and a third piece was wrapped around the column, taking great care to ensure that no insulation touched any portion of the sample column. By allowing contact with both the source and sink, the radiation shield had a temperature gradient similar to the sample column maximizing its effectiveness.

The test procedure for the sintered samples was essentially the same: a sample was installed between the flux meters, the ends of which were coated in a thin layer of Dow Corning 340 heat sink compound. The heat sink compound served to promote even contact between the irregular porous structure and the flux meter surface, and did not obstruct the surface pores. The sample column was wrapped in the reflective insulation and placed under vacuum to minimize radiation and convection losses respectively. Settings on the Variac and chiller were then incrementally adjusted resulting in temperature gradients in the flux meters between approximately 480 and 1600^{o}C/m.

Calibration procedure

The stainless steel heat flux meters were calibrated using a NIST standard reference bar of electrolytic iron, SRM8421 [18]. The NIST standard was 25.45 mm in diameter, 50.80 mm in length and was polished on both ends; it was instrumented with

three Omega 30-gauge SLE thermocouples spaced evenly in 12.7 mm increments. The thermocouples for both the flux meters and the calibration standard were mounted with Dow Corning 340 heat sink compound in centerline-depth holes machined with a #58 drill bit and held in place with a small amount of epoxy resin. During the calibration procedure, the NIST standard was placed between the flux meters with a thin layer of heat sink compound applied at each end. The Variac setting and chiller temperature were incrementally increased and allowed to reach steady state between each point. This typically took between 6 and 10 h; data was averaged over a 5 min period to determine the temperature profile within the sample column. A table of Variac and chiller settings is given in Appendix A. A typical temperature profile is shown in Figure 2-2. To determine the heat flux through the column, the temperature gradient in the NIST standard was found by a linear fit of the three temperature measurements.

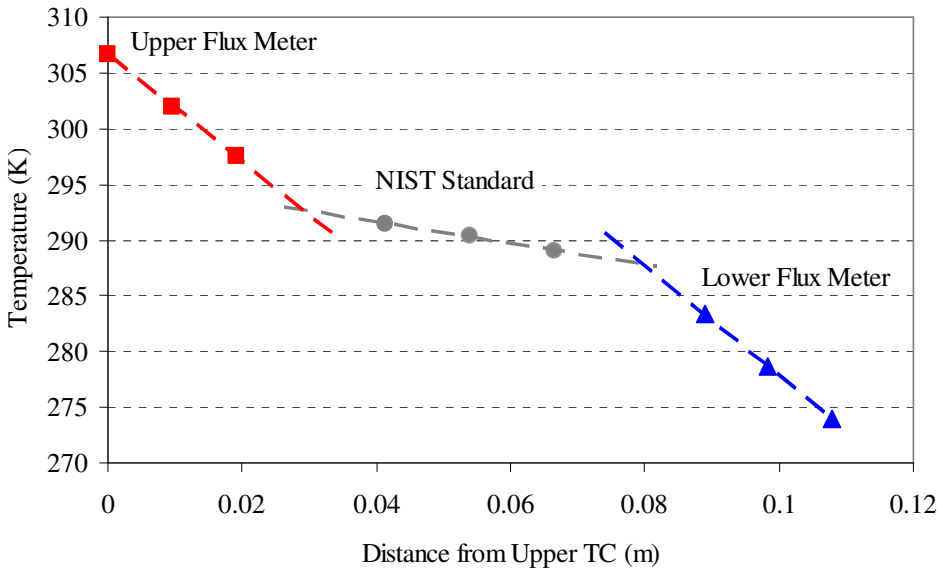

Figure 2-2: Typical temperature profile from calibration tests.

The linear profile was extrapolated to the ends of the NIST sample to give a temperature range over which the average value of *k(T)* was determined. The conductivity of the NIST standard is presented in Figure 2-3. The curve shown is the best fit line used in determining this value, the expression for which is given by

$$k_{NIST} = 110.31e^{-1.2083E-03T} \tag{12}$$

The average value theorem is given as

$$k_{NIST,avg} = \frac{\int_{T_{low}}^{T_{high}} k_{NIST}\,dT}{\left(T_{high} - T_{low}\right)} \tag{13}$$

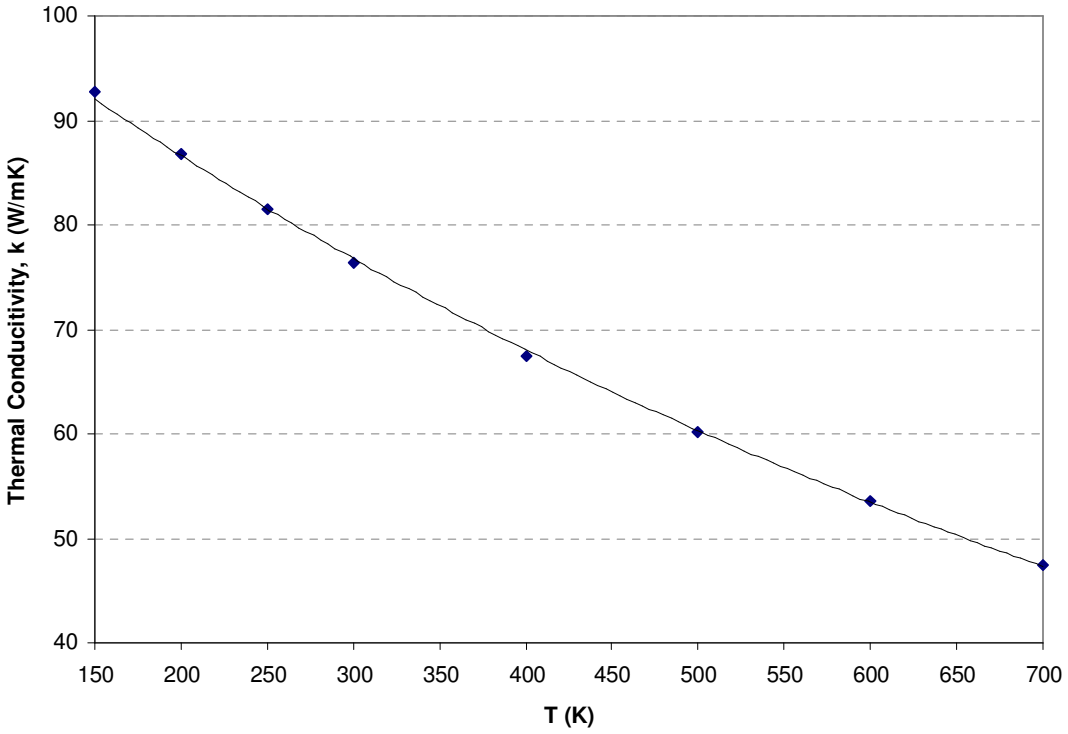

Figure 2-3: Effective thermal conductivity of NIST SRM 8421.

The temperature gradient and thermal conductivity were used to determine the heat flux through the NIST sample, given by

$$q''_{NIST} = -k_{NIST,avg} \left(\frac{dT}{dx} \right)_{NIST} \tag{14}$$

Dividing by the temperature gradient of the upper and lower flux meters, the conductivity of each meter at its average temperature is given as

$$k_{meter}\left(T_{meter,avg}\right) = \frac{-q''_{NIST}}{\left(dT \big/ dx \right)_{meter}} \tag{15}$$

This data is presented in Figure 2-4 along with reference curves for 304 and 316 stainless steel [19].

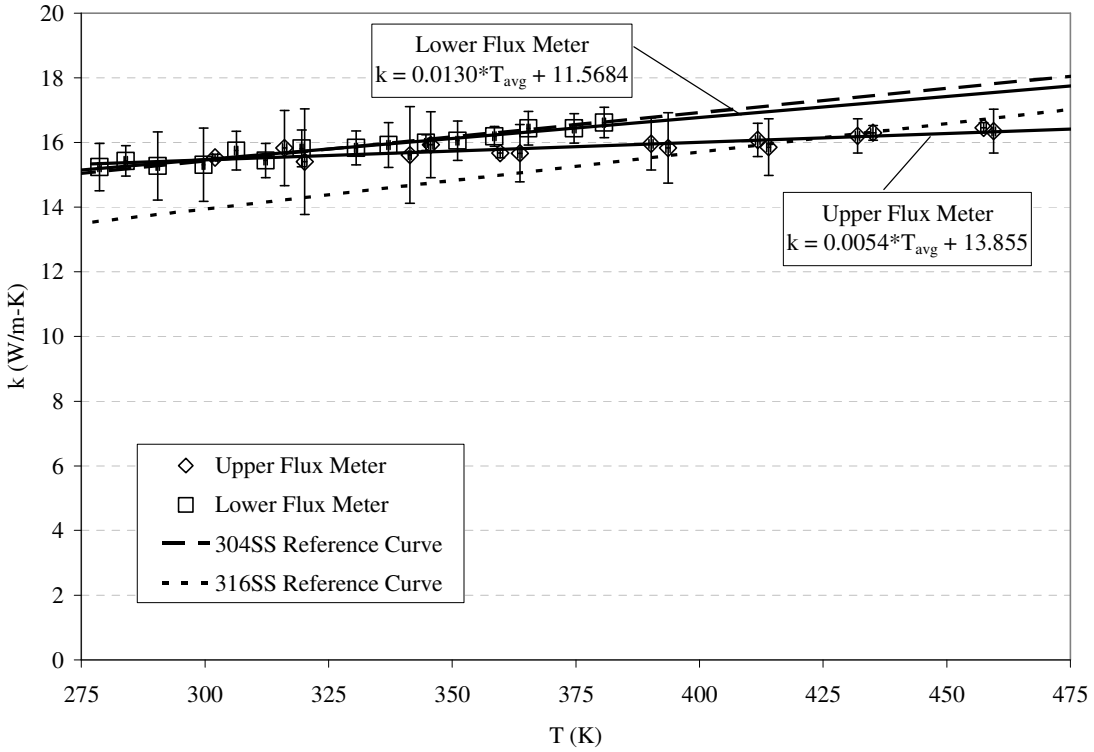

Figure 2-4: Calibration curves for stainless steel flux meters.

The different slopes of the calibration curves are most likely due to greater radiation losses in the upper flux meter. For each data point, the upper flux meter was at a significantly higher temperature than the lower flux meter (see Table A-2). Given the fourth-order dependence of radiation heat transfer on temperature, it is clear that the upper flux meter would lose proportionally more energy to radiation heat transfer and would thus have a lower apparent conductivity since the heat flux was calculated below the upper flux meter. Regardless, the goal was to correlate heat flow through the sample with temperature gradients in the flux meters; every effort was made to minimize radiation heat transfer through careful shielding and the resulting curves are quite close to the reference data for 304 stainless steel. The calibration curves are given as

$$k_{meter,low}\left(T_{meter,avg}\right) = 0.0130T_{meter,avg} + 11.5684 \tag{16}$$

$$k_{meter,up}\left(T_{meter,avg}\right) = 0.0054T_{meter,avg} + 13.855 \tag{17}$$

Capillary Flow Porometry

Sample pore size information such as bubble point, mean flow pore size, and pore size distribution were measured using a Capillary Flow Porometer (CFP) manufactured by Porous Materials Incorporated. The CFP is pictured in Figure 2-5. Seen in the photo are the sample chamber {1}, the penetrometer fill valve {2}, the liquid permeability fitting {3}, and the penetrometer {4}. A gas line, which supplies high pressure nitrogen to the system, connects to the machine at {5}, while a bottle for filling the penetrometer tube connects at {6}. A schematic of the sample chamber is shown in Figure 2-6. The machine has automated and manual modes of operation within the dedicated software

package CapWin™. All of the testing presented in this work was conducted in the automated mode. To illustrate typical operation, the manual operation setup is shown in Figure 2-7.

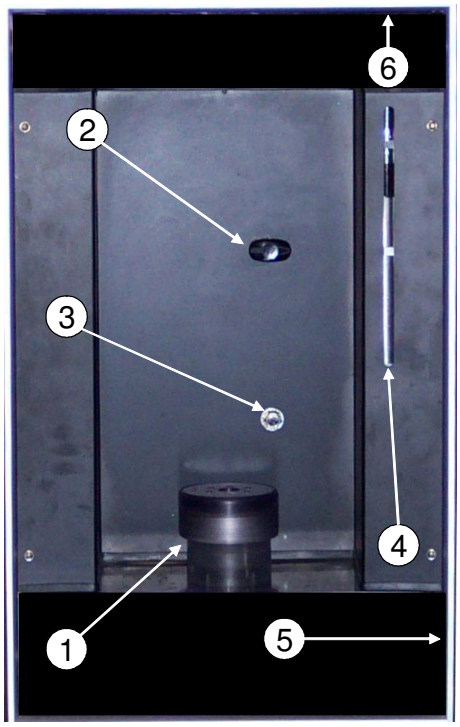

Figure 2-5: PMI capillary flow porometer (front view)

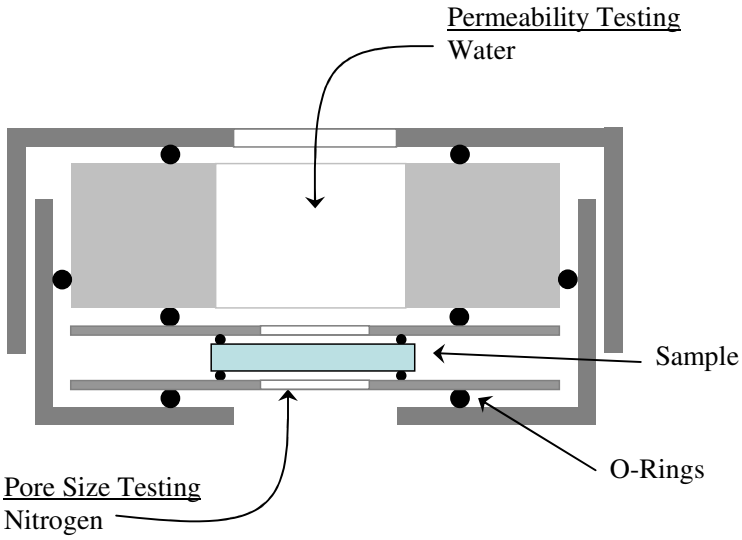

Figure 2-6: Capillary flow porometer sample chamber schematic.

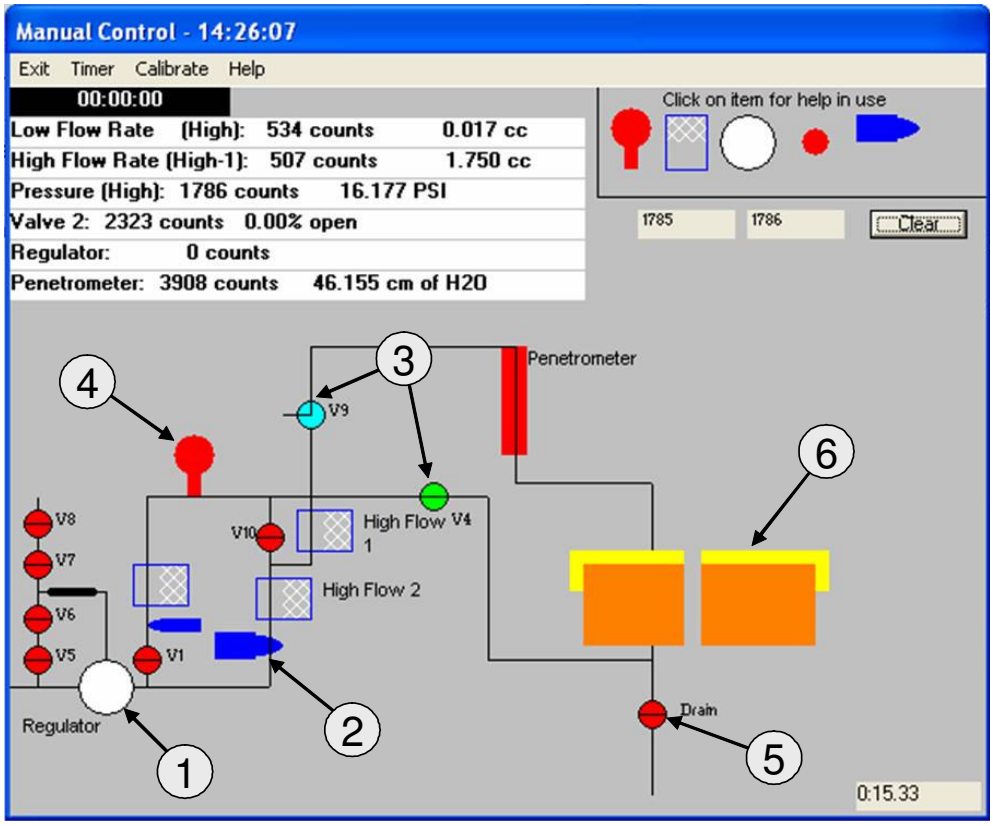

Figure 2-7: Manual control interface for CFP in CapWin™.

The primary features of the system control are the regulator {1}, the motorized needle valve {2}, and the valves V4 and V9 {3}. The regulator is technically a volume booster, accepting a pulse of air from the bank of valves V5 to V8, and increasing the volume such that the desired pressure is achieved. Valve V4 controls flow to the bottom of the sample chamber for gas permeability or CFP testing. Valve V9 controls flow to the top of the penetrometer tube for elevated pressure liquid permeability tests. The other valves, V1 and V10, direct gas through the various flow meters depending on the flow range in question. The pressure transducer {4} measures the differential pressure in the system. The drain valve {5}, which allows fluid to flow out the bottom of the sample chamber during liquid permeability testing, is closed during other tests as the gas must

flow up through the sample chamber {6}. A summary of the instruments in the machine is presented in Table 2-1.

Table 2-1: Instrument list for CFP.

Instrument	Manufacturer	Range
Regulator	Fairchild	0-1375 kPa
High Flow Meter	Hastings	200 SLPM
Low Flow Meter 1	Hastings	10 SLPM
Low Flow Meter 2	Hastings	5 SLPM
Motorized Valve	PMI	0-100%
Pressure Transducer	MKS Instruments	1720 kPa
Displacement Sensor	MTS	40 cm

Using a series of valves, pressure transducers, and flow meters, the machine determines pressure and flow rate data for dry and fully saturated samples. The difference between these curves is then analyzed to provide information concerning the pore structure of the sample. The device uses a bank of valves to allow a pulse of compressed nitrogen at 1375 kPa to enter a regulator. The regulator lowers the pressure to whatever pressure is specified by the software. In a typical CFP test, the pressure is increased slowly while the flow rate through the dry sample is recorded – this is the "dry curve". Next the sample saturated with wetting fluid, isopropanol in this work, is loaded into the sample chamber and the same process is repeated yielding the "wet curve". The two curves are then analyzed using PMI's CapRep™ data reduction software. An example of a typical CFP curve is shown in Figure 2-8.

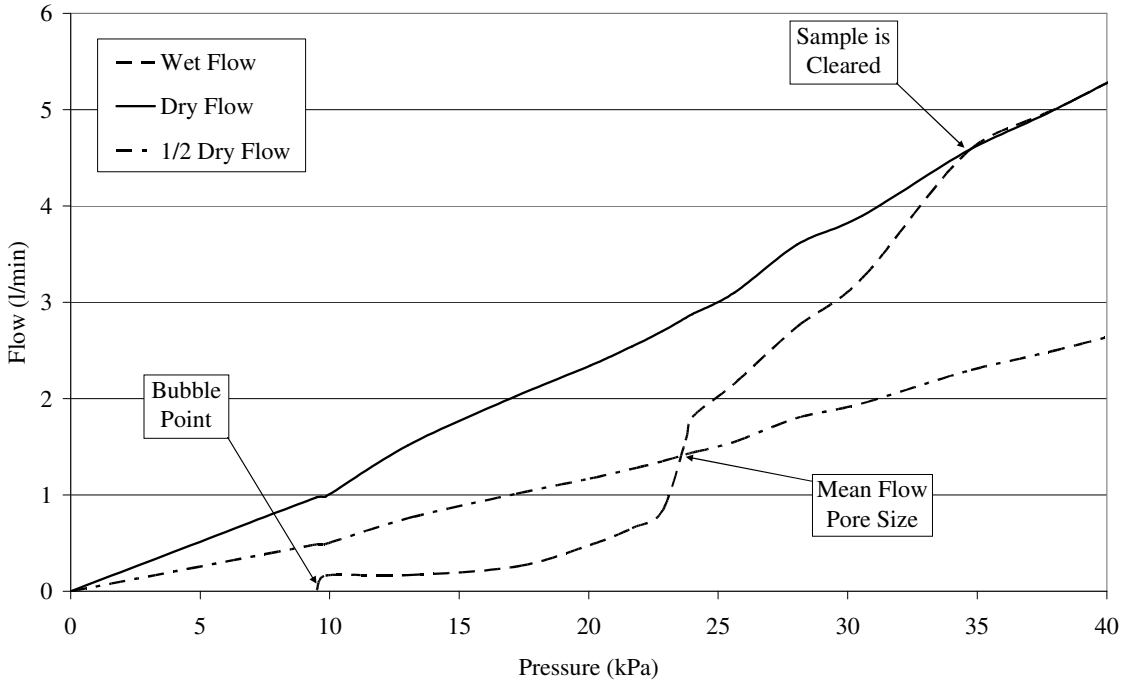

Figure 2-8: Typical CFP curve

The capillary pressure, P_c generated by the wick is a governing parameter in heat pipe operation. It is a function of the effective pore radius, r_c, the surface tension of the working fluid, σ, and the contact angle θ, and is given by the well-known Young-LaPlace equation [6, 20]

$$P_c = \frac{2\sigma\cos(\theta)}{r_c} \tag{18}$$

For wetting fluids with low surface tension such as isopropanol, the contact angle is assumed to be small, such that the cosine term is taken as unity. An implicit assumption is that the measured pore radius is an effective radius, as the pore geometries in sintered

wicks and many other porous structures are not circular pores. The actual formula used to calculate pore size is the ASTM F316-80 standard, and is given by

$$d = \frac{C\lambda\sigma}{P} \tag{19}$$

$$C = 0.58402$$
$$\lambda = 0.415$$

where C is a unit correction constant, d is the pore diameter in μm, σ is surface tension in dynes/cm, and P is in psi. The PMI software uses a tortuosity factor, λ, to correct for non-circular pores. The default value used in the ASTM relation is 0.415 and seems to be applicable to a wide range of pore shapes. PMI includes the option to change it for uniquely shaped pores but the default value was used in this investigation. The value does not affect the data collected, only the calculation of pore size.

The first detected flow value on the wet curve corresponds to the bubble point. This is determined from (19), where the surface tension of isopropanol is taken as 23.0 dynes/cm [21]. The pore size distribution is determined from this data as well [20]. Q_{wet} is the wet flow at a given pressure and Q_{dry} is the dry flow at that same pressure (interpolating between points if necessary), the flow percentage at each point is given by

$$\left(\left.\frac{Q_{wet}}{Q_{dry}}\right|_{n} - \left.\frac{Q_{wet}}{Q_{dry}}\right|_{n-1} \right) \times 100 \tag{20}$$

The pore size distribution is then found as

$$d_{dist,n} = \frac{F_n - F_{n-1}}{d_{n-1} - d_n} \left(\frac{d_{n-1} - d_n}{F_n - F_{n-1}} \right)_{\max} \times 100 \tag{21}$$

The pore size distribution is not a physical quantity, but the magnitude of the function plotted against pore diameter (or equivalent pressures) gives an indication as to the number of pores in a given size range.

Liquid Permeability

Liquid permeability testing was carried out using the CFP as well. The test requires that the drain valve be closed; the sample chamber is subsequently flooded with liquid, deionized water in this case, and the sample is inserted into the chamber. The chamber is completely filled with liquid taking care to ensure no air bubbles of any appreciable size exist within. The chamber is connected to the penetrometer by way of the liquid permeability fitting. Again, this hose must be connected carefully to prevent any air bubbles from being trapped in the line. Once this is complete, the decision to use ambient or elevated pressure at the top of the penetrometer water column must be made. For the samples tested here, all were sufficiently permeable that ambient pressure was adequate. A magnetic float in the water column enables the potentiometer to measure the change in height of the column and hence the change in hydrostatic pressure applied to the sample. Combined with the diameter of the column, the flow rate through the sample can be determined. This information is analyzed using the CapRep™ software to determine the liquid permeability of the sample.

The CFP measures permeability by forcing fluid through a sample while measuring the differential pressure and flow rate. Examining Darcy's law for flow

through porous media, the flow rate, Q, through a sample with cross sectional area, A, driven by a pressure gradient, $\frac{dP}{dx}$, depends on the permeability constant, K, where

$$Q = \frac{KA}{\mu}\frac{dP}{dx} \tag{22}$$

Permeability has units of m^2, and can be thought of as the equivalent area of an orifice yielding the same flow-rate at the same differential pressure. The following restrictions apply to Darcy's law [20, 22]:

1) Laminar, viscous flow (creeping flow)
2) Steady state flow
3) Incompressible flow
4) Homogeneous structure

Darcy's law can be used to predict the flow rate through a porous medium of known permeability or determine the permeability based on flow rate and pressure data. Here, permeability was calculated from the measured flow rate and hydrostatic pressure of deionized water through the wick sample. Rearranging (22) and assuming a constant pressure gradient, $\frac{\Delta P}{L}$, the following expression for permeability is obtained

$$K = \frac{Q\mu L}{A(\Delta P)} \tag{23}$$

Heat Leak

The heat leak measurement apparatus consisted of a high density polyethylene fluid reservoir, silicone tubing, a variable flow peristaltic pump, a liquid flow meter, a Mettler PE-22 balance, and a test stand into which the wick was inserted. Two Minco HM6800 thermofoil heaters (R = 4.5 Ω) were mechanically clamped to solid copper heater blocks backed by ceramic insulation. The heater blocks had relieved passages for vapor exit and were bolted together to support the wick. A schematic of the apparatus is shown in Figure 2-9.

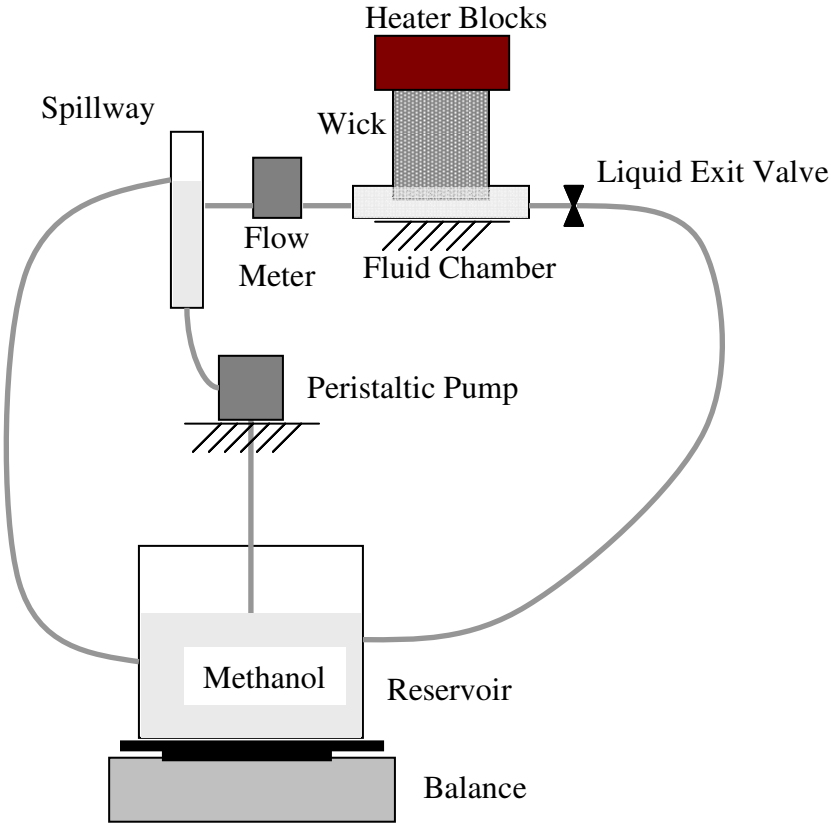

Figure 2-9: Heat leak measurement apparatus

The test stand was constructed from a section of 31.75 mm PVC pipe with a 4.8 mm slot cut longitudinally through the top wall of the pipe. The slot was slightly longer

than the wick samples and wide enough that the samples did not touch any portion of the slot once inserted. Flow through the pipe was measured using a MacMillan S-112 liquid flow meter. A ball valve on the exit end of the pipe allowed the liquid flow rate through the test stand to be regulated. Methanol was used as the working fluid due to its excellent wetting characteristics. Liquid level in the test stand was maintained at a constant level by the peristaltic pump and a spillway system with overflow directed back to the reservoir. Mass flow rate was measured by recording the mass lost from the system in 15 min increments. Each wick was instrumented with six Omega 30-gauge SLE T-type thermocouples spaced in 12.7 mm increments from the bottom edge of the sample as shown in Figure 2-10. The thermocouples were attached with a small amount of solder using a drop of phosphoric acid as flux.

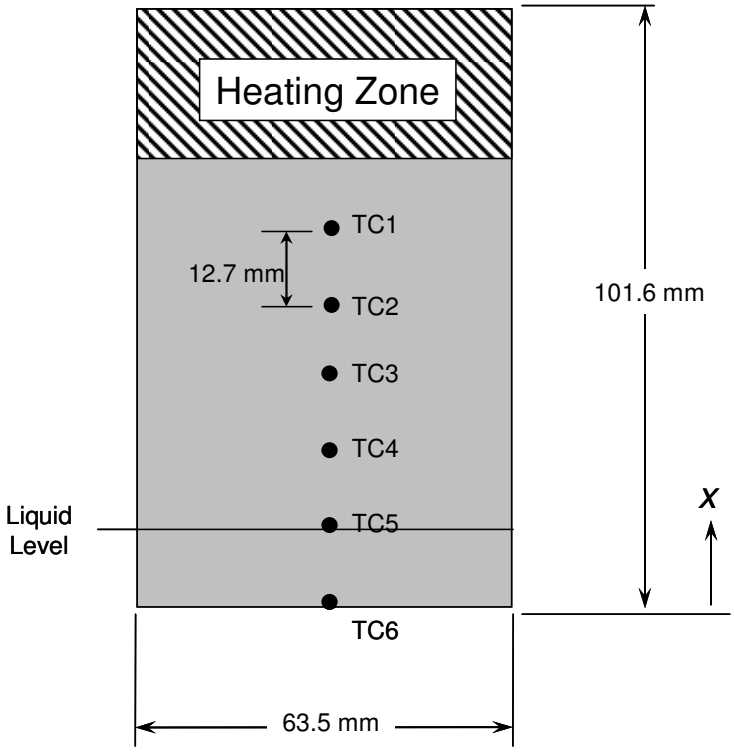

Figure 2-10: Wick sample configuration.

An additional thermocouple was used to monitor the liquid exit temperature to ensure a steady fluid temperature. The entire heater block/wick/fluid chamber assembly was surrounded with several layers of reflective thermal insulation to minimize losses to the surroundings. Baffles were included to minimize air currents within the chamber, as shown in Figure 2-11.

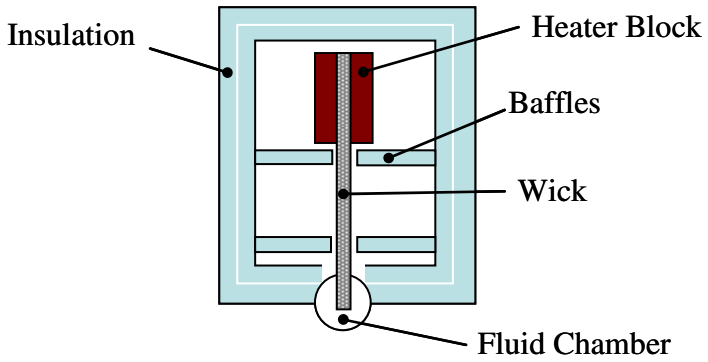

Figure 2-11: Insulation schematic for heat leak testing.

The reservoir was maintained at room temperature and the flow through the silicone tubing was sufficient to dissipate the small amount of heat transmitted through the wick into the fluid. The samples were inserted into the flow-through fluid chamber up to the height of the second thermocouple, i.e., 12.7 mm. The wick was given several minutes to fully saturate before each test. The liquid front in the wick could be seen visually and confirmed with the drop in measured temperature as the methanol evaporated.

An evaporative loss calibration was performed for each sample by immersing the wetted portion of the wick in the fluid and allowing the temperature profile to reach steady state with no applied power. The mass flow rate was then recorded over a period of approximately 2 h to ensure a steady mass flow had been achieved. The resolution of the balance was 0.1 g translating to a resolution of approximately 0.03 W in steady state

evaporative power based on the latent heat of methanol, h_{fg} = 1101.8 kJ/kg and a time period of 1 h over which the measurements were recorded. Power was then applied to the heaters in 5 W increments until 1) heater backing plate temperature reached 150°C, or 2) the temperature of the uppermost thermocouple exceeded the saturation temperature of methanol at atmospheric pressure (64.1°C). Power to the heaters was controlled by a Variac, 120 V input, and measured using an Ohio Semitronics GW5-010X5 power transducer. Evaporative power was measured independently of the applied heat load using the mass loss measurement such that the resulting data is unaffected by the power setting, so long as the setting is constant for the duration of the test. The power transducer was periodically checked to ensure that the applied power was not drifting appreciably. Applied power not dissipated in evaporative heat transfer or conducted through the wick was considered lost to the environment; the power setting served as a convenient measure for designating test settings. Steady state temperature profiles were used to determine the heat leak into the fluid supply. The plane of the thermocouple TC5 was taken as the plane of interest and the temperature gradient between TC4 and TC5 was used to determine heat leak based on the effective conductivity of the saturated wick structure.

CHAPTER THREE
RESULTS AND DISCUSSION

Porosity

The porosity of each sample was calculated based on the average of 4 trials of the following measurements: diameter, thickness, dry mass, and saturated mass. Of the four, the saturated mass had the greatest uncertainty due to the variable thickness of the fluid that collected on the surface of the sample due to surface tension. Diameter and thickness were both measured at 4 distinct locations using Mitutoyo CD-6" BS calipers with a resolution of 0.01 mm. The results of those measurements are presented in Appendix C. The expression for volumetric porosity is

$$\phi = \frac{V_{pore}}{V_{tot}} \tag{24}$$

The expressions for the pore volume and total volume are given by

$$V_{pore} = \frac{\left(m_{sat} - m_{dry}\right)}{\rho_f} \tag{25}$$

$$V_{tot} = \frac{\pi D^2 t}{4} \tag{26}$$

The resulting porosity values are presented in Figure 3-1.

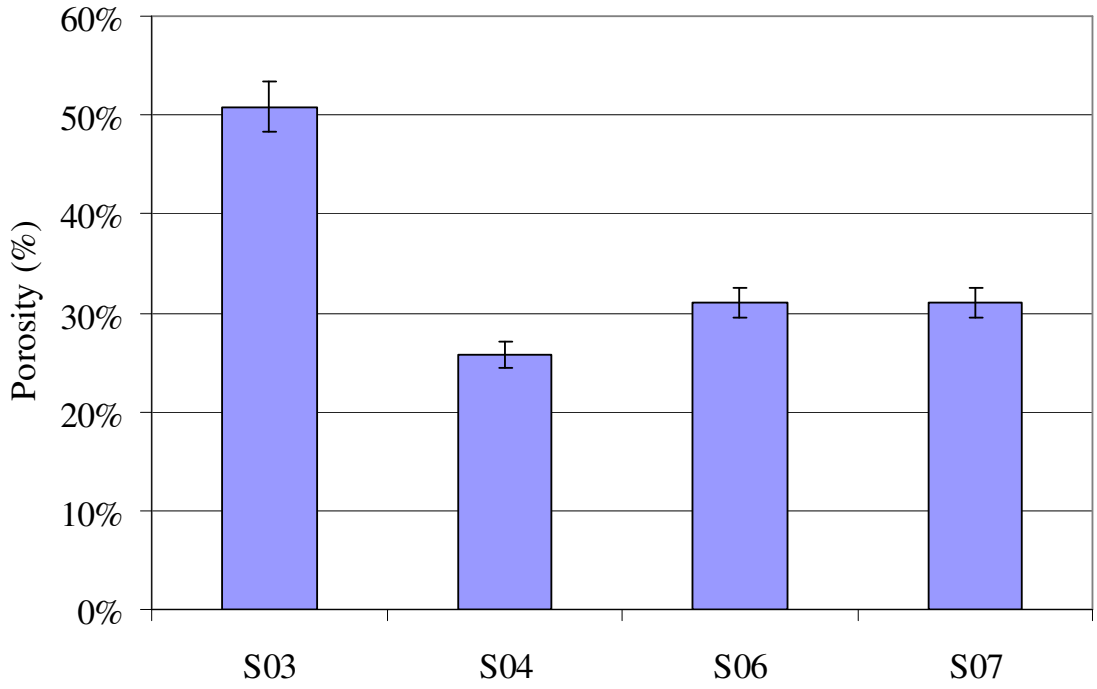

Figure 3-1: Sample porosity results

Effective Thermal Conductivity

Effective thermal conductivity measurements were obtained for each sample using the heat flux meters and calibration curves presented in chapter two. An average of the three thermocouple readings for each flux meter was used to determine its thermal conductivity. Heat flux through each meter was then determined using the temperature gradients measured at steady state, taken as a linear fit of the 3 thermocouples. The measurements for the two heat flux meters were averaged to yield the heat flux through the sample. This is in keeping with the calibration procedure of using the heat flux through the sample in the center of the column as being equivalent to the heat flux through each meter, effectively averaging the heat flux. In testing the measured upper

and lower heat flux differed by 2-9%, increasing with temperature gradient. To calculate the temperature gradient in the sample, temperature profiles were extrapolated to the surface of the sample as shown in Figure 3-2. Thus, the heat fluxes are determined from

$$q''_{meter} = -k_{meter}\left(T_{meter,avg}\right)\left.\frac{dT}{dx}\right)_{meter} \tag{27}$$

$$q''_{samp} = \frac{q''_{meter,low} + q''_{meter,up}}{2} \tag{28}$$

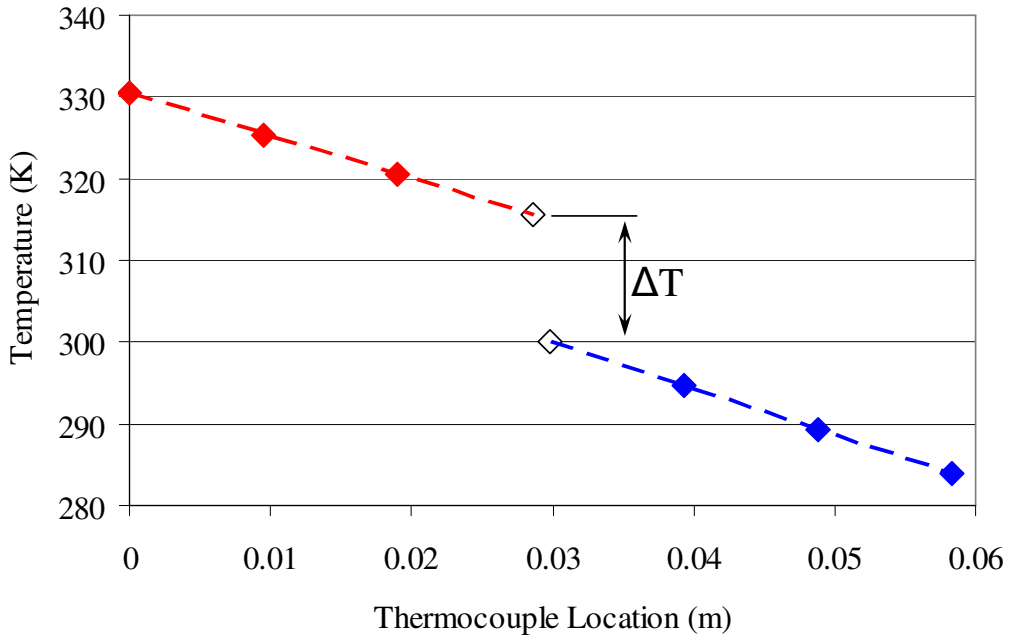

Figure 3-2: Graphical example of sample temperature drop calculation.

The temperature gradient is calculated as he difference in these extrapolated temperatures divided by the sample thickness. The conductivity of the sample was determined by dividing the average heat flux by the temperature gradient

$$k_{eff}\left(T_{samp,avg}\right) = \frac{-q''_{samp}}{\left.dT/dx\right)_{samp}} \tag{29}$$

Samples S06 and S07 were tested first with seven data points taken for each. Due to the good linearity of the data, only three points were collected for samples S03 and S04 in the interest of time. The data for each sample are presented in Figure 3-3 to Figure 3-6. The raw temperature data for each point are presented in Appendices B1-B4.

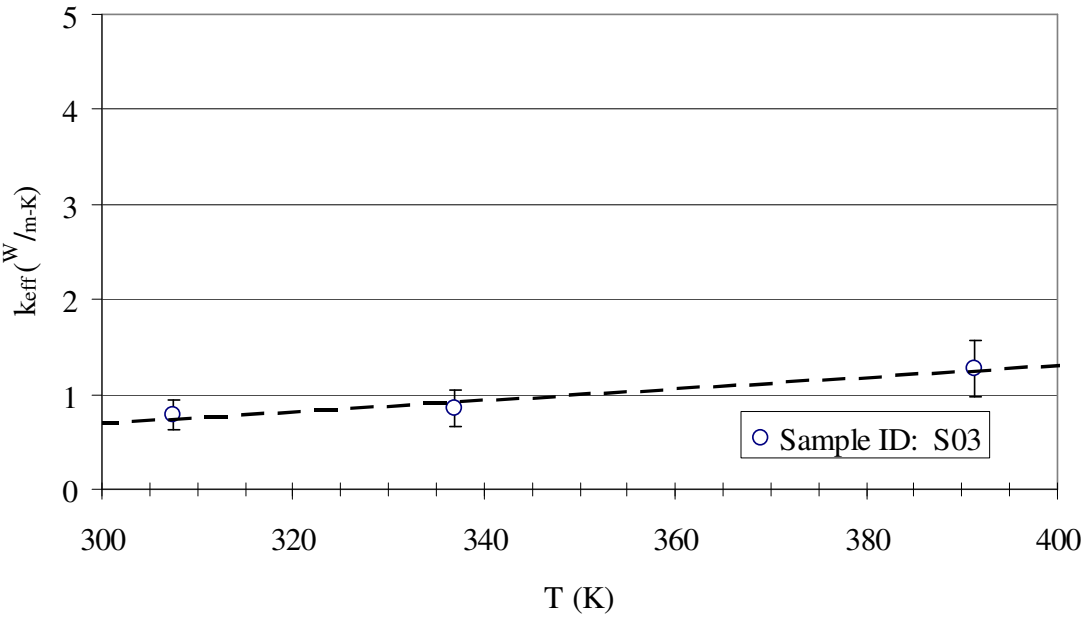

Figure 3-3: Effective thermal conductivity results for S03.

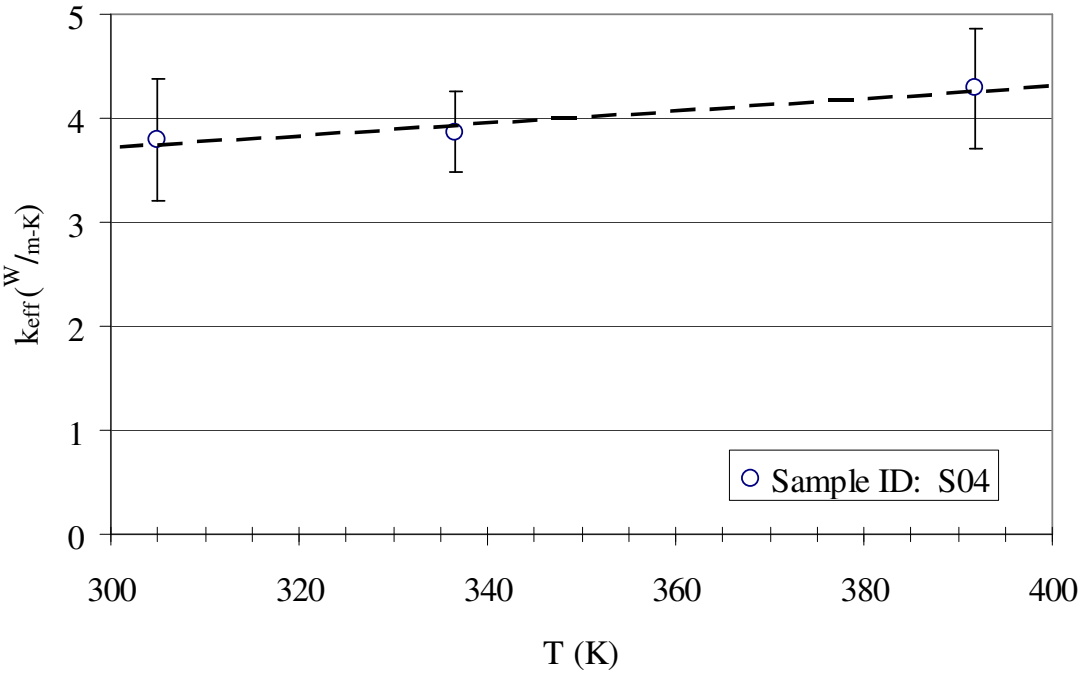

Figure 3-4: Effective thermal conductivity results for S04.

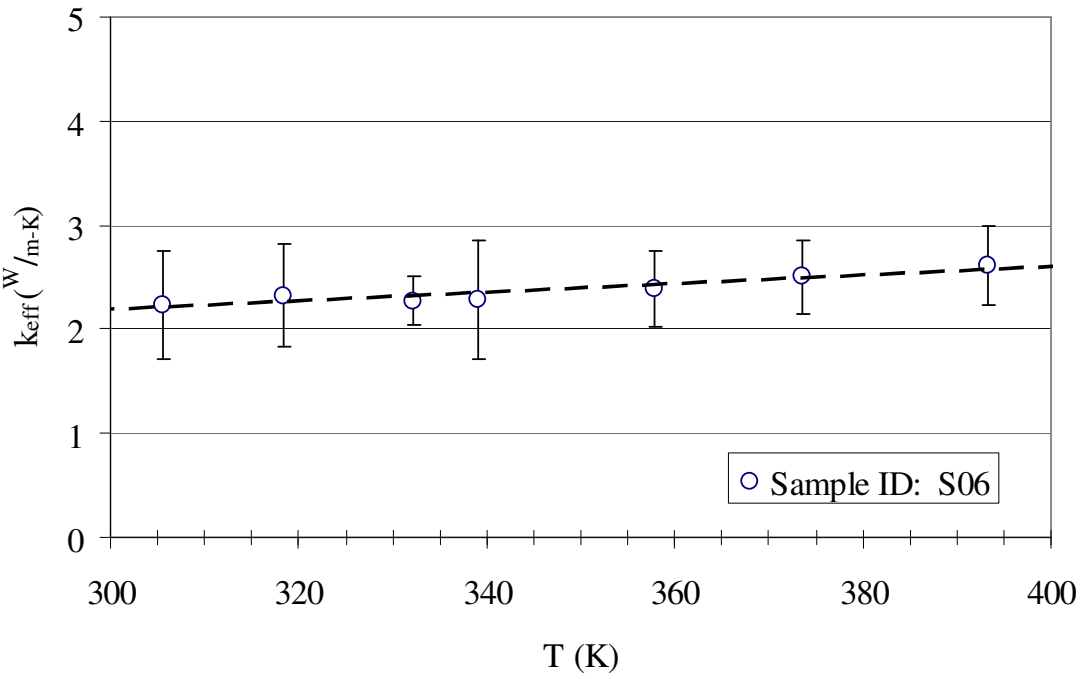

Figure 3-5: Effective thermal conductivity results for S06.

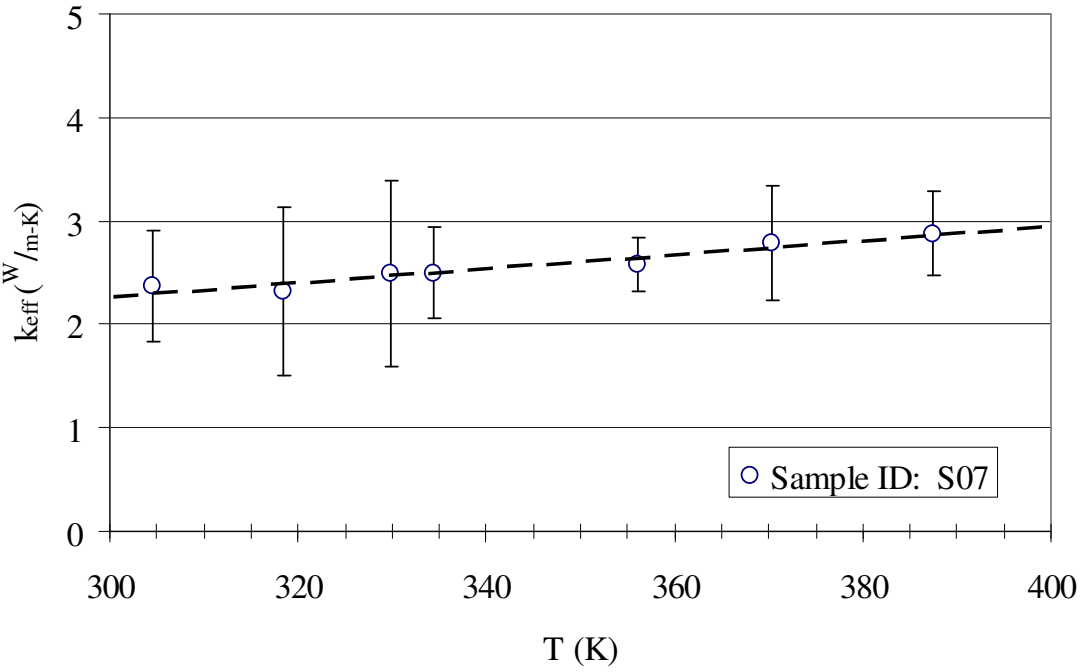

Figure 3-6: Effective thermal conductivity results for S07.

For each sample, a linear fit of the data was used in calculating subsequent results requiring effective thermal conductivity. The equations were of the form $k_{eff} = A \cdot T_{samp} + B$, where A and B are the coefficients presented in Table 3-1.

Table 3-1: Linear coefficients for sample conductivity in vacuum.

Coefficient	S03	S04	S06	S07
A	0.006	0.006	0.004	0.007
B	-1.113	1.939	0.934	0.242

Using these values for effective conductivity in vacuum, the Chi model found by Bonnefoy et al.[5] to be the most consistent for sintered metal wicks was used to predict the saturated effective conductivity of the wick samples. Of the parameters in the model

only r_s is unknown. Thermal conductivity of stainless steel and methanol are known from reference data [19, 21] while capillary radius and porosity are measured (mean flow pore radius is used for r_c). With this information, the model can be iteratively tailored to yield the measured k_{eff} (with k_f set to zero for vacuum) by changing the value of r_s. Once the appropriate value of r_s is found the value of k_f is changed to that of methanol, thereby giving a good approximation of the effective conductivity. This procedure was performed for two temperatures, 300 and 400K. The results of this approach along with the results of other models in the literature are presented in Figure 3-7 to Figure 3-10 [6, 7, 9].

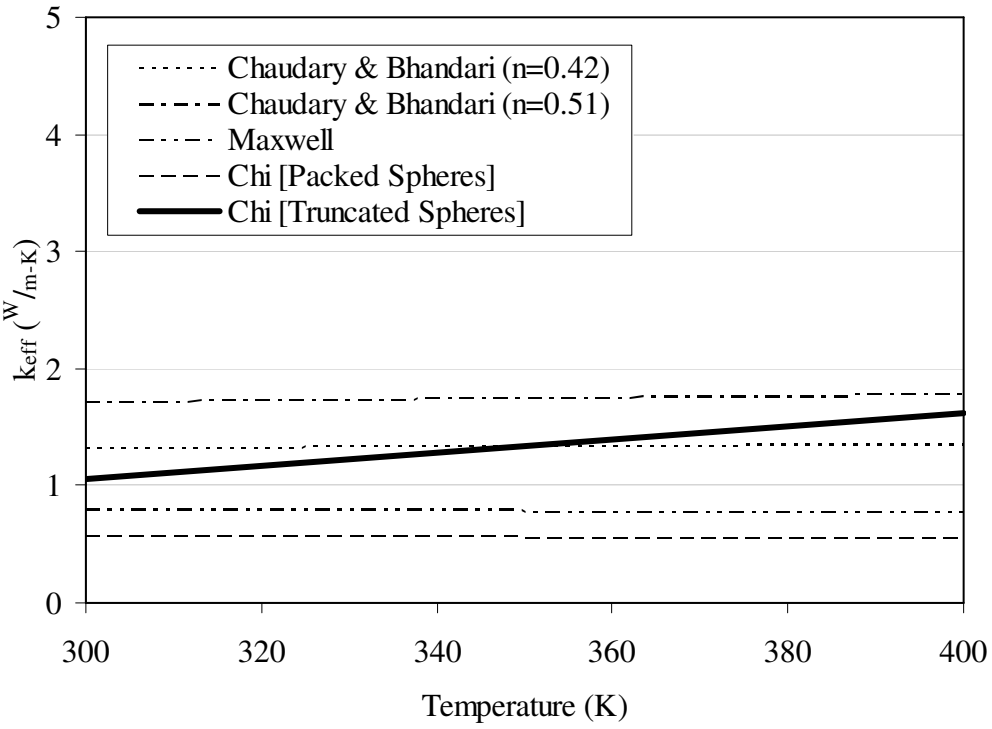

Figure 3-7: S03 saturated effective conductivity results and comparisons.

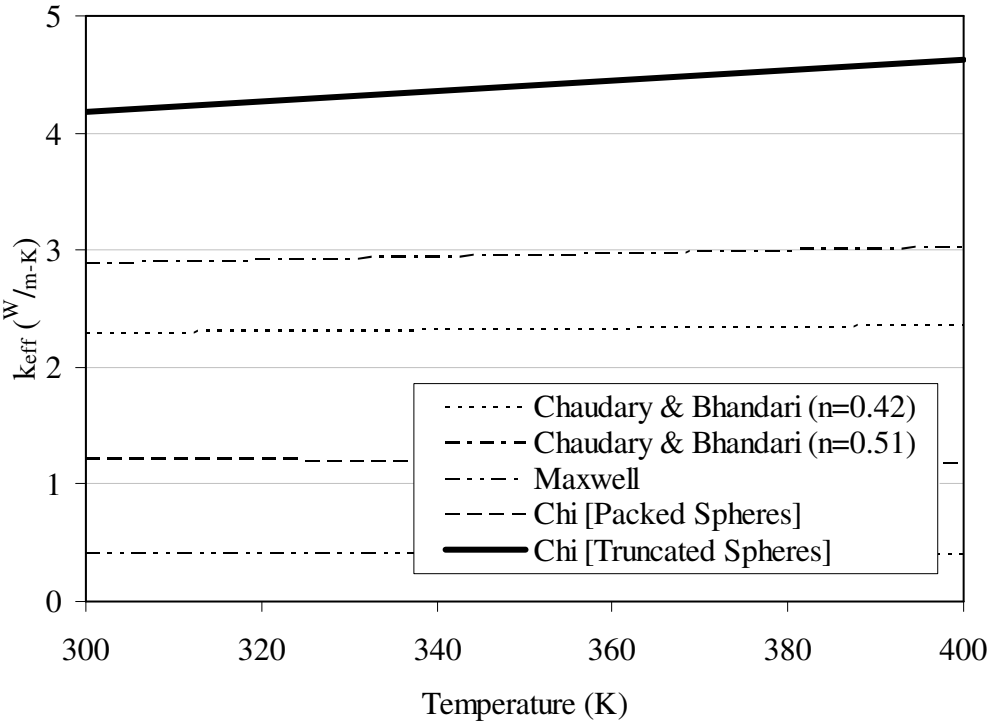

Figure 3-8: S04 saturated effective conductivity results and comparisons.

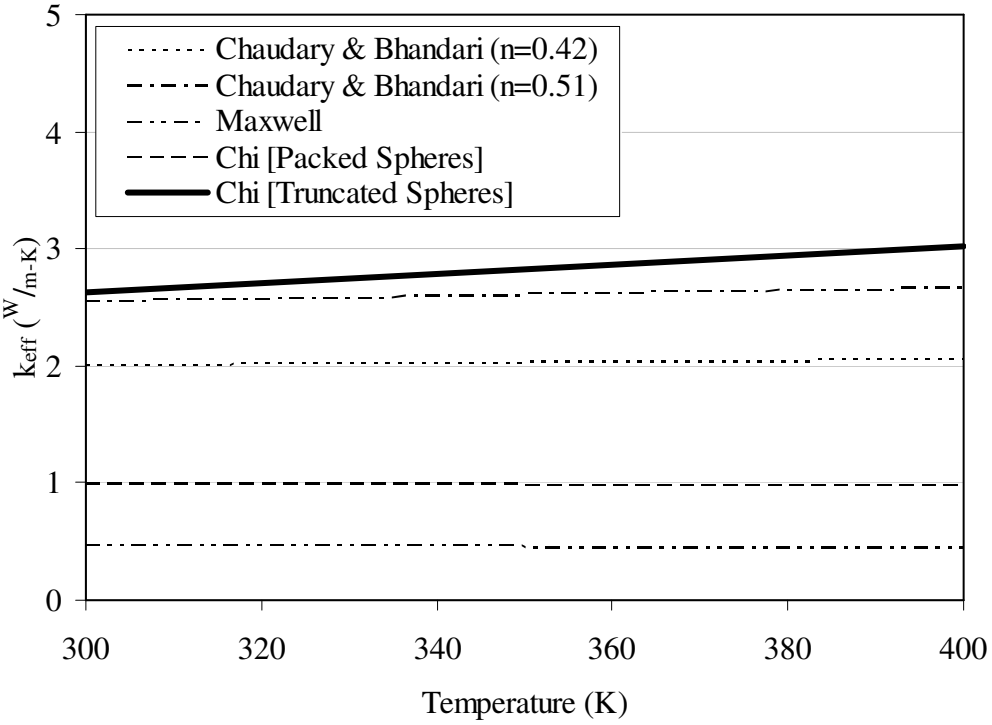

Figure 3-9: S06 saturated effective conductivity results and comparisons.

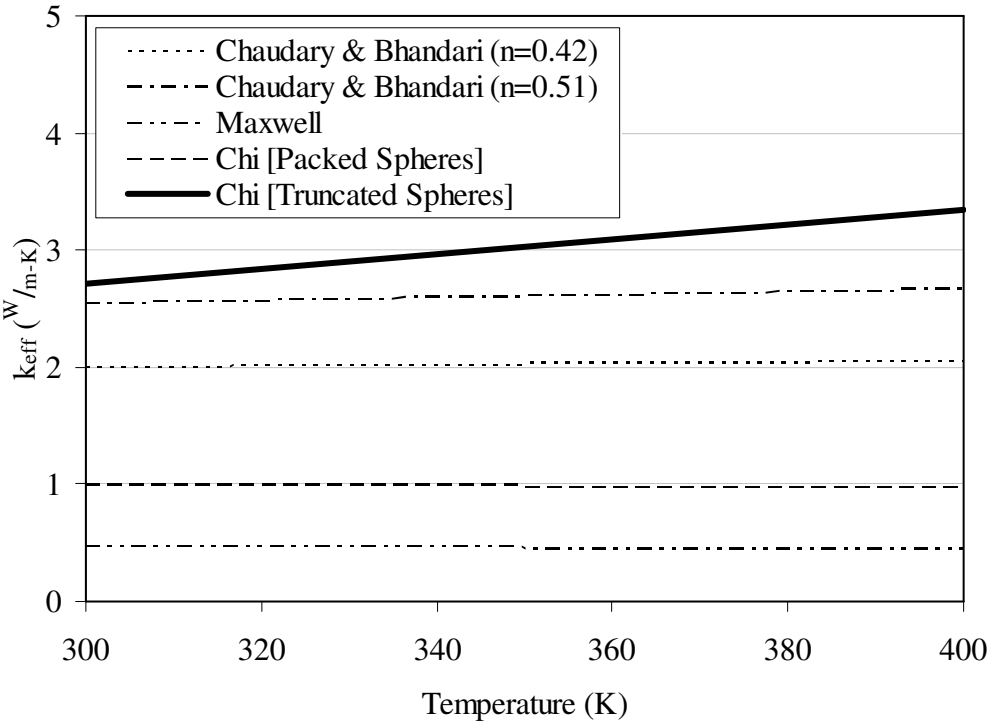

Figure 3-10: S07 saturated effective conductivity results and comparisons.

Examining these results, it is clear that while the data matches the models to within an order of magnitude the temperature dependence of the conductivity is not reflected despite using temperature-dependent values for k_f and k_s as inputs. Indeed, the Chi truncated spheres model only includes this effect due to the measured conductivity in vacuum that was used in determining $k_{eff,sat}$ at each temperature. As with vacuum, linear models of methanol-saturated effective thermal conductivity were used in subsequent calculations. The models were of the form $k_{eff,sat} = C \cdot T_{samp} + D$; values for C and D are presented in Table 3-2. A plot showing the relative conductivities of the saturated samples is presented in Figure 3-11.

Table 3-2: Linear coefficients for saturated sample conductivity.

Coefficient	S03	S04	S06	S07
C	0.006	0.006	0.004	0.006
D	-0.660	2.420	1.460	0.820

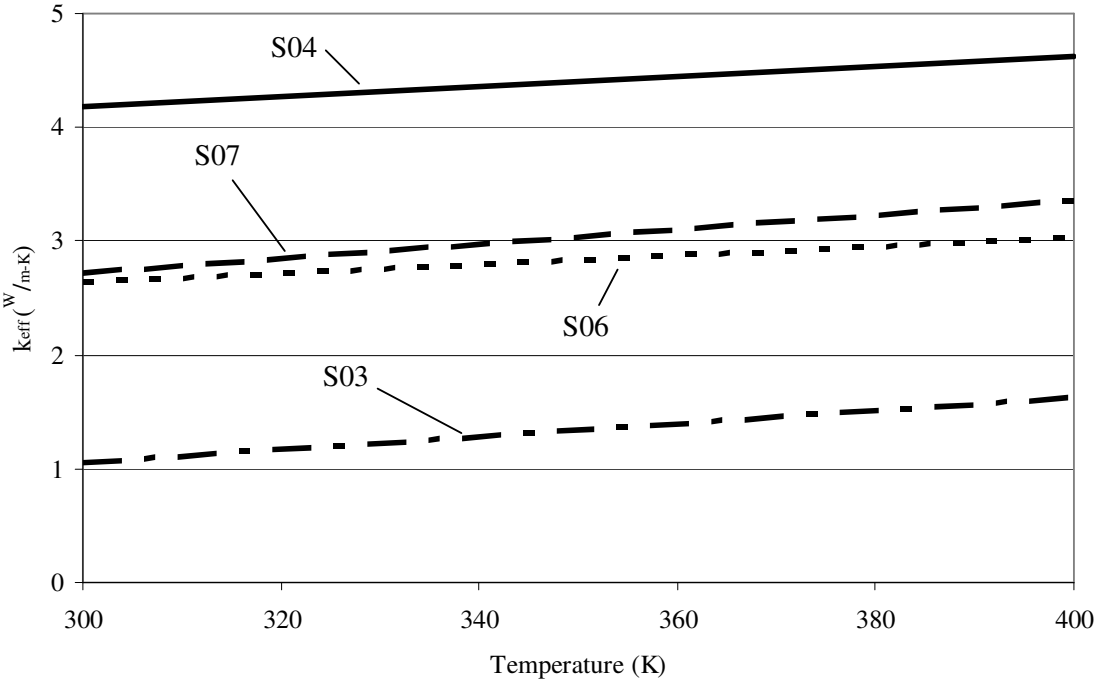

Figure 3-11: Saturated sample effective thermal conductivities.

Pore Size Distribution

Presented in Figure 3-12 through Figure 3-15 are the wet and dry curves for each sample. Also included in each figure is the 1/2 dry curve, which at its intersection with the wet curve corresponds to the mean flow pore size. The uncertainties in these measurements are very low, such that they aren't visible on the charts. The stated uncertainties for the instruments are 0.15% for pressure and 1/60,000th full scale for flow rate.

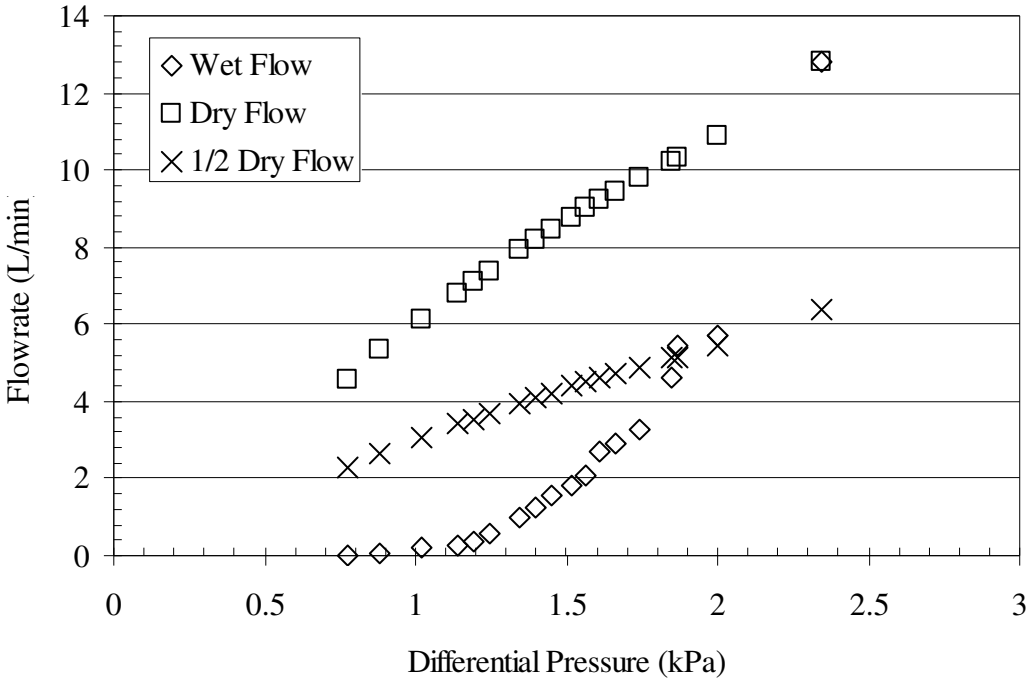

Figure 3-12: S03 CFP results – pressure and flow rate data.

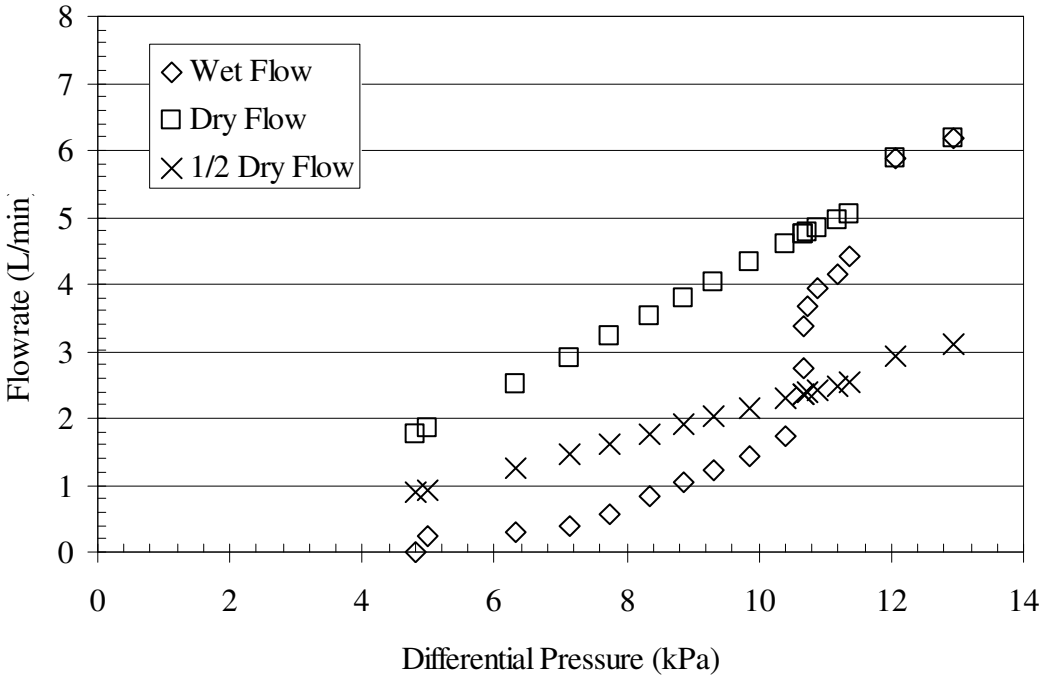

Figure 3-13: S04 CFP results – pressure and flow rate data.

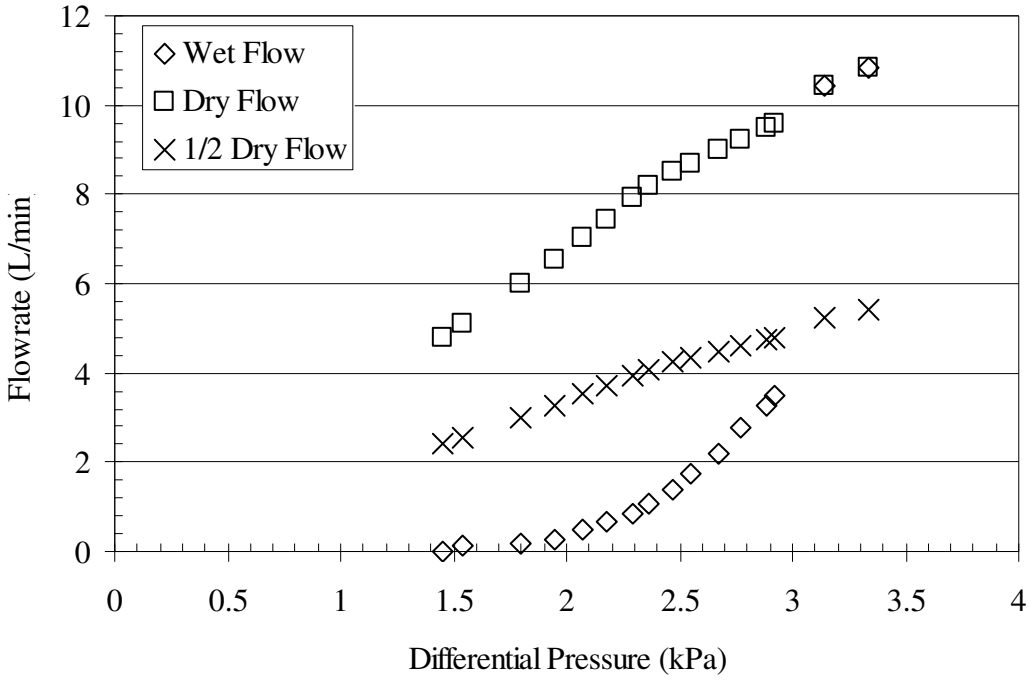

Figure 3-14: S06 CFP results – pressure and flow rate data.

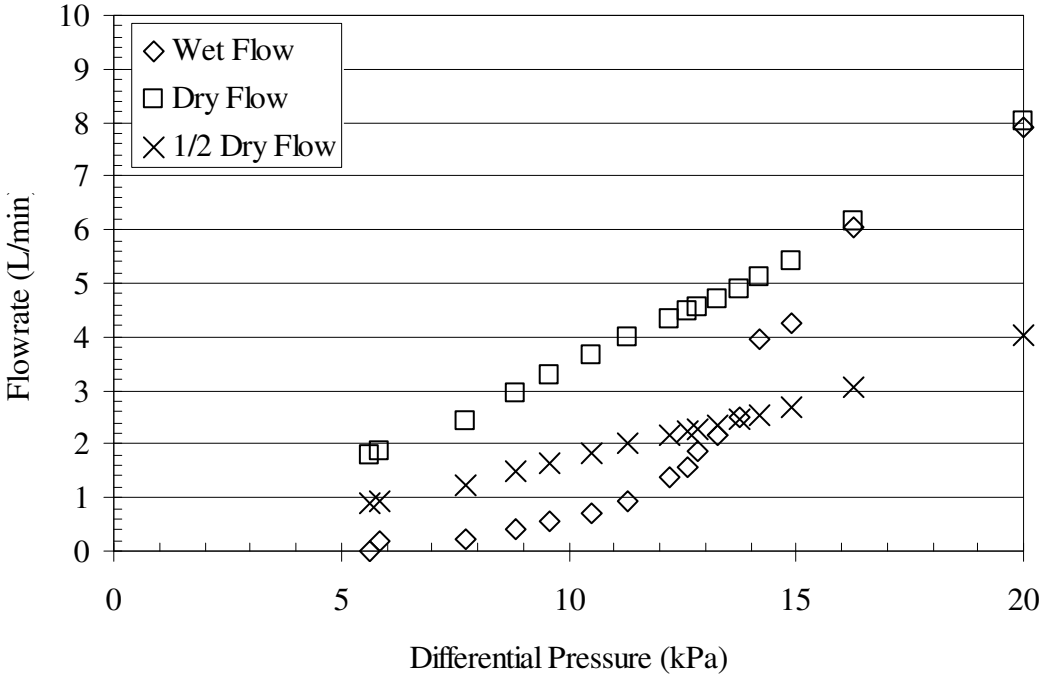

Figure 3-15: S07 CFP results – pressure and flow rate data.

Pore size distributions for the four samples are plotted against average pore diameter in Figure 3-16 to Figure 3-19. The peaks in these plots correspond well with the mean flow pore size data. A summary of bubble point, mean flow, and minimum detectable pore diameters are presented in Table 3-3.

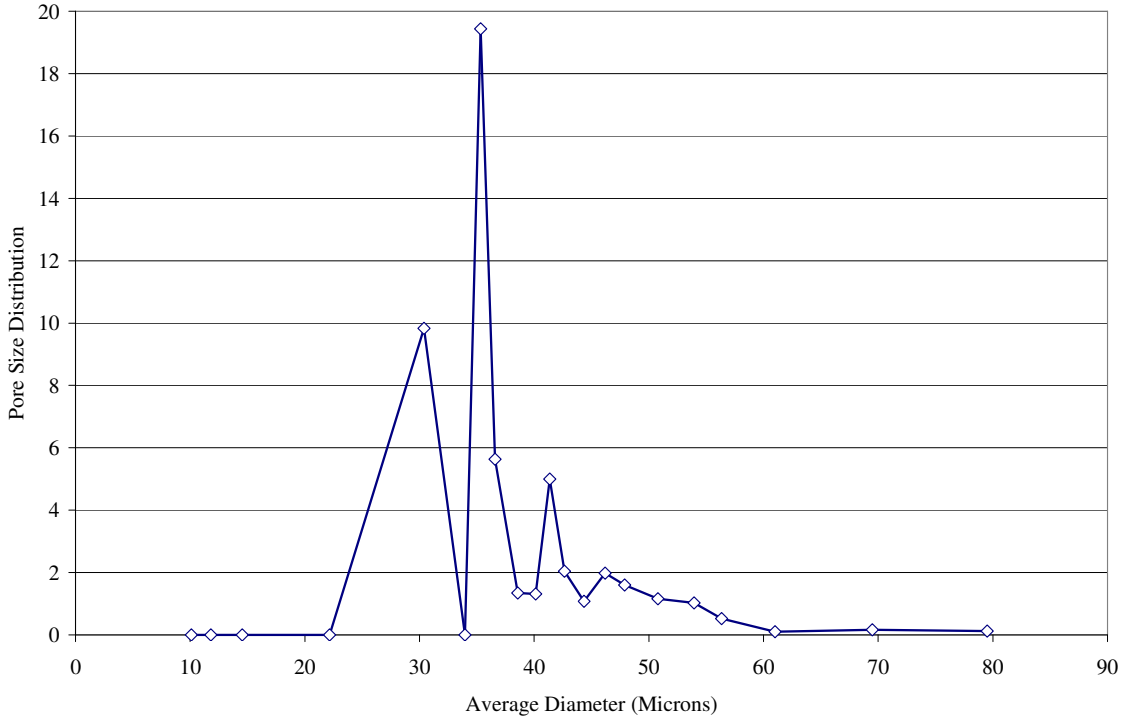

Figure 3-16: S03 pore size distribution.

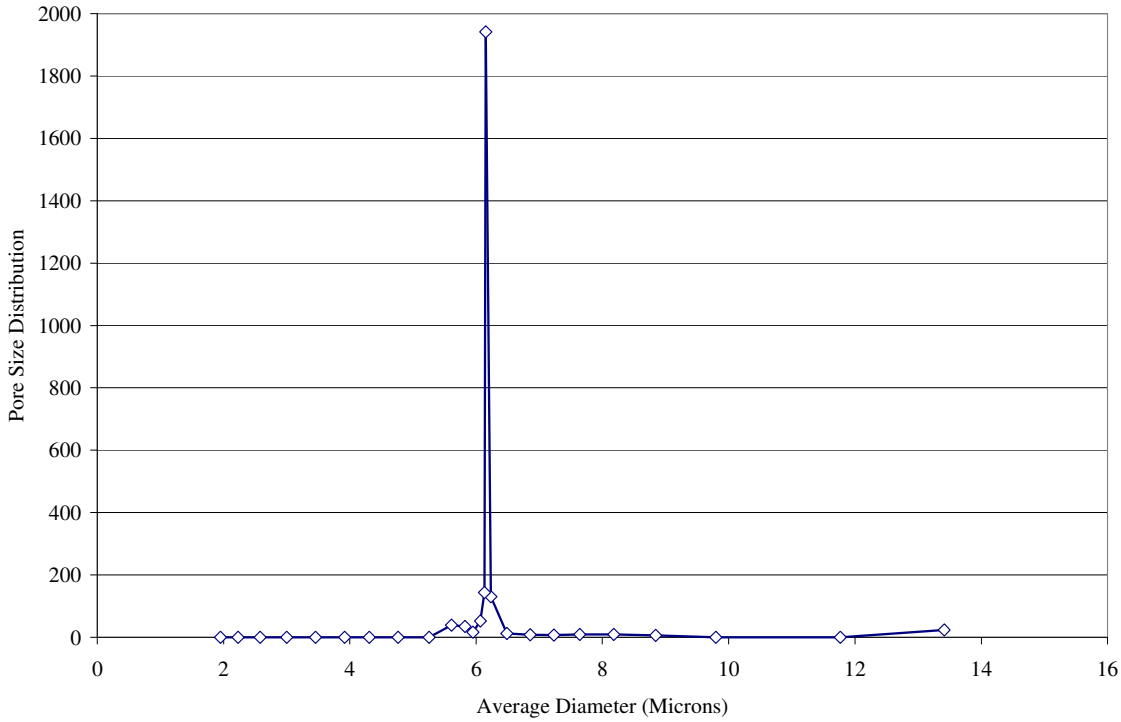

Figure 3-17: S04 pore size distribution.

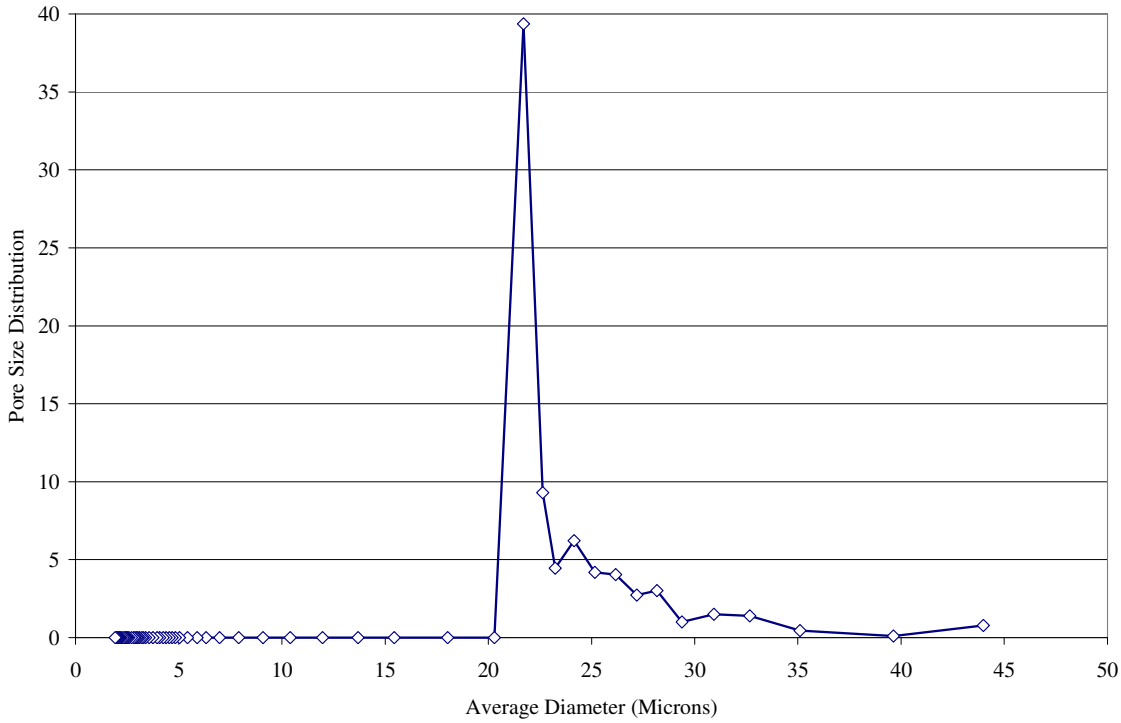

Figure 3-18: S06 pore size distribution.

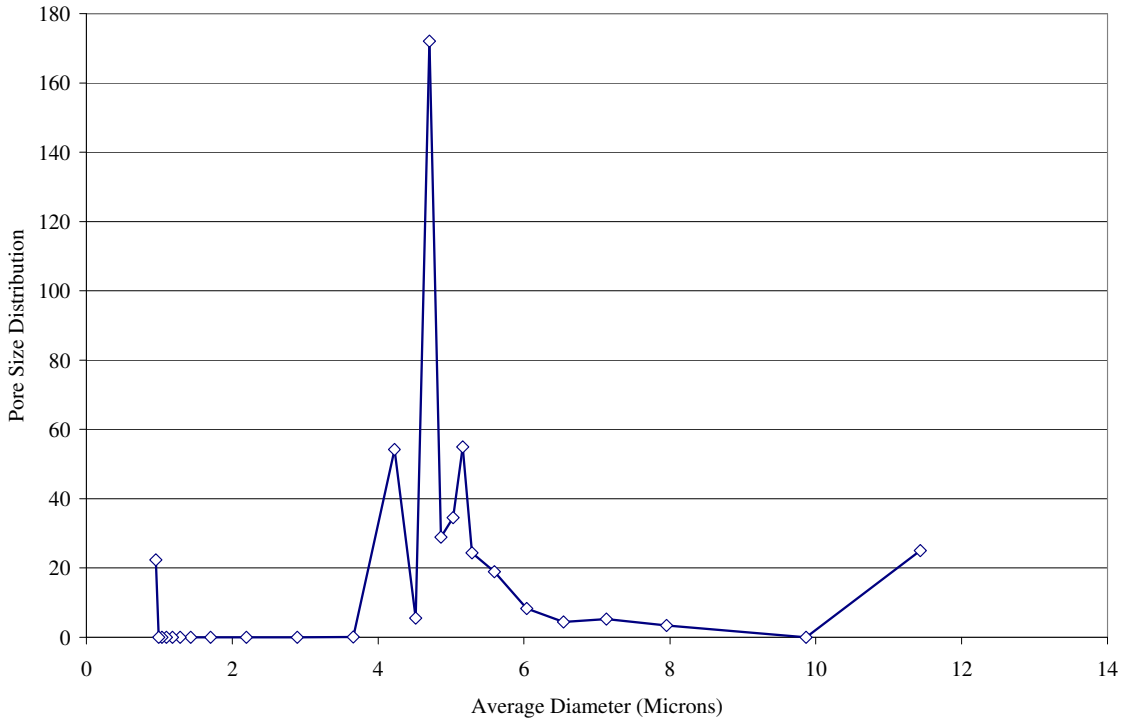

Figure 3-19: S07 pore size distribution.

Table 3-3: Pore diameter summary.

Sample ID:	S03	S04	S06	S07
Bubble Point (μm)	84.5	13.7	45.3	11.6
MFP (μm)	35.3	6.2	22.2	4.8
Minimum Pore (μm)	9.3	1.8	1.9	0.9

Liquid Permeability

The liquid permeability of the four samples was measured using the Capillary Flow Porometer. As with the porometry results the uncertainties are very low: 0.15% in pressure and 1/20,000th resolution in the position sensor. A summary of permeability results and comparison to the well known Blake-Kozeny equation [6] is provided in Figure 3-20. This model is given again as

$$K = \frac{r_s^2 \phi^3}{37.5(1-\phi)^2} \tag{30}$$

Where:

$$r_s = \frac{r_c}{0.41}$$

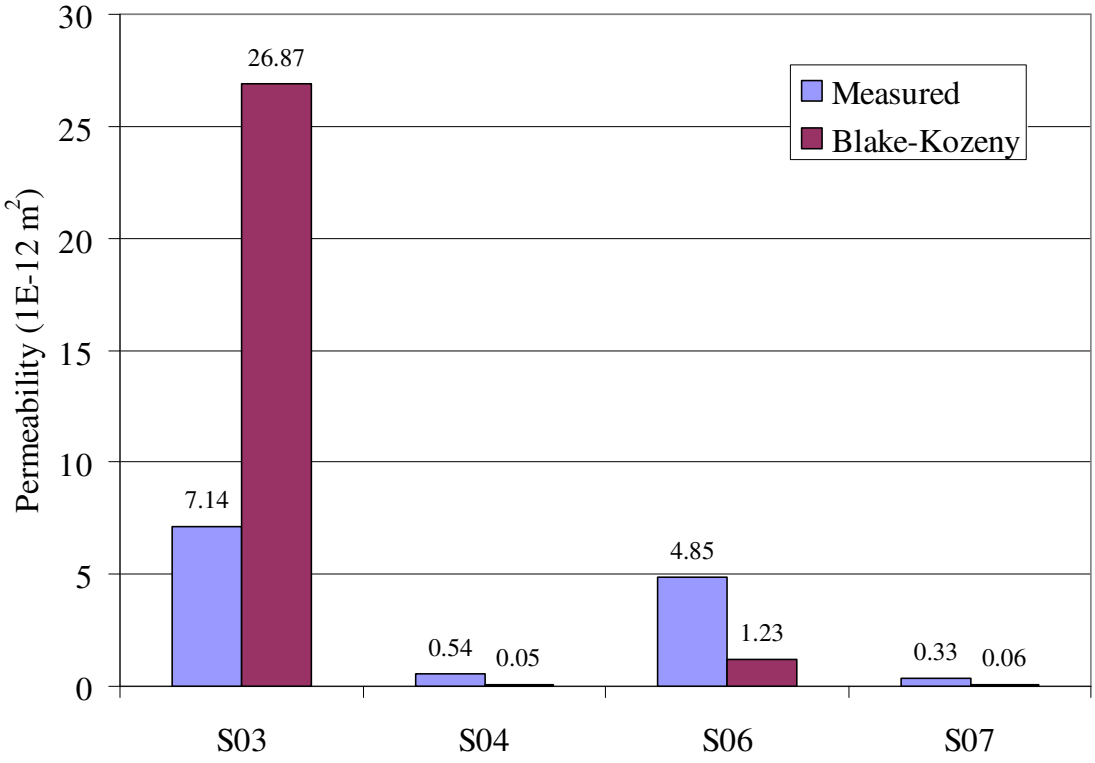

Figure 3-20: Sample permeability results.

The differences among the three samples between the measured permeability and the value predicted by the Blake-Kozeny equation are likely rooted in the sample manufacturing. Since the Blake-Kozeny equation determines permeability using an r_s value based on a packed-spheres assumption, different packing methods, non-uniform particle sizing, or other departures from the packed spheres assumption lead to significant error resulting from this equation. To further indicate the potential for processing

differences, sample S03 was obtained from Mott Corporation in the 1998-1999 timeframe, while S04, S06, and S07 were obtained from the manufacturer in 2006. Additionally, S03 is of larger pore size and greater wick thickness than the other samples. A comparison of the of the wick properties is presented in Figure 3-21.

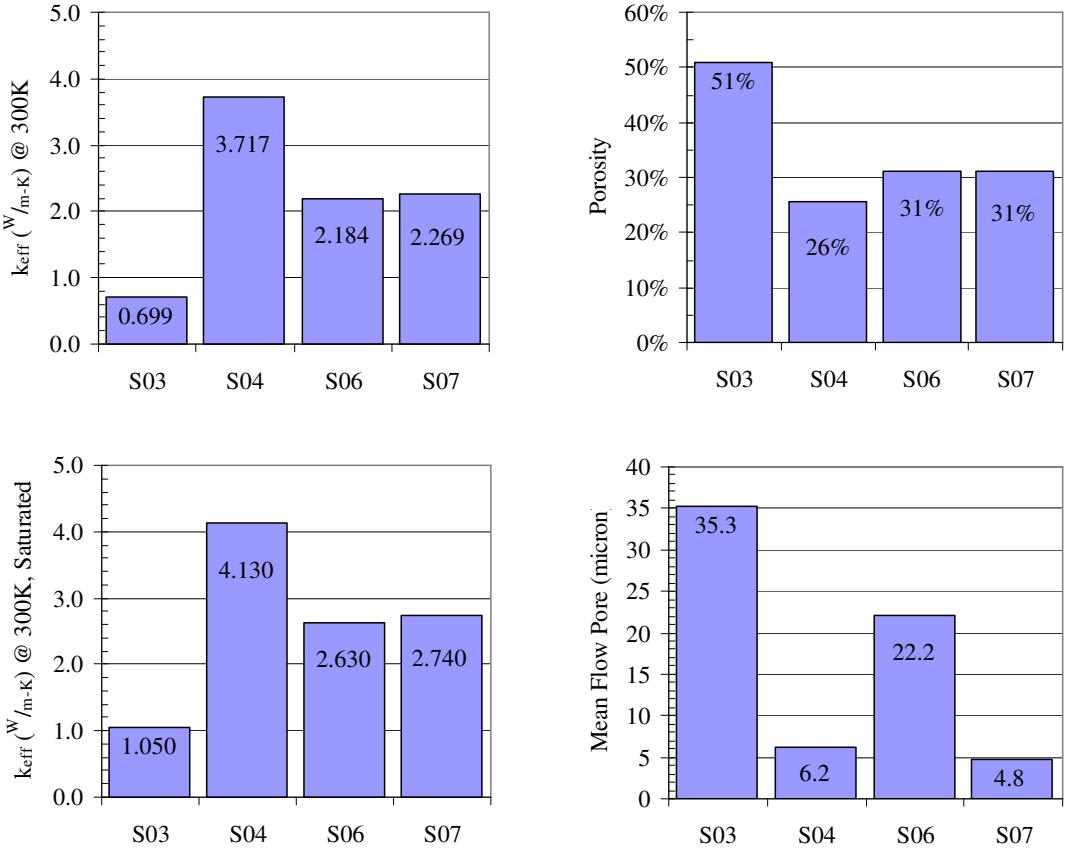

Figure 3-21: Comparison of sample property results.

Heat Leak

As discussed earlier, heat leak testing consisted of immersing the bottom 12.7 mm of each wick sample in a slow moving stream of methanol. Temperature gradients in the

wick were measured and used to determine heat flow through the wick into the fluid stream. System mass was monitored to determine the mass flow rate of fluid evaporation at steady state. For each sample tested, an evaporative loss calibration was performed. By measuring the mass lost to atmospheric evaporation without any heat input, parasitic losses to the wick could be evaluated (the latent heat of methanol at room temperature is h_{fg} = 1101.8 kJ/kg) using

$$q''_{evap,loss} = \frac{\dot{m} h_{fg}}{A} \tag{31}$$

Any additional mass lost was due to heat input from the heater block through the wick structure. These evaporation losses also created a temperature gradient in the wick which resulted in heat leak losses in the wick. These were evaluated using the effective thermal conductivity of the saturated wick and the temperature gradient above the liquid surface to calculate the heat leak loss, given as

$$q''_{leak,loss} = \frac{-k_{e,meth}\left(\frac{T_4 - T_5}{x_4 - x_5}\right)}{A} \tag{32}$$

The results of the evaporative loss calibrations are presented in Table 3-4. Note that the evaporative loss results are presented with a positive sign and are subtracted from the measured values while the leak loss results are negative and subtracted from the measured values.

Table 3-4: Heat loss calibration values.

Sample ID	S03	S04	S06	S07
$q''_{evap,loss}\ (W/m^2)$	10961.3	16794.9	14450.5	15147.5
$q''_{leak,loss}\ (W/m^2)$	-522.5	-2261.6	-1456.2	-1243.6

This procedure and calculation was repeated again for the operating wicks; leak heat flux was calculated according to

$$q''_{leak} = \frac{-k_{eff,meth}\left(\frac{T_4 - T_5}{x_4 - x_5}\right)}{A} - q''_{leak,loss} \tag{33}$$

while evaporative power was calculated using

$$q''_{evap} = \frac{\dot{m}\left(c_{p,f}(T_{sat} - T_f) + h_{fg}\right)}{A} - q''_{evap,loss} \tag{34}$$

Power was increased in approximately 5W increments from 0 to 25W. Sample S06 reached the limit temperature more quickly and the 25W test was aborted. Leak heat flux is plotted against evaporative heat flux for each sample in Figure 3-22, while heat leak as a percentage of the total evaporative and leak heat flux is plotted in Figure 3-23. Large uncertainties resulted for several data points where very little temperature difference was present across the thermocouples of interest. This result is evident looking at ΔT between TC4 and TC5 in the heat leak data presented in Appendix D.

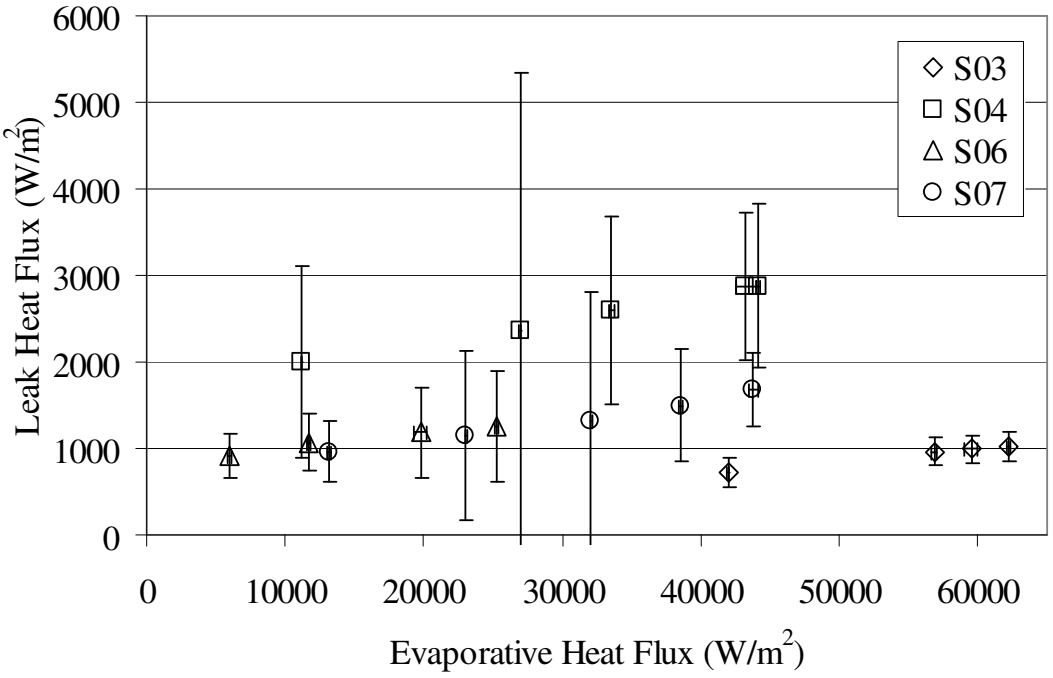

Figure 3-22: Leak v. evaporative heat flux.

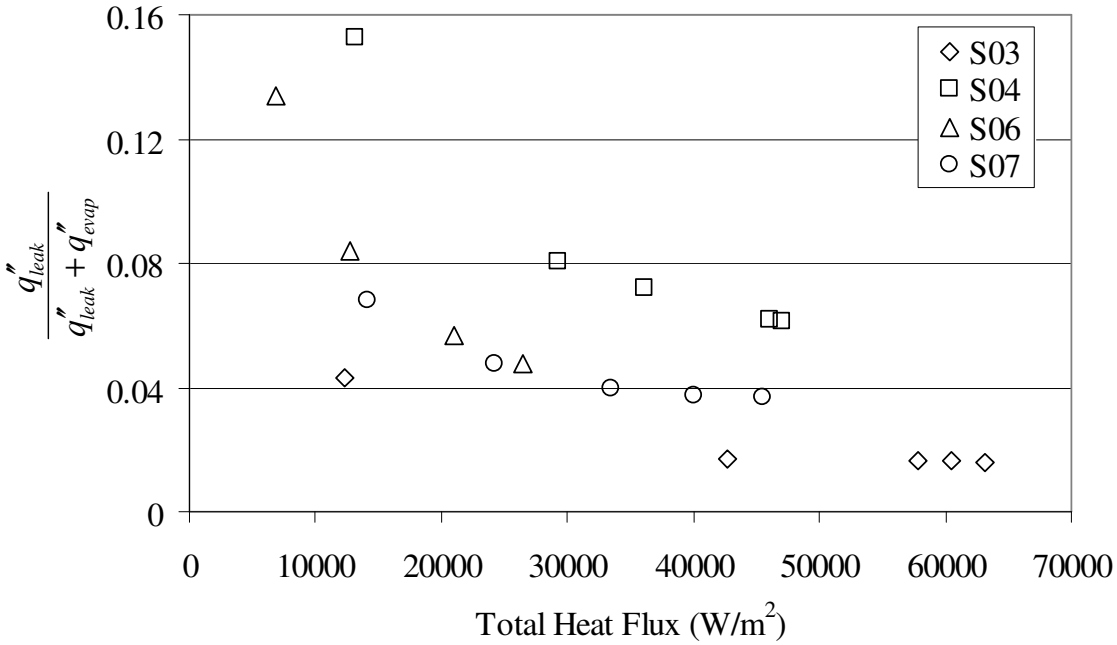

Figure 3-23: Leak heat flux as a fraction of total heat flux.

If the two points with abnormally high uncertainty are discarded, it can be seen that for increasing evaporative power the absolute leak heat flux increases linearly for each sample; however, the heat leak as a percentage of the total dissipated power decreases in a power law fashion approaching a minimum value. If it is assumed that the relationship between heat leak and applied heat flux is in fact linear, then this minimum value is equal to the slope of the linear relationship, determined from

$$\lim_{x\to\infty}\left(\frac{ax+b}{x}\right)=a \tag{35}$$

This relationship must surely break down however, as at some point the applied power will outstrip the ability of the wick to deliver the working fluid to the evaporation zone and dryout will ensue. These results are consistent with those of Iverson et al. [15], and show very similar trends in terms of heat leak fraction of total dissipated power. The results of Ren and Wu [12], who found that heat leak was reduced with increasing conductivity, are at odds with the results presented here. The absolute heat leak and fractional heat leak are each proportional to the effective thermal conductivity and porosity of the wick structure, which are themselves related. Figure 3-24 shows the leak heat flux for a specified evaporative heat flux plotted against the effective thermal conductivity. These results were generated using a linear fit for each data set in Figure 3-22. Specific values of $q"_{evap}$ were used to determine the leak heat flux. Figure 3-25 is a plot of the same data against sample porosity. Performing the same comparison for fractional heat leak gives Figure 3-26 and Figure 3-27:

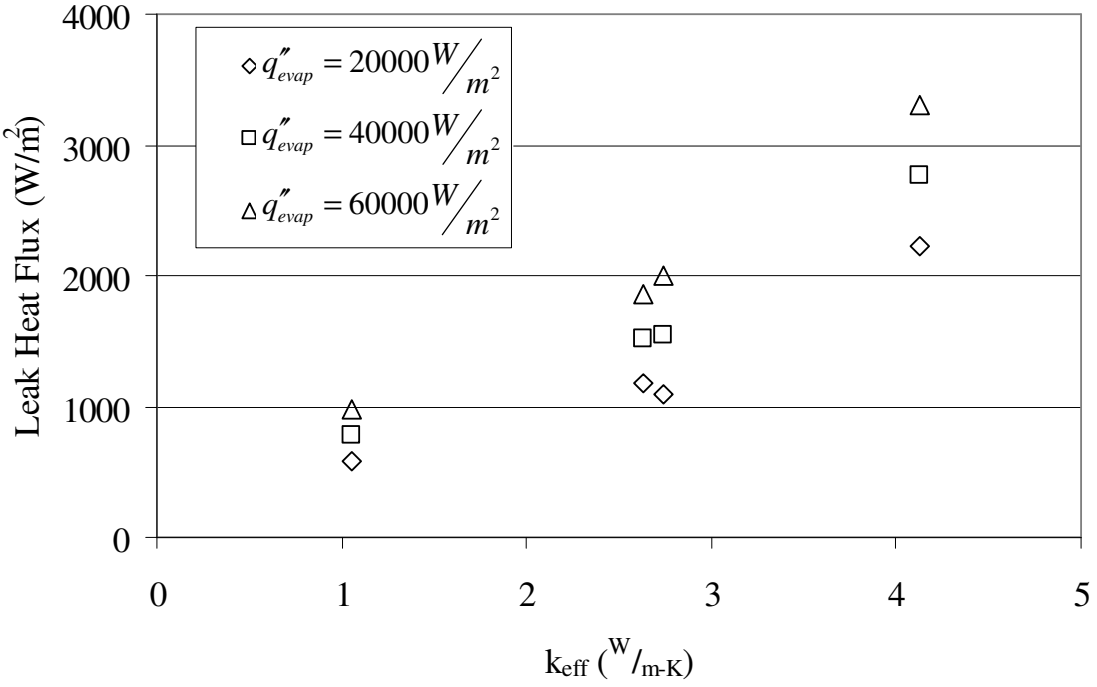

Figure 3-24: Leak heat flux v. effective conductivity

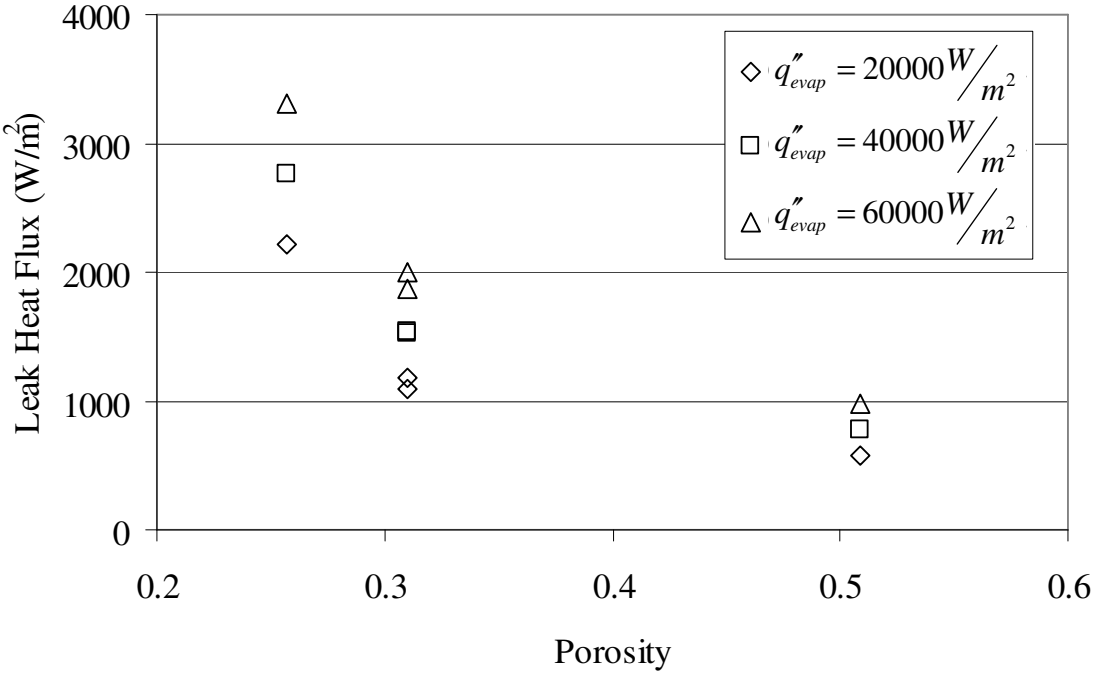

Figure 3-25: Leak heat flux v. sample porosity

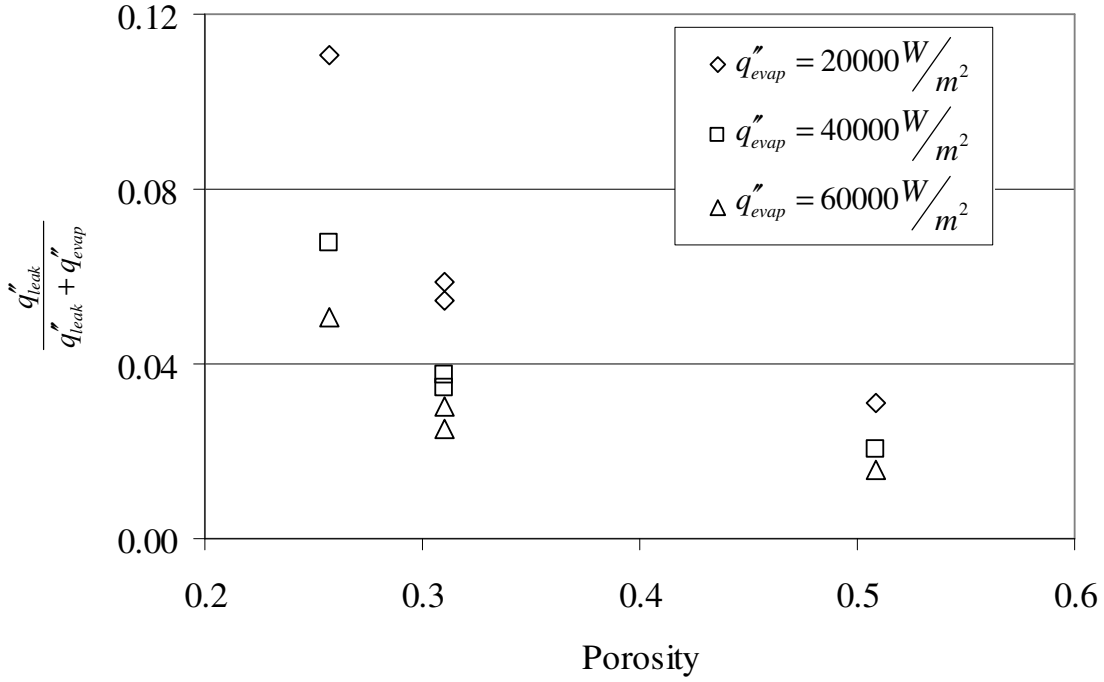

Figure 3-26: Fractional heat leak v. porosity.

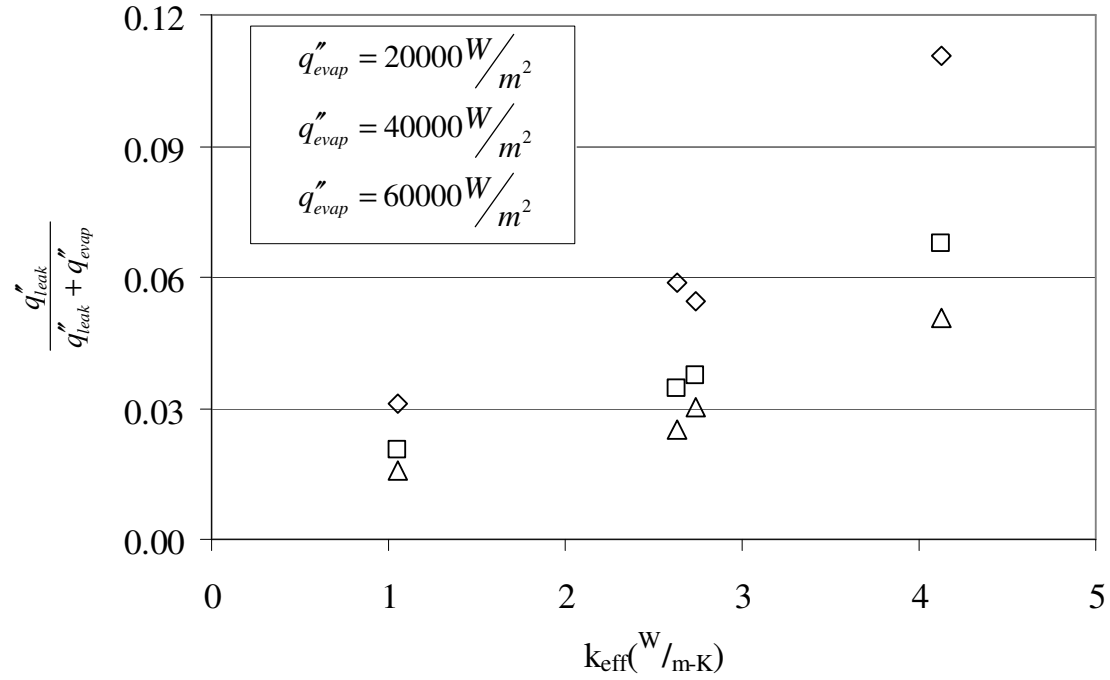

Figure 3-27: Fractional heat leak v. effective conductivity.

CHAPTER FOUR
CONCLUSIONS

Four sintered stainless wick samples were tested for porosity, pore size characterization, effective thermal conductivity, and conductive heat leak with methanol as a working fluid. The goal of the study was to determine the fractional heat leak through each wick for increasing evaporative power levels. The samples were tested in a vertical orientation for heat leak in operation as a capillary wick. In general, the results agreed with the experimental results in the literature [14, 15]. Heat leak was found to vary linearly with evaporative power, while the heat leak fraction of the total dissipated power decreased monotonically in a power law relationship with total dissipated power. For each sample, this fractional loss approached a limit proportional to the sample effective conductivity. This limit was on the order of 1% of the total dissipated power. In certain test results, the uncertainties were very high, in excess of 100% in two cases, due to very small temperature gradients that resulted under the conditions of these points. The trends observed above are based on neglecting these high uncertainty points, although the resulting values fit the trends observed.

With regard to wick properties, porosity, pore size, permeability, and effective thermal conductivity were determined for each sample. Wick porosity was measured using the samples' physical dimensions along with dry and saturated sample mass. Measured porosities fell between 26 and 51%, values which are within the range frequently cited for sintered wicks.

Pore sizes were found to correlate well with the nominal pore size and pores were very narrowly distributed within a size range of approximately 1-10 μm depending on the sample. As no information was available regarding the particle size used in the wick fabrication, comparison to models for pore size was not possible.

The sample permeabilities were measured using a penetrometer to measure the flow rate and pressure of deionized water through the samples. Values between 0.33 x 10^{-12} and 7.14 x 10^{-12} m^2 were measured, values not well-approximated by the frequently cited Blake-Kozeny equation for sintered wicks.

Effective thermal conductivity was measured in vacuum using calibrated stainless steel flux meters, and found to vary linearly with temperature over the range of 300-400K for all samples within the range of 0.7 W/m-K to 3.7 W/m-K in vacuum. Using the correlation put forth by Chi [6] for truncated packed spheres, the conductivity of the samples saturated in methanol was determined. These values ranged from 1.1 W/m-K to 4.1 W/m-K. The models in the literature predicted the effective thermal conductivity to within an order of magnitude for all samples; however, the models did not capture the measured temperature dependence of conductivity and errors of 100% or more were found.

APPENDICES

Appendix A

Thermal Conductivity Calibration Data

Table A-1: Calibration settings.

Point #	Variac (%)	Chiller (^{o}C)
1	5	-15
2	10	-15
3	10	-5
4	15	-5
5	15	5
6	20	5
7	20	15
8	25	15
9	25	25
10	30	25
11	30	35
12	35	35
13	35	45
14	40	45
15	40	55

Table A-2: Average flux meter temperatures in calibration data.

Point #	$T_{low,avg}$ (K)	$T_{up,avg}$ (K)	ΔT (K)
1	278.66	302.04	23.38
2	283.97	316.07	32.10
3	290.43	320.13	29.70
4	299.68	341.40	41.71
5	306.31	345.65	39.35
6	312.24	359.67	47.44
7	319.52	363.64	44.12
8	330.52	390.19	59.67
9	337.12	393.61	56.49
10	344.69	411.76	67.06
11	351.05	413.97	62.92
12	358.51	431.92	73.41
13	365.38	435.10	69.72
14	374.63	457.41	82.78
15	380.69	459.48	78.78

POINT 1

Settings ==> Variac: 5 Chiller -15

	Upper Flux Meter			Calibration Standard			Lower Flux Meter		
Time	TC1	TC2	TC3	TC4	TC9	TC5	TC8	TC12	TC10
10:17:34 AM	33.882	28.774	24.346	18.401	17.209	15.905	10.190	5.614	0.600
10:18:06 AM	33.705	28.826	24.406	18.234	17.201	15.920	10.167	5.409	0.876
10:18:39 AM	32.969	28.828	24.246	18.145	17.240	15.915	10.149	5.469	1.118
10:19:12 AM	32.861	28.798	24.226	18.325	17.257	15.913	10.161	5.575	0.944
10:19:45 AM	33.918	28.806	24.456	18.464	17.186	15.915	10.179	5.416	0.747
10:20:17 AM	33.894	28.806	24.391	18.406	17.201	15.907	10.182	5.393	0.731
10:20:50 AM	33.295	28.783	24.389	18.203	17.214	15.910	10.164	5.484	0.876
10:21:23 AM	33.521	28.791	24.381	18.441	17.222	15.918	10.174	5.456	0.863
10:21:55 AM	33.298	28.830	24.359	18.173	17.232	15.915	10.167	5.385	1.081
10:22:28 AM	33.639	28.761	24.429	18.712	17.214	15.907	10.179	5.664	0.758
Avg:	33.498	28.800	24.363	18.350	17.218	15.913	10.171	5.487	0.859
T (K)	306.648	301.950	297.513	291.500	290.368	289.063	283.321	278.637	274.009
Y (in):	0.000	0.375	0.750	1.625	2.125	2.625	3.500	3.875	4.250
Y (m)	0.000	0.010	0.019	0.041	0.054	0.067	0.089	0.098	0.108

DATA TABLE									
	Upper Flux			**Calibration**			**Lower Flux**		
	dT/dY	-479.543		T Lower	289.063		dT/dY	-488.808	
	Avg. T	302.037		T Upper	291.500		Avg. T	278.656	
	k (W/mK)	15.534		Avg. K	77.610		k (W/mK)	15.239	
				dT/dY	-95.980				
				q" (W/m^2)	**7449.004**				

POINT 2

Settings ==> Variac: 10 Chiller -15

	Upper Flux Meter			Calibration Standard			Lower Flux Meter		
Time	TC1	TC2	TC3	TC4	TC9	TC5	TC8	TC12	TC10
9:07:53 AM	48.854	42.931	36.744	28.040	26.870	25.048	17.151	10.633	4.772
9:08:26 AM	49.146	42.854	36.736	28.612	26.870	25.046	17.179	10.816	4.347
9:08:58 AM	48.611	42.886	36.671	28.414	26.902	25.046	17.146	10.821	4.681
9:09:31 AM	49.520	42.869	36.731	28.630	26.842	25.041	17.199	10.944	4.339
9:10:04 AM	49.465	42.850	36.790	28.736	26.860	25.043	17.201	10.847	4.180
9:10:36 AM	48.977	42.941	36.785	28.315	26.885	25.046	17.166	10.749	4.679
9:11:09 AM	49.104	42.924	36.783	28.347	26.860	25.053	17.171	10.718	4.564
9:11:42 AM	48.854	42.871	36.741	28.528	26.895	25.053	17.179	10.803	4.425
9:12:15 AM	49.035	42.939	36.761	28.325	26.890	25.056	17.173	10.841	4.652
9:12:47 AM	49.648	42.883	36.824	28.573	26.842	25.061	17.214	10.795	4.316
Avg:	49.121	42.895	36.757	28.452	26.872	25.049	17.178	10.797	4.496
T (K)	322.271	316.045	309.907	301.602	300.022	298.199	290.328	283.947	277.646
Y (in):	0.000	0.375	0.750	1.625	2.125	2.625	3.500	3.875	4.250
Y (m)	0.000	0.010	0.019	0.041	0.054	0.067	0.089	0.098	0.108

DATA TABLE									
Upper Flux				**Calibration**			**Lower Flux**		
	dT/dY	-649.071		T Lower	298.199		dT/dY	-665.743	
	Avg. T	316.074		T Upper	301.602		Avg. T	283.973	
	k (W/mK)	15.827		Avg. K	76.683		k (W/mK)	15.431	
				dT/dY	-133.965				
				q" (W/m^2)	**10272.773**				

POINT 3

Settings ==> Variac: 10 Chiller -5

	Upper Flux Meter			Calibration Standard			Lower Flux Meter		
Time	TC1	TC2	TC3	TC4	TC9	TC5	TC8	TC12	TC10
9:55:53 AM	52.517	46.930	41.193	33.551	32.035	30.374	23.129	17.389	11.441
9:56:26 AM	52.503	46.988	41.222	33.173	32.018	30.369	23.094	17.207	11.634
9:56:59 AM	52.292	46.981	41.145	33.183	32.040	30.374	23.097	17.252	11.688
9:57:32 AM	53.081	46.918	41.212	33.683	32.010	30.366	23.140	17.275	11.320
9:58:04 AM	52.975	46.976	41.304	33.288	31.988	30.374	23.122	17.196	11.536
9:58:37 AM	52.779	46.930	41.147	33.666	32.035	30.371	23.127	17.293	11.310
9:59:10 AM	52.984	47.000	41.309	33.352	32.000	30.376	23.114	17.176	11.546
9:59:42 AM	53.192	46.928	41.350	33.798	31.995	30.371	23.142	17.278	11.227
10:00:15 AM	52.418	46.918	41.034	33.509	32.047	30.366	23.114	17.354	11.505
10:00:48 AM	53.121	46.904	41.227	33.695	32.008	30.366	23.140	17.232	11.292
Avg:	52.786	46.947	41.214	33.490	32.018	30.371	23.122	17.265	11.450
T (K)	325.936	320.097	314.364	306.640	305.168	303.521	296.272	290.415	284.600
Y (in):	0.000	0.375	0.750	1.625	2.125	2.625	3.500	3.875	4.250
Y (m)	0.000	0.010	0.019	0.041	0.054	0.067	0.089	0.098	0.108

DATA TABLE

Upper Flux			**Calibration**			**Lower Flux**		
	dT/dY	-607.449	T Lower	303.521		dT/dY	-612.703	
	Avg. T	320.133	T Upper	306.640		Avg. T	290.429	
	k (W/mK)	15.402	Avg. K	76.188		k (W/mK)	15.270	
			dT/dY	-122.799				
			q" (W/m^2)	**9355.851**				

POINT 4

Settings ==> Variac: 15 Chiller -5

	Upper Flux Meter			Calibration Standard			Lower Flux Meter		
Time	TC1	TC2	TC3	TC4	TC9	TC5	TC8	TC12	TC10
6:55:59 AM	76.170	68.269	60.198	49.351	47.243	44.870	34.692	26.489	18.504
6:56:31 AM	76.242	68.282	60.228	49.237	47.246	44.861	34.678	26.534	18.484
6:57:04 AM	76.425	68.230	60.265	49.544	47.226	44.861	34.702	26.604	18.218
6:57:37 AM	76.186	68.214	60.142	49.570	47.250	44.863	34.697	26.574	18.363
6:58:09 AM	75.887	68.280	60.277	49.056	47.241	44.863	34.670	26.472	18.560
6:58:42 AM	76.211	68.276	60.291	49.182	47.210	44.858	34.680	26.529	18.461
6:59:15 AM	76.437	68.248	60.384	49.391	47.215	44.851	34.687	26.516	18.236
6:59:48 AM	76.281	68.292	60.258	49.215	47.236	44.856	34.675	26.516	18.426
7:00:20 AM	76.156	68.241	60.202	49.234	47.210	44.861	34.687	26.584	18.317
7:00:53 AM	76.346	68.253	60.240	49.313	47.224	44.846	34.692	26.417	18.335
Avg:	76.234	68.259	60.249	49.309	47.230	44.859	34.686	26.524	18.390
T (K)	349.384	341.409	333.399	322.459	320.380	318.009	307.836	299.674	291.540
Y (in):	0.000	0.375	0.750	1.625	2.125	2.625	3.500	3.875	4.250
Y (m)	0.000	0.010	0.019	0.041	0.054	0.067	0.089	0.098	0.108

DATA TABLE

Upper Flux			**Calibration**			**Lower Flux**		
	dT/dY	-839.139	T Lower	318.009		dT/dY	-855.412	
	Avg. T	341.397	T Upper	322.459		Avg. T	299.683	
	k (W/mK)	15.609	Avg. K	74.759		k (W/mK)	15.312	
			dT/dY	-175.209				
			q" (W/m^2)	**13098.489**				

POINT 5

Settings ==> Variac: 15 Chiller 5

	Upper Flux Meter			Calibration Standard			Lower Flux Meter		
Time	TC1	TC2	TC3	TC4	TC9	TC5	TC8	TC12	TC10
9:29:37 AM	79.653	72.561	64.927	54.488	52.659	50.336	40.739	33.114	25.667
9:30:10 AM	80.060	72.600	65.077	54.213	52.607	50.336	40.753	33.001	25.669
9:30:42 AM	80.531	72.522	65.054	54.839	52.614	50.344	40.787	33.106	25.308
9:31:15 AM	79.974	72.559	64.957	54.752	52.654	50.341	40.756	33.239	25.575
9:31:48 AM	80.051	72.586	64.948	54.479	52.644	50.336	40.765	33.062	25.582
9:32:21 AM	79.761	72.577	64.948	54.514	52.670	50.336	40.753	33.153	25.689
9:32:53 AM	79.758	72.531	64.906	54.879	52.680	50.334	40.753	33.200	25.552
9:33:26 AM	79.801	72.525	64.897	54.860	52.668	50.336	40.756	33.217	25.582
9:33:59 AM	80.630	72.550	65.066	54.780	52.614	50.332	40.794	33.114	25.323
9:34:31 AM	79.655	72.579	64.902	54.528	52.663	50.336	40.732	33.200	25.714
Avg:	79.987	72.559	64.968	54.633	52.647	50.337	40.759	33.141	25.566
T (K)	353.137	345.709	338.118	327.783	325.797	323.487	313.909	306.291	298.716
Y (in):	0.000	0.375	0.750	1.625	2.125	2.625	3.500	3.875	4.250
Y (m)	0.000	0.010	0.019	0.041	0.054	0.067	0.089	0.098	0.108

DATA TABLE

Upper Flux			**Calibration**			**Lower Flux**		
	dT/dY	-788.409		T Lower	323.487		dT/dY	-797.517
	Avg. T	345.655		T Upper	327.783		Avg. T	306.305
	k (W/mK)	15.932		Avg. K	74.257		k (W/mK)	15.750
				dT/dY	-169.154			
				q" (W/m^2)	**12560.783**			

POINT6

Settings ==> Variac: 20 Chiller 5

	Upper Flux Meter			Calibration Standard			Lower Flux Meter		
Time	TC1	TC2	TC3	TC4	TC9	TC5	TC8	TC12	TC10
12:19:48 PM	95.897	86.590	77.607	64.705	62.505	59.760	48.249	39.029	29.800
12:20:21 PM	95.329	86.553	77.415	64.996	62.556	59.769	48.230	39.179	29.909
12:20:53 PM	96.030	86.575	77.591	64.987	62.519	59.764	48.261	39.046	29.768
12:21:26 PM	95.231	86.584	77.497	64.805	62.554	59.778	48.228	39.051	30.072
12:21:59 PM	95.176	86.588	77.456	64.802	62.570	59.769	48.230	39.015	30.223
12:22:32 PM	96.074	86.559	77.621	65.017	62.517	59.778	48.276	39.027	29.795
12:23:04 PM	95.877	86.533	77.463	65.204	62.551	59.778	48.268	39.158	29.684
12:23:37 PM	95.332	86.542	77.388	65.061	62.568	59.771	48.252	39.182	29.922
12:24:10 PM	95.150	86.597	77.379	64.682	62.568	59.778	48.242	39.044	30.119
12:24:42 PM	95.113	86.568	77.408	64.842	62.568	59.771	48.240	39.049	30.117
Avg:	95.521	86.569	77.483	64.910	62.548	59.772	48.248	39.078	29.941
T (K)	368.671	359.719	350.633	338.060	335.698	332.922	321.398	312.228	303.091
Y (in):	0.000	0.375	0.750	1.625	2.125	2.625	3.500	3.875	4.250
Y (m)	0.000	0.010	0.019	0.041	0.054	0.067	0.089	0.098	0.108

DATA TABLE

Upper Flux			**Calibration**			**Lower Flux**		
	dT/dY	-946.898		T Lower	332.922		dT/dY	-960.982
	Avg. T	359.674		T Upper	338.060		Avg. T	312.239
	k (W/mK)	15.671		Avg. K	73.348		k (W/mK)	15.441
				dT/dY	-202.303			
				q" (W/m^2)	**14838.580**			

POINT 7

Settings ==> Variac: 20 Chiller: 15

	Upper Flux Meter			Calibration Standard			Lower Flux Meter		
Time	TC1	TC2	TC3	TC4	TC9	TC5	TC8	TC12	TC10
10:42:14 AM	99.164	90.382	81.996	70.499	68.023	65.444	54.820	46.445	37.844
10:42:47 AM	98.734	90.393	81.920	70.492	68.048	65.446	54.801	46.479	37.890
10:43:19 AM	99.312	90.413	82.101	70.316	68.016	65.453	54.850	46.295	37.895
10:43:52 AM	98.789	90.382	81.927	70.497	68.048	65.449	54.808	46.448	37.941
10:44:25 AM	98.512	90.450	81.958	69.950	68.046	65.449	54.773	46.319	38.209
10:44:58 AM	99.309	90.402	82.052	70.355	68.007	65.439	54.848	46.335	37.800
10:45:30 AM	99.307	90.408	82.092	70.314	68.007	65.444	54.839	46.345	37.824
10:46:03 AM	98.845	90.388	81.850	70.554	68.067	65.444	54.813	46.472	37.900
10:46:36 AM	99.323	90.483	82.086	70.216	68.019	65.442	54.825	46.314	38.024
10:47:08 AM	99.318	90.441	82.070	70.179	68.007	65.446	54.853	46.304	37.927
Avg:	99.061	90.414	82.005	70.337	68.029	65.446	54.823	46.376	37.925
T (K)	372.211	363.564	355.155	343.487	341.179	338.596	327.973	319.526	311.075
Y (in):	0.000	0.375	0.750	1.625	2.125	2.625	3.500	3.875	4.250
Y (m)	0.000	0.010	0.019	0.041	0.054	0.067	0.089	0.098	0.108

DATA TABLE									
Upper Flux			**Calibration**			**Lower Flux**			
	dT/dY	-895.333		T Lower	338.596		dT/dY	-887.013	
	Avg. T	363.644		T Upper	343.487		Avg. T	319.525	
	k (W/mK)	15.668		Avg. K	72.842		k (W/mK)	15.815	
				dT/dY	-192.583				
				q" (W/m^2)	**14028.041**				

POINT 8

Settings ==> Variac: 25 Chiller 15

	Upper Flux Meter			Calibration Standard			Lower Flux Meter		
Time	TC1	TC2	TC3	TC4	TC9	TC5	TC8	TC12	TC10
9:16:25 AM	128.563	117.107	105.845	89.732	86.717	83.157	68.750	57.260	46.072
9:16:58 AM	128.303	117.020	105.692	90.147	86.739	83.160	68.755	57.443	45.888
9:17:30 AM	127.867	117.090	105.729	89.582	86.755	83.162	68.707	57.291	46.235
9:18:03 AM	128.545	117.015	105.735	90.254	86.730	83.162	68.766	57.457	45.816
9:18:36 AM	127.931	117.075	105.675	89.865	86.762	83.160	68.716	57.420	46.151
9:19:08 AM	128.098	117.056	105.658	89.944	86.746	83.164	68.723	57.347	46.039
9:19:41 AM	128.123	117.060	105.699	89.811	86.739	83.166	68.741	57.342	46.024
9:20:14 AM	128.146	117.085	105.740	89.743	86.739	83.162	68.732	57.305	46.132
9:20:47 AM	128.732	117.062	105.826	89.984	86.717	83.162	68.766	57.305	45.824
9:21:19 AM	128.749	117.058	105.850	90.015	86.715	83.171	68.796	57.307	45.888
Avg:	128.306	117.063	105.745	89.908	86.736	83.163	68.745	57.348	46.007
T (K)	401.456	390.213	378.895	363.058	359.886	356.313	341.895	330.498	319.157
Y (in):	0.000	0.375	0.750	1.625	2.125	2.625	3.500	3.875	4.250
Y (m)	0.000	0.010	0.019	0.041	0.054	0.067	0.089	0.098	0.108

DATA TABLE									
Upper Flux			**Calibration**			**Lower Flux**			
	dT/dY	-1184.294		T Lower	356.313		dT/dY	-1193.612	
	Avg. T	390.188		T Upper	363.058		Avg. T	330.517	
	k (W/mK)	15.958		Avg. K	71.167		k (W/mK)	15.833	
				dT/dY	-265.555				
				q" (W/m^2)	**18898.700**				

POINT 9

Settings ==> Variac: 25 Chiller 25

	Upper Flux Meter			Calibration Standard			Lower Flux Meter		
Time	TC1	TC2	TC3	TC4	TC9	TC5	TC8	TC12	TC10
10:40:08 AM	131.548	120.462	109.780	94.856	91.622	88.251	74.675	64.084	53.058
10:40:41 AM	131.519	120.458	109.780	94.814	91.613	88.253	74.672	64.028	53.043
10:41:14 AM	131.053	120.466	109.598	94.856	91.648	88.249	74.625	64.042	53.348
10:41:46 AM	131.169	120.521	109.795	94.351	91.626	88.244	74.634	63.878	53.447
10:42:19 AM	131.433	120.447	109.727	94.904	91.624	88.233	74.643	64.031	53.128
10:42:52 AM	130.779	120.508	109.720	94.424	91.639	88.240	74.602	63.975	53.525
10:43:24 AM	130.864	120.479	109.684	94.466	91.637	88.233	74.616	63.964	53.473
10:43:57 AM	131.581	120.471	109.806	94.773	91.600	88.235	74.650	63.832	53.192
10:44:30 AM	130.887	120.502	109.746	94.367	91.628	88.229	74.598	63.880	53.555
10:45:03 AM	130.987	120.460	109.630	94.602	91.620	88.226	74.618	64.047	53.267
Avg:	131.182	120.477	109.727	94.641	91.626	88.239	74.633	63.976	53.304
T (K)	404.332	393.627	382.877	367.791	364.776	361.389	347.783	337.126	326.454
Y (in):	0.000	0.375	0.750	1.625	2.125	2.625	3.500	3.875	4.250
Y (m)	0.000	0.010	0.019	0.041	0.054	0.067	0.089	0.098	0.108

DATA TABLE

Upper Flux			**Calibration**			**Lower Flux**		
	dT/dY	-1126.268	T Lower	361.389		dT/dY	-1119.669	
	Avg. T	393.612	T Upper	367.791		Avg. T	337.121	
	k (W/mK)	15.829	Avg. K	70.733		k (W/mK)	15.923	
			dT/dY	-252.047				
			q" (W/m^2)	**17828.029**				

POINT 10

Settings ==> Variac: 30 Chiller 25

	Upper Flux Meter			Calibration Standard			Lower Flux Meter		
Time	TC1	TC2	TC3	TC4	TC9	TC5	TC8	TC12	TC10
1:28:48 AM	150.973	138.618	125.967	108.090	104.471	100.369	84.183	71.558	58.946
1:29:21 AM	151.243	138.649	126.002	108.135	104.464	100.376	84.223	71.551	58.857
1:29:53 AM	151.018	138.622	125.950	108.072	104.473	100.373	84.201	71.549	58.916
1:30:26 AM	151.168	138.641	125.914	108.105	104.464	100.376	84.210	71.599	58.906
1:30:59 AM	151.210	138.631	125.969	108.154	104.467	100.373	84.210	71.611	58.869
1:31:31 AM	151.554	138.606	126.050	108.264	104.441	100.378	84.250	71.549	58.631
1:32:04 AM	151.595	138.614	126.025	108.283	104.449	100.382	84.250	71.577	58.654
1:32:37 AM	150.613	138.639	125.822	108.152	104.516	100.382	84.185	71.688	59.021
1:33:10 AM	151.176	138.678	126.076	107.838	104.473	100.376	84.203	71.442	59.086
1:33:42 AM	151.558	138.608	126.071	108.380	104.454	100.389	84.256	71.522	58.635
Avg:	151.211	138.631	125.985	108.147	104.467	100.377	84.217	71.565	58.852
T (K)	424.361	411.781	399.135	381.297	377.617	373.527	357.367	344.715	332.002
Y (in):	0.000	0.375	0.750	1.625	2.125	2.625	3.500	3.875	4.250
Y (m)	0.000	0.010	0.019	0.041	0.054	0.067	0.089	0.098	0.108

DATA TABLE

Upper Flux			**Calibration**			**Lower Flux**		
	dT/dY	-1324.210	T Lower	373.527		dT/dY	-1331.496	
	Avg. T	411.759	T Upper	381.297		Avg. T	344.695	
	k (W/mK)	16.081	Avg. K	69.612		k (W/mK)	15.993	
			dT/dY	-305.902				
			q" (W/m^2)	**21294.493**				

POINT 11

Settings ==> Variac: 30 Chiller 35

	Upper Flux Meter			Calibration Standard			Lower Flux Meter		
Time	TC1	TC2	TC3	TC4	TC9	TC5	TC8	TC12	TC10
12:26:48 PM	152.476	140.828	128.885	112.080	108.650	104.750	89.643	77.840	66.161
12:27:21 PM	152.713	140.849	128.928	112.095	108.650	104.752	89.628	77.932	66.172
12:27:53 PM	152.658	140.830	128.889	112.069	108.648	104.756	89.639	77.928	66.170
12:28:26 PM	152.854	140.837	128.949	112.092	108.609	104.754	89.628	77.921	66.096
12:28:59 PM	152.599	140.882	128.905	111.746	108.631	104.756	89.632	77.819	66.308
12:29:32 PM	152.577	140.886	128.947	111.702	108.627	104.756	89.617	77.779	66.352
12:30:04 PM	152.114	140.839	128.812	112.144	108.676	104.756	89.637	77.970	66.223
12:30:37 PM	153.123	140.896	129.001	111.984	108.624	104.754	89.643	77.720	66.193
12:31:10 PM	153.054	140.822	128.943	112.310	108.622	104.758	89.674	77.923	65.831
12:31:42 PM	152.559	140.898	128.941	111.817	108.644	104.752	89.624	77.831	66.324
Avg:	152.673	140.857	128.920	112.004	108.638	104.754	89.637	77.866	66.183
T (K)	425.823	414.007	402.070	385.154	381.788	377.904	362.787	351.016	339.333
Y (in):	0.000	0.375	0.750	1.625	2.125	2.625	3.500	3.875	4.250
Y (m)	0.000	0.010	0.019	0.041	0.054	0.067	0.089	0.098	0.108

DATA TABLE									
Upper Flux			**Calibration**			**Lower Flux**			
	dT/dY	-1246.861		T Lower	377.904		dT/dY	-1231.155	
	Avg. T	413.966		T Upper	385.154		Avg. T	351.045	
	k (W/mK)	15.853		Avg. K	69.256		k (W/mK)	16.055	
				dT/dY	-285.413				
				q" (W/m^2)	**19766.727**				

POINT 12

Settings ==> Variac: 35 Chiller 35

	Upper Flux Meter			Calibration Standard			Lower Flux Meter		
Time	TC1	TC2	TC3	TC4	TC9	TC5	TC8	TC12	TC10
9:24:53 AM	172.589	158.852	145.093	125.420	121.379	116.793	99.113	85.304	71.720
9:25:25 AM	172.508	158.814	145.028	125.640	121.383	116.795	99.127	85.384	71.579
9:25:58 AM	172.534	158.806	145.054	125.630	121.373	116.782	99.122	85.393	71.609
9:26:31 AM	172.577	158.806	145.050	125.487	121.354	116.774	99.098	85.266	71.688
9:27:04 AM	171.849	158.812	144.975	125.336	121.390	116.772	99.083	85.469	71.764
9:27:36 AM	172.641	158.828	145.048	125.322	121.335	116.770	99.087	85.157	71.695
9:28:09 AM	172.459	158.752	144.962	125.657	121.352	116.759	99.118	85.529	71.442
9:28:42 AM	172.812	158.792	145.107	125.433	121.316	116.755	99.094	85.271	71.590
9:29:14 AM	171.976	158.802	145.001	125.148	121.347	116.748	99.037	85.280	71.898
9:29:47 AM	172.781	158.748	145.075	125.559	121.303	116.746	99.098	85.282	71.428
Avg:	172.473	158.801	145.039	125.463	121.353	116.769	99.098	85.334	71.641
T (K)	445.623	431.951	418.189	398.613	394.503	389.919	372.248	358.484	344.791
Y (in):	0.000	0.375	0.750	1.625	2.125	2.625	3.500	3.875	4.250
Y (m)	0.000	0.010	0.019	0.041	0.054	0.067	0.089	0.098	0.108

DATA TABLE									
Upper Flux			**Calibration**			**Lower Flux**			
	dT/dY	-1440.068		T Lower	389.919		dT/dY	-1441.281	
	Avg. T	431.921		T Upper	398.613		Avg. T	358.508	
	k (W/mK)	16.202		Avg. K	68.169		k (W/mK)	16.189	
				dT/dY	-342.276				
				q" (W/m^2)	**23332.466**				

POINT 13

Settings ==> Variac: 35 Chiller 45

	Upper Flux Meter			Calibration Standard			Lower Flux Meter		
Time	TC1	TC2	TC3	TC4	TC9	TC5	TC8	TC12	TC10
10:19:09 AM	175.378	162.076	148.916	130.201	126.281	121.899	105.162	92.215	79.185
10:19:41 AM	175.317	162.092	148.912	130.151	126.276	121.899	105.162	92.221	79.194
10:20:14 AM	174.551	162.092	148.839	130.128	126.308	121.897	105.108	92.254	79.475
10:20:47 AM	174.744	162.070	148.892	130.415	126.306	121.887	105.116	92.366	79.360
10:21:19 AM	175.440	162.110	148.936	130.128	126.266	121.891	105.157	92.148	79.194
10:21:52 AM	174.510	162.094	148.798	130.192	126.316	121.891	105.099	92.263	79.522
10:22:25 AM	174.538	162.102	148.843	130.117	126.310	121.887	105.099	92.252	79.464
10:22:58 AM	175.260	162.052	148.831	130.436	126.266	121.884	105.147	92.272	78.993
10:23:30 AM	174.510	162.076	148.756	130.284	126.316	121.882	105.093	92.382	79.464
10:24:03 AM	174.789	162.058	148.849	130.377	126.293	121.876	105.123	92.294	79.149
Avg:	174.904	162.082	148.857	130.243	126.294	121.889	105.127	92.267	79.300
T (K)	448.054	435.232	422.007	403.393	399.444	395.039	378.277	365.417	352.450
Y (in):	0.000	0.375	0.750	1.625	2.125	2.625	3.500	3.875	4.250
Y (m)	0.000	0.010	0.019	0.041	0.054	0.067	0.089	0.098	0.108

DATA TABLE

Upper Flux			**Calibration**			**Lower Flux**		
	dT/dY	-1367.270	T Lower	395.039		dT/dY	-1355.727	
	Avg. T	435.098	T Upper	403.393		Avg. T	365.381	
	k (W/mK)	16.297	Avg. K	67.751		k (W/mK)	16.436	
			dT/dY	-328.882				
			q" (W/m^2)	**22282.080**				

POINT 14

Settings ==> Variac: 40 Chiller 45

	Upper Flux Meter			Calibration Standard			Lower Flux Meter		
Time	TC1	TC2	TC3	TC4	TC9	TC5	TC8	TC12	TC10
9:34:58 AM	199.997	184.398	169.012	146.998	142.029	136.692	116.810	101.429	85.801
9:35:31 AM	199.136	184.453	168.913	146.639	142.072	136.699	116.736	101.472	86.426
9:36:03 AM	199.900	184.427	168.970	146.871	142.042	136.694	116.786	101.366	85.977
9:36:36 AM	199.770	184.422	168.990	146.817	142.050	136.694	116.774	101.451	86.181
9:37:09 AM	199.812	184.435	169.030	146.719	142.029	136.694	116.776	101.353	86.128
9:37:42 AM	199.048	184.441	168.858	146.650	142.072	136.699	116.736	101.479	86.373
9:38:14 AM	199.038	184.424	168.867	146.790	142.081	136.686	116.729	101.537	86.344
9:38:47 AM	199.023	184.412	168.861	146.861	142.085	136.692	116.742	101.585	86.326
9:39:20 AM	199.216	184.435	168.913	146.644	142.072	136.686	116.736	101.416	86.439
9:39:52 AM	199.255	184.443	168.911	146.605	142.070	136.692	116.740	101.344	86.339
Avg:	199.420	184.429	168.933	146.759	142.060	136.693	116.757	101.443	86.233
T (K)	472.570	457.579	442.083	419.909	415.210	409.843	389.907	374.593	359.383
Y (in):	0.000	0.375	0.750	1.625	2.125	2.625	3.500	3.875	4.250
Y (m)	0.000	0.010	0.019	0.041	0.054	0.067	0.089	0.098	0.108

DATA TABLE

Upper Flux			**Calibration**			**Lower Flux**		
	dT/dY	-1600.367	T Lower	409.843		dT/dY	-1602.262	
	Avg. T	457.410	T Upper	419.909		Avg. T	374.628	
	k (W/mK)	16.456	Avg. K	66.449		k (W/mK)	16.436	
			dT/dY	-396.323				
			q" (W/m^2)	**26335.230**				

POINT 15

Settings ==> Variac: 40 Chiller 55

	Upper Flux Meter			Calibration Standard			Lower Flux Meter		
Time	TC1	TC2	TC3	TC4	TC9	TC5	TC8	TC12	TC10
11:30:56 AM	201.057	186.385	171.569	150.743	145.971	140.808	121.962	107.761	92.965
11:31:29 AM	201.185	186.439	171.650	150.455	145.945	140.810	121.960	107.374	93.079
11:32:01 AM	200.405	186.447	171.563	150.364	145.984	140.810	121.920	107.608	93.444
11:32:34 AM	200.982	186.467	171.650	150.340	145.959	140.808	121.933	107.415	93.277
11:33:07 AM	200.606	186.418	171.543	150.589	145.986	140.812	121.948	107.649	93.139
11:33:39 AM	200.839	186.439	171.632	150.475	145.957	140.810	121.948	107.546	93.033
11:34:12 AM	201.038	186.451	171.644	150.546	145.969	140.812	121.950	107.505	93.068
11:34:45 AM	201.175	186.439	171.747	150.461	145.947	140.818	121.964	107.413	93.060
11:35:18 AM	200.900	186.461	171.687	150.295	145.959	140.820	121.950	107.426	93.172
11:35:50 AM	200.877	186.455	171.624	150.370	145.965	140.824	121.952	107.580	93.229
Avg:	200.906	186.440	171.631	150.464	145.964	140.813	121.949	107.528	93.147
T (K)	474.056	459.590	444.781	423.614	419.114	413.963	395.099	380.678	366.297
Y (in):	0.000	0.375	0.750	1.625	2.125	2.625	3.500	3.875	4.250
Y (m)	0.000	0.010	0.019	0.041	0.054	0.067	0.089	0.098	0.108

DATA TABLE									
Upper Flux			**Calibration**			**Lower Flux**			
	dT/dY	-1536.772		T Lower	413.963		dT/dY	-1511.921	
	Avg. T	459.476		T Upper	423.614		Avg. T	380.691	
	k (W/mK)	16.349		Avg. K	66.128		k (W/mK)	16.618	
				dT/dY	-379.945				
				q" (W/m^2)	**25125.023**				

Appendix B1

S03 Effective Conductivity Data

S03	Chiller:	-5	Variac:	10		
	Sample Thickness:		2.00E-03	m		
Y Stations:	0	0.375	0.75			
	0	0.009525	0.01905	4.01E-02	0.049625	0.05915

	Upper Flux Meter			Lower Flux Meter		
Time	TC6	TC7	TC8	TC2	TC3	TC4
12:31:10 PM	57.417	52.918	48.495	20.017	14.855	10.446
12:31:42 PM	57.417	52.921	48.466	20.006	14.870	10.437
12:32:14 PM	57.424	52.859	48.190	19.726	14.931	10.079
12:32:46 PM	57.417	52.888	48.128	19.639	14.985	10.151
12:33:18 PM	57.420	52.840	48.335	19.925	14.819	10.075
12:33:50 PM	57.424	52.831	48.245	19.810	14.834	10.059
12:34:22 PM	57.424	52.923	48.361	19.834	14.873	10.409
12:34:54 PM	57.429	52.897	48.487	20.011	14.794	10.332
12:35:26 PM	57.429	52.857	48.383	20.006	14.681	10.207
12:35:58 PM	57.434	52.914	48.478	20.016	14.763	10.399

Average:	57.424	52.885	48.357	19.899	14.841	10.259
	332.574	328.035	323.507	295.049	289.991	285.409

y	T
0.00000	330.574
0.00953	326.035
0.01905	321.507
0.02858	316.972
0.03058	297.789
0.04010	293.049
0.04963	287.991
0.05915	283.409

kupper	15.61561
klower	15.31394

dTdyupper	-475.9423
dTdylower	-506.021

qhigh	7432.127
qlow	7749.178
qavg	7590.652
Tavg	307.3805
ksamp	0.79142

Figure B1-1

S03	Chiller:	5	Variac:	20		
	Sample Thickness:		2.00E-03	m		
Y Stations:	0	0.375	0.75			
	0	0.009525	0.01905	4.01E-02	0.049625	0.05915

	Upper Flux Meter			Lower Flux Meter		
Time	TC6	TC7	TC8	TC2	TC3	TC4
12:54:22 PM	99.196	92.135	84.867	42.194	34.956	27.595
12:54:54 PM	99.190	92.078	84.972	42.375	34.920	27.223
12:55:26 PM	99.174	92.144	84.874	42.014	34.952	27.615
12:55:58 PM	99.170	92.153	85.137	42.676	34.824	27.886
12:56:30 PM	99.177	92.113	84.798	41.825	34.961	27.272
12:57:03 PM	99.177	92.096	84.823	41.973	34.952	27.282
12:57:35 PM	99.179	92.091	84.870	42.163	34.895	27.277
12:58:07 PM	99.177	92.126	85.052	42.573	34.763	27.628
12:58:39 PM	99.198	92.140	85.044	42.519	34.925	27.598
12:59:11 PM	99.194	92.122	85.012	42.479	34.927	27.672

Average:	99.183	92.120	84.945	42.279	34.908	27.505
	374.333	367.270	360.095	317.429	310.058	302.655

y	T
0.00000	372.333
0.00953	365.270
0.01905	358.095
0.02858	350.994
0.03058	322.821
0.04010	315.429
0.04963	308.058
0.05915	300.655

kupper	15.82726
klower	15.57261

dTdyupper	-747.4173
dTdylower	-775.5538

qhigh	11829.57
qlow	12077.4
qavg	11953.48
Tavg	336.9079
ksamp	0.84858

Figure B1-2

S03	Chiller:	20	Variac:	35		
	Sample Thickness:		2.00E-03	m		
Y Stations:	0	0.375	0.75			
	0	0.009525	0.01905	4.01E-02	0.049625	0.05915

	Upper Flux Meter			Lower Flux Meter		
Time	TC6	TC7	TC8	TC2	TC3	TC4
5:17:59 PM	174.577	161.646	148.520	86.644	73.871	59.990
5:18:31 PM	174.579	161.666	148.551	86.762	73.819	60.121
5:19:03 PM	174.581	161.650	148.603	86.777	73.814	60.021
5:19:35 PM	174.591	161.608	148.642	87.252	73.669	59.697
5:20:07 PM	174.589	161.644	148.662	86.810	73.876	60.116
5:20:39 PM	174.591	161.648	148.551	86.710	73.880	59.869
5:21:11 PM	174.587	161.650	148.882	87.665	73.573	60.363
5:21:43 PM	174.581	161.666	148.585	86.659	73.926	59.951
5:22:15 PM	174.589	161.632	148.477	86.642	73.935	59.564
5:22:47 PM	174.587	161.622	148.847	87.670	73.587	60.275

Average:	174.585	161.643	148.632	86.959	73.795	59.997
	449.735	436.793	423.782	362.109	348.945	335.147

y	T
0.00000	447.735
0.00953	434.793
0.01905	421.782
0.02858	408.817
0.03058	373.696
0.04010	360.109
0.04963	346.945
0.05915	333.147

kupper	16.20276
klower	16.07554

dTdyupper	-1362.373
dTdylower	-1415.349

qhigh	22074.2
qlow	22752.5
qavg	22413.35
Tavg	391.2565
ksamp	1.276353

Figure B1-3

Appendix B2

S04 Effective Conductivity Data

S04	Chiller:	-5	Variac:	10		
	Sample Thickness:		1.63E-03	m		
Y Stations:	0	0.375	0.75			
	0	0.009525	0.01905	3.97E-02	0.049255	0.05878

	Upper Flux Meter			Lower Flux Meter		
Time	TC6	TC7	TC8	TC2	TC3	TC4
8:28:12 AM	50.769	45.117	39.344	23.926	18.272	12.389
8:28:43 AM	50.797	45.110	39.516	23.941	18.292	12.455
8:29:14 AM	50.637	45.187	39.301	23.933	18.163	12.132
8:29:45 AM	50.663	45.175	39.347	23.923	18.274	12.119
8:30:15 AM	50.786	45.119	39.456	23.928	18.223	12.437
8:30:46 AM	50.680	45.167	39.366	23.936	18.299	12.162
8:31:17 AM	50.728	45.232	39.594	23.933	17.907	12.204
8:31:48 AM	50.642	45.218	39.405	23.918	18.011	12.044
8:32:18 AM	50.810	45.117	39.519	23.926	18.074	12.482
8:32:49 AM	50.645	45.220	39.339	23.936	17.975	12.024

Average:	50.716	45.166	39.419	23.930	18.149	12.245
	323.866	318.316	312.569	297.080	291.299	285.395

y	T
0.00000	323.866
0.00953	318.316
0.01905	312.569
0.02858	306.953
0.03021	302.943
0.03973	297.080
0.04926	291.299
0.05878	285.395

kupper	15.57355
klower	15.35435

dTdyupper	-593.0184
dTdylower	-613.3911

qhigh	9235.402
qlow	9418.223
qavg	9326.813
Tavg	304.9481
ksamp	3.791072

Figure B2-1

S04	Chiller:	5	Variac:	20		
	Sample Thickness:		1.63E-03	m		
Y Stations:	0	0.375	0.75			
	0	0.009525	0.01905	3.97E-02	0.049255	0.05878

	Upper Flux Meter			Lower Flux Meter		
Time	TC6	TC7	TC8	TC2	TC3	TC4
9:03:32 AM	93.576	84.798	75.652	50.808	41.352	31.934
9:04:02 AM	93.827	84.796	75.729	50.808	41.290	31.823
9:04:33 AM	93.592	84.736	75.534	50.797	41.490	31.875
9:05:04 AM	93.741	84.727	75.717	50.811	41.384	31.666
9:05:35 AM	93.671	84.707	75.563	50.808	41.468	31.801
9:06:05 AM	93.747	84.765	75.731	50.811	41.413	31.754
9:06:36 AM	93.365	84.772	75.466	50.789	41.352	32.128
9:07:07 AM	93.541	84.783	75.808	50.806	41.326	31.953
9:07:38 AM	93.446	84.752	75.645	50.787	41.401	31.956
9:08:08 AM	93.526	84.729	75.543	50.801	41.413	31.917

Average:						
	93.603	84.757	75.639	50.803	41.389	31.881
	366.753	357.907	348.789	323.953	314.539	305.031

y	T
0.00000	366.753
0.00953	357.907
0.01905	348.789
0.02858	339.852
0.03021	333.429
0.03973	323.953
0.04926	314.539
0.05878	305.031

kupper	15.78721
klower	15.6566

dTdyupper	-943.0131
dTdylower	-993.2756

qhigh	14887.54
qlow	15551.31
qavg	15219.43
Tavg	336.6405
ksamp	3.862639

Figure B2-2

S04	Chiller:	20	Variac:	35		
	Sample Thickness:		1.63E-03	m		
Y Stations:	0	0.375	0.75			
	0	0.009525	0.01905	3.97E-02	0.049255	0.05878

	Upper Flux Meter			Lower Flux Meter		
Time	TC6	TC7	TC8	TC2	TC3	TC4
7:47:03 AM	167.478	153.468	138.268	97.515	81.584	65.910
7:47:33 AM	168.455	153.379	138.458	97.513	81.557	65.259
7:48:04 AM	168.451	153.389	138.452	97.519	81.680	65.169
7:48:35 AM	167.989	153.393	138.347	97.521	81.862	65.407
7:49:05 AM	167.571	153.417	138.336	97.497	81.653	65.596
7:49:36 AM	168.394	153.353	138.388	97.500	81.673	65.139
7:50:07 AM	168.098	153.345	138.322	97.508	81.828	65.273
7:50:38 AM	167.799	153.399	138.312	97.506	81.642	65.541
7:51:08 AM	168.023	153.409	138.316	97.486	81.631	65.571
7:51:39 AM	167.995	153.377	138.275	97.504	81.729	65.513

Average:						
	168.025	153.393	138.347	97.507	81.684	65.438
	441.175	426.543	411.497	370.657	354.834	338.588

y	T
0.00000	441.175
0.00953	426.543
0.01905	411.497
0.02858	396.727
0.03021	386.762
0.03973	370.657
0.04926	354.834
0.05878	338.588

kupper	16.15759
klower	16.17901

dTdyupper	-1557.895
dTdylower	-1683.417

qhigh	25171.83
qlow	27236.02
qavg	26203.92
Tavg	391.7446
ksamp	4.286098

Figure B2-3

Appendix B3

S06 Effective Conductivity Data

S06	Chiller:	-5	Variac:	15		
	Sample Thickness:		1.62E-03	m		
Y Stations:	0	0.375	0.75			
	0	0.009525	0.01905	3.97E-02	0.049245	0.05877

	Upper Flux Meter			Lower Flux Meter		
Time	TC6	TC7	TC8	TC2	TC3	TC4
8:58:12 AM	71.079	63.975	56.604	33.160	25.500	17.805
8:58:43 AM	70.992	63.954	56.581	33.148	25.535	17.706
8:59:13 AM	71.458	63.968	56.686	33.151	25.540	17.643
8:59:44 AM	71.152	63.931	56.651	33.148	25.562	17.607
9:00:15 AM	71.314	63.922	56.593	33.151	25.704	17.564
9:00:45 AM	70.791	63.998	56.626	33.151	25.378	17.990
9:01:16 AM	71.068	63.929	56.546	33.146	25.567	17.658
9:01:47 AM	70.565	63.901	56.494	33.143	25.630	17.699
9:02:18 AM	71.517	63.908	56.675	33.146	25.542	17.371
9:02:48 AM	70.931	63.985	56.731	33.136	25.230	17.907

Average:	71.087	63.947	56.619	33.148	25.519	17.695
	344.237	337.097	329.769	306.298	298.669	290.845

y	T
0.00000	344.237
0.00953	337.097
0.01905	329.769
0.02858	322.566
0.03020	314.057
0.03972	306.298
0.04925	298.669
0.05877	290.845

kupper	15.67498
klower	15.44985

dTdyupper	-759.4751
dTdylower	-811.1811

qhigh	11904.76
qlow	12532.63
qavg	12218.69
Tavg	318.3116
ksamp	2.326212

Figure B3-1

S06	Chiller:	-5	Variac:	20		
	Sample Thickness:		1.62E-03	m		
Y Stations:	0	0.375	0.75			
	0	0.009525	0.01905	3.97E-02	0.049245	0.05877

	Upper Flux Meter			Lower Flux Meter		
Time	TC6	TC7	TC8	TC2	TC3	TC4
11:38:25 AM	91.719	82.851	73.519	43.737	33.980	24.279
11:38:55 AM	91.694	82.822	73.621	43.756	33.967	23.991
11:39:26 AM	91.679	82.851	73.630	43.756	33.950	24.136
11:39:57 AM	91.824	82.829	73.603	43.749	33.989	24.224
11:40:28 AM	91.875	82.835	73.596	43.756	34.026	24.199
11:40:58 AM	91.829	82.820	73.612	43.747	33.999	24.008
11:41:29 AM	91.904	82.831	73.632	43.756	33.970	23.908
11:42:00 AM	91.278	82.842	73.551	43.747	33.980	24.246
11:42:30 AM	91.496	82.860	73.596	43.754	33.918	24.169
11:43:01 AM	91.659	82.876	73.628	43.747	33.896	24.249

Average:	91.696	82.842	73.599	43.751	33.968	24.141
	364.846	355.992	346.749	316.901	307.118	297.291

y	T
0.00000	364.846
0.00953	355.992
0.01905	346.749
0.02858	337.765
0.03020	326.713
0.03972	316.901
0.04925	307.118
0.05877	297.291

kupper	15.77666
klower	15.56034

dTdyupper	-949.9685
dTdylower	-1029.375

qhigh	14987.33
qlow	16017.43
qavg	15502.38
Tavg	332.2389
ksamp	2.272212

Figure B3-2

S06	Chiller:	5	Variac:	20		
	Sample Thickness:		1.62E-03	m		
Y Stations:	0	0.375	0.75			
	0	0.009525	0.01905	3.97E-02	0.049245	0.05877

	Upper Flux Meter			Lower Flux Meter		
Time	TC6	TC7	TC8	TC2	TC3	TC4
9:46:54 AM	96.932	88.771	79.758	51.097	41.794	32.200
9:47:25 AM	97.923	88.780	80.004	51.100	41.669	32.064
9:47:56 AM	97.456	88.818	79.959	51.100	41.661	32.320
9:48:26 AM	97.541	88.802	79.882	51.112	41.746	32.126
9:48:57 AM	97.316	88.798	79.871	51.100	41.755	32.259
9:49:28 AM	97.100	88.798	79.772	51.095	41.770	32.359
9:49:59 AM	96.984	88.825	79.792	51.100	41.765	32.554
9:50:29 AM	97.877	88.880	80.062	51.100	41.683	32.278
9:51:00 AM	97.310	88.845	79.979	51.105	41.649	32.394
9:51:31 AM	97.801	88.763	79.875	51.105	41.796	31.949

Average:	97.424	88.808	79.895	51.101	41.729	32.250
	370.574	361.958	353.045	324.251	314.879	305.400

y	T
0.00000	370.574
0.00953	361.958
0.01905	353.045
0.02858	344.331
0.03020	333.695
0.03972	324.251
0.04925	314.879
0.05877	305.400

kupper	15.80904
klower	15.66097

dTdyupper	-920.1365
dTdylower	-989.5591

qhigh	14546.47
qlow	15497.45
qavg	15021.96
Tavg	339.0126
ksamp	2.288053

Figure B3-3

S06	Chiller:	15	Variac:	25			
	Sample Thickness:		1.62E-03	m			
Y Stations:	0	0.375	0.75				
	0	0.009525	0.01905	3.97E-02	0.049245	0.05877	
		Upper Flux Meter			Lower Flux Meter		

Time	TC6	TC7	TC8	TC2	TC3	TC4
10:00:59 AM	120.639	110.727	100.541	67.966	57.300	46.237
10:01:30 AM	120.333	110.712	100.528	67.963	57.216	46.323
10:02:01 AM	120.508	110.692	100.543	67.954	57.317	46.319
10:02:31 AM	120.411	110.688	100.532	67.947	57.230	46.271
10:03:02 AM	120.200	110.686	100.445	67.943	57.230	46.436
10:03:33 AM	120.905	110.720	100.619	67.947	57.181	46.216
10:04:04 AM	120.947	110.692	100.641	67.931	57.176	46.170
10:04:34 AM	120.500	110.626	100.541	67.929	57.314	46.194
10:05:05 AM	120.930	110.662	100.597	67.936	57.218	46.111
10:05:36 AM	120.059	110.686	100.480	67.918	57.202	46.555

Average:						
	120.543	110.689	100.547	67.943	57.238	46.283
	393.693	383.839	373.697	341.093	330.388	319.433

y	T
0.00000	393.693
0.00953	383.839
0.01905	373.697
0.02858	363.747
0.03020	351.965
0.03972	341.093
0.04925	330.388
0.05877	319.433

kupper	15.92721
klower	15.86197

dTdyupper	-1049.685
dTdylower	-1137.018

qhigh	16718.56
qlow	18035.35
qavg	17376.95
Tavg	357.8559
ksamp	2.389436

Figure B3-4

S06	Chiller:	15	Variac:	30		
	Sample Thickness:		1.62E-03	m		
Y Stations:	0	0.375	0.75			
	0	0.009525	0.01905	3.97E-02	0.049245	0.05877
		Upper Flux Meter			Lower Flux Meter	

Time	TC6	TC7	TC8	TC2	TC3	TC4
9:32:49 AM	143.754	131.957	119.542	80.046	66.752	53.553
9:33:20 AM	143.564	131.880	119.409	80.035	66.969	53.265
9:33:51 AM	144.305	131.878	119.550	80.055	66.925	53.032
9:34:21 AM	144.285	131.917	119.578	80.048	66.824	53.133
9:34:52 AM	143.978	131.911	119.514	80.053	66.858	53.289
9:35:23 AM	143.792	131.911	119.500	80.044	66.826	53.168
9:35:54 AM	143.684	131.903	119.462	80.033	66.833	53.393
9:36:24 AM	143.584	131.928	119.447	80.035	66.778	53.489
9:36:55 AM	144.136	131.861	119.436	80.039	66.948	53.020
9:37:26 AM	143.339	131.934	119.394	80.042	66.844	53.602

Average:						
	143.842	131.908	119.483	80.043	66.856	53.294
	416.992	405.058	392.633	353.193	340.006	326.444

y	T
0.00000	416.992
0.00953	405.058
0.01905	392.633
0.02858	380.536
0.03020	366.630
0.03972	353.193
0.04925	340.006
0.05877	326.444

kupper	16.04143
klower	15.98645

dTdyupper	-1278.682
dTdylower	-1404.126

qhigh	20511.89
qlow	22446.99
qavg	21479.44
Tavg	373.5826
ksamp	2.502298

Figure B3-5

S06	Chiller:	20	Variac:	35		
	Sample Thickness:		1.62E-03	m		
Y Stations:	0	0.375	0.75			
	0	0.009525	0.01905	3.97E-02	0.049245	0.05877

	Upper Flux Meter			Lower Flux Meter		
Time	TC6	TC7	TC8	TC2	TC3	TC4
7:43:14 PM	170.917	156.678	142.322	96.477	80.936	64.948
7:43:44 PM	171.028	156.656	142.312	96.486	81.007	64.856
7:44:15 PM	170.065	156.674	142.128	96.483	81.001	65.220
7:44:46 PM	170.039	156.664	142.013	96.475	80.987	65.370
7:45:17 PM	170.810	156.686	142.252	96.486	80.951	65.190
7:45:47 PM	170.729	156.608	142.076	96.479	81.129	64.883
7:46:18 PM	170.972	156.616	142.164	96.490	81.066	64.766
7:46:49 PM	170.907	156.646	142.265	96.488	80.936	65.040
7:47:20 PM	170.427	156.660	142.164	96.486	80.947	65.202
7:47:50 PM	170.460	156.650	142.166	96.490	81.003	65.146

Average:	170.635	156.654	142.186	96.484	80.996	65.062
	443.785	429.804	415.336	369.634	354.146	338.212

y	T
0.00000	443.785
0.00953	429.804
0.01905	415.336
0.02858	401.193
0.03020	385.419
0.03972	369.634
0.04925	354.146
0.05877	338.212

kupper	16.17507
klower	16.16997

dTdyupper	-1493.396
dTdylower	-1649.444

qhigh	24155.78
qlow	26671.45
qavg	25413.62
Tavg	393.306
ksamp	2.610122

Figure B3-6

Appendix B4

S07 Effective Conductivity Data

S07	Chiller:	-5	Variac:	10		
	Sample Thickness:		1.68E-03	m		
Y Stations:	0	0.375	0.75			
	0	0.009525	0.01905	3.98E-02	0.049305	0.05883

	Upper Flux Meter			Lower Flux Meter		
Time	TC6	TC7	TC8	TC2	TC3	TC4
12:32:07 PM	50.867	45.440	39.969	22.580	17.036	11.397
12:32:37 PM	50.844	45.467	39.894	22.580	17.034	11.315
12:33:08 PM	50.953	45.462	39.989	22.583	16.940	11.330
12:33:39 PM	50.780	45.440	39.986	22.585	17.031	11.392
12:34:10 PM	50.628	45.431	39.962	22.575	17.047	11.317
12:34:40 PM	50.401	45.457	40.001	22.570	16.958	11.577
12:35:11 PM	51.280	45.457	40.146	22.575	16.988	11.222
12:35:42 PM	51.206	45.436	40.107	22.590	16.963	11.114
12:36:13 PM	50.922	45.417	39.984	22.590	17.082	11.245
12:36:43 PM	50.666	45.424	39.984	22.583	16.935	11.364

Average:	50.855	45.443	40.002	22.581	17.001	11.327
	324.005	318.593	313.152	295.731	290.151	284.477

y	T
0.00000	324.005
0.00953	318.593
0.01905	313.152
0.02858	307.731
0.03026	301.374
0.03978	295.731
0.04931	290.151
0.05883	284.477

kupper	15.57535
klower	15.33956

dTdyupper	-569.685
dTdylower	-590.7507

qhigh	8873.044
qlow	9061.855
qavg	8967.449
Tavg	304.5523
ksamp	2.369841

Figure B4-1

S07	Chiller:	-5	Variac:	15			
	Sample Thickness:		1.68E-03	m			
Y Stations:	0	0.375	0.75				
	0	0.009525	0.01905	3.98E-02	0.049305	0.05883	
		Upper Flux Meter			Lower Flux Meter		

Time	TC6	TC7	TC8	TC2	TC3	TC4
10:15:26 AM	71.524	64.283	56.937	33.124	25.438	17.853
10:15:56 AM	71.033	64.313	56.827	33.124	25.470	18.041
10:16:27 AM	72.001	64.308	57.078	33.126	25.395	17.557
10:16:58 AM	71.335	64.336	56.944	33.121	25.418	17.970
10:17:29 AM	71.989	64.264	57.022	33.119	25.395	17.338
10:17:59 AM	71.237	64.260	56.836	33.119	25.480	17.792
10:18:30 AM	71.595	64.341	57.038	33.121	25.343	17.836
10:19:01 AM	71.056	64.322	56.834	33.116	25.492	17.922
10:19:32 AM	71.853	64.253	56.902	33.114	25.445	17.450
10:20:02 AM	71.198	64.243	56.801	33.131	25.438	17.737

Average:						
	71.482	64.292	56.922	33.122	25.431	17.750
	344.632	337.442	330.072	306.272	298.581	290.900

y	T
0.00000	344.632
0.00953	337.442
0.01905	330.072
0.02858	322.822
0.03026	313.956
0.03978	306.272
0.04931	298.581
0.05883	290.900

kupper	15.67686
klower	15.44959

dTdyupper	-764.315
dTdylower	-806.9239

qhigh	11982.06
qlow	12466.65
qavg	12224.35
Tavg	318.389
ksamp	2.316411

Figure B4-2

S07	Chiller:	-5	Variac:	20		
	Sample Thickness:		1.68E-03	m		
Y Stations:	0	0.375	0.75			
	0	0.009525	0.01905	3.98E-02	0.049305	0.05883

	Upper Flux Meter			Lower Flux Meter		
Time	TC6	TC7	TC8	TC2	TC3	TC4
9:40:15 AM	89.079	79.803	70.933	41.982	32.480	22.936
9:40:46 AM	89.011	79.743	70.794	41.980	32.613	22.640
9:41:17 AM	88.189	79.815	70.727	41.973	32.475	23.405
9:41:48 AM	88.131	79.817	70.725	41.963	32.490	23.222
9:42:18 AM	88.838	79.736	70.707	41.970	32.623	22.718
9:42:49 AM	89.059	79.761	70.894	41.977	32.536	22.756
9:43:20 AM	88.902	79.738	70.732	41.973	32.652	22.681
9:43:51 AM	88.217	79.729	70.590	41.977	32.684	22.889
9:44:21 AM	89.059	79.749	70.901	41.975	32.500	22.645
9:44:52 AM	89.068	79.774	70.903	41.977	32.446	22.924

Average:	88.755	79.767	70.791	41.975	32.550	22.882
	361.905	352.917	343.941	315.125	305.700	296.032

y	T
0.00000	361.905
0.00953	352.917
0.01905	343.941
0.02858	334.956
0.03026	324.712
0.03978	315.125
0.04931	305.700
0.05883	296.032

kupper	15.76077
klower	15.54104

dTdyupper	-943.0289
dTdylower	-1002.262

qhigh	14862.86
qlow	15576.2
qavg	15219.53
Tavg	329.834
ksamp	2.495915

Figure B4-3

S07	Chiller:	5	Variac:	20		
	Sample Thickness:		1.68E-03	m		
Y Stations:	0	0.375	0.75			
	0	0.009525	0.01905	3.98E-02	0.049305	0.05883

	Upper Flux Meter			Lower Flux Meter		
Time	TC6	TC7	TC8	TC2	TC3	TC4
2:22:41 PM	91.406	82.860	74.491	47.587	38.743	29.786
2:23:12 PM	90.887	82.882	74.391	47.577	38.765	30.057
2:23:42 PM	91.542	82.858	74.434	47.587	38.840	29.736
2:24:13 PM	91.328	82.916	74.518	47.587	38.719	30.099
2:24:44 PM	90.678	82.869	74.314	47.572	38.794	30.094
2:25:15 PM	91.207	82.824	74.373	47.582	38.879	29.726
2:25:45 PM	91.600	82.842	74.475	47.589	38.784	29.736
2:26:16 PM	91.141	82.827	74.289	47.575	38.854	29.907
2:26:47 PM	90.951	82.889	74.343	47.582	38.779	29.976
2:27:18 PM	91.214	82.824	74.391	47.582	38.864	29.771

Average:	91.195	82.859	74.402	47.582	38.802	29.889
	364.345	356.009	347.552	320.732	311.952	303.039

y	T
0.00000	364.345
0.00953	356.009
0.01905	347.552
0.02858	339.175
0.03026	329.601
0.03978	320.732
0.04931	311.952
0.05883	303.039

kupper	15.77723
klower	15.6228

dTdyupper	-881.5486
dTdylower	-928.7769

qhigh	13908.4
qlow	14510.1
qavg	14209.25
Tavg	334.3881
ksamp	2.493249

Figure B4-4

S07	Chiller:	15	Variac:	25			
	Sample Thickness:		1.68E-03	m			
Y Stations:	0	0.375	0.75				
	0	0.009525	0.01905	3.98E-02	0.049305	0.05883	
		Upper Flux Meter			Lower Flux Meter		

Time	TC6	TC7	TC8	TC2	TC3	TC4
11:01:15 AM	119.417	109.073	98.950	66.478	55.889	44.745
11:01:45 AM	119.396	109.064	98.887	66.481	55.854	44.781
11:02:16 AM	118.914	109.114	98.795	66.474	55.816	45.012
11:02:47 AM	119.212	109.122	98.808	66.474	55.814	44.899
11:03:18 AM	119.007	109.116	98.774	66.472	55.765	44.942
11:03:48 AM	118.956	109.103	98.811	66.458	55.776	44.973
11:04:19 AM	119.180	109.090	98.878	66.455	55.809	44.942
11:04:50 AM	119.178	109.064	98.824	66.455	55.866	44.753
11:05:21 AM	119.506	109.064	98.909	66.465	55.835	44.695
11:05:51 AM	118.866	109.060	98.734	66.458	55.880	44.930

Average:						
	119.163	109.087	98.837	66.467	55.830	44.867
	392.313	382.237	371.987	339.617	328.980	318.017

y	T
0.00000	392.313
0.00953	382.237
0.01905	371.987
0.02858	361.853
0.03026	350.471
0.03978	339.617
0.04931	328.980
0.05883	318.017

kupper	15.91877
klower	15.84333

dTdyupper	-1066.992
dTdylower	-1133.848

qhigh	16985.2
qlow	17963.92
qavg	17474.56
Tavg	356.1621
ksamp	2.579377

Figure B4-5

S07	Chiller:	15	Variac:	30		
	Sample Thickness:		1.68E-03	m		
Y Stations:	0	0.375	0.75			
	0	0.009525	0.01905	3.98E-02	0.049305	0.05883

	Upper Flux Meter			Lower Flux Meter		
Time	TC6	TC7	TC8	TC2	TC3	TC4
10:14:16 AM	140.424	128.169	115.817	77.634	64.546	51.573
10:14:47 AM	140.586	128.142	115.806	77.623	64.618	51.422
10:15:17 AM	139.615	128.161	115.611	77.632	64.731	51.834
10:15:48 AM	140.586	128.138	115.859	77.639	64.618	51.247
10:16:19 AM	140.387	128.207	115.893	77.639	64.592	51.607
10:16:49 AM	140.590	128.115	115.812	77.636	64.634	51.247
10:17:20 AM	140.586	128.105	115.785	77.650	64.675	51.171
10:17:51 AM	139.751	128.184	115.711	77.643	64.657	51.912
10:18:22 AM	140.268	128.171	115.749	77.641	64.675	51.415
10:18:52 AM	139.972	128.136	115.732	77.643	64.752	51.509

Average:	140.277	128.153	115.778	77.638	64.650	51.494
	413.427	401.303	388.928	350.788	337.800	324.644

y	T
0.00000	413.427
0.00953	401.303
0.01905	388.928
0.02858	376.720
0.03026	363.888
0.03978	350.788
0.04931	337.800
0.05883	324.644

kupper	16.02158
klower	15.95867

dTdyupper	-1286.037
dTdylower	-1372.404

qhigh	20604.34
qlow	21901.75
qavg	21253.04
Tavg	370.304
ksamp	2.782549

Figure B4-6

S07	Chiller:	20	Variac:	35			
	Sample Thickness:		1.68E-03	m			
Y Stations:	0	0.375	0.75				
	0	0.009525	0.01905	3.98E-02	0.049305	0.05883	
		Upper Flux Meter			Lower Flux Meter		

Time	TC6	TC7	TC8	TC2	TC3	TC4
11:01:09 AM	162.722	149.387	135.148	91.981	77.203	62.011
11:01:40 AM	162.918	149.446	135.260	91.983	77.020	62.173
11:02:11 AM	163.504	149.381	135.371	91.977	77.047	61.865
11:02:41 AM	163.223	149.403	135.338	91.979	77.088	61.883
11:03:12 AM	163.085	149.364	135.243	91.988	77.223	61.753
11:03:43 AM	162.842	149.356	135.173	91.977	77.210	61.876
11:04:14 AM	163.476	149.344	135.305	91.977	77.108	61.674
11:04:44 AM	162.503	149.395	135.088	91.972	77.185	62.206
11:05:15 AM	163.448	149.334	135.270	91.972	77.153	61.623
11:05:46 AM	163.381	149.369	135.340	91.974	77.081	61.872

Average:	163.110	149.378	135.254	91.978	77.132	61.894
	436.260	422.528	408.404	365.128	350.282	335.044

y	T
0.00000	436.260
0.00953	422.528
0.01905	408.404
0.02858	394.541
0.03026	380.236
0.03978	365.128
0.04931	350.282
0.05883	335.044

kupper	16.13595
klower	16.11996

dTdyupper	-1462.289
dTdylower	-1579.234

qhigh	23595.41
qlow	25457.19
qavg	24526.3
Tavg	387.3881
ksamp	2.880384

Figure B4-7

Appendix C

Porosity Measurements

Table C-1: Dimensional and mass measurements for porosity calculations.

S03				
Trial	**Diameter (mm)**	**Thickness (mm)**	**Dry Mass (g)**	**Saturated Mass (g)**
1	64.53	2.01	4.106	4.507
2	64.55	2.02	4.103	4.519
3	64.55	2.01	4.105	4.510
4	64.54	2.01	4.107	4.521
Average	64.54	2.01	4.105	4.514
S04				
1	64.68	1.66	4.103	4.282
2	64.66	1.66	4.104	4.279
3	64.67	1.66	4.102	4.268
4	64.66	1.65	4.106	4.270
Average	64.67	1.66	4.104	4.275
S06				
1	64.61	1.66	3.419	3.628
2	64.62	1.66	3.417	3.619
3	64.63	1.66	3.418	3.631
4	64.61	1.65	3.421	3.621
Average	64.62	1.66	3.419	3.625
S07				
1	64.64	1.61	4.104	4.299
2	64.63	1.60	4.108	4.301
3	64.63	1.61	4.106	4.310
4	64.65	1.61	4.105	4.313
Average	64.64	1.61	4.106	4.306

Appendix D

Heat Leak Temperature Profiles

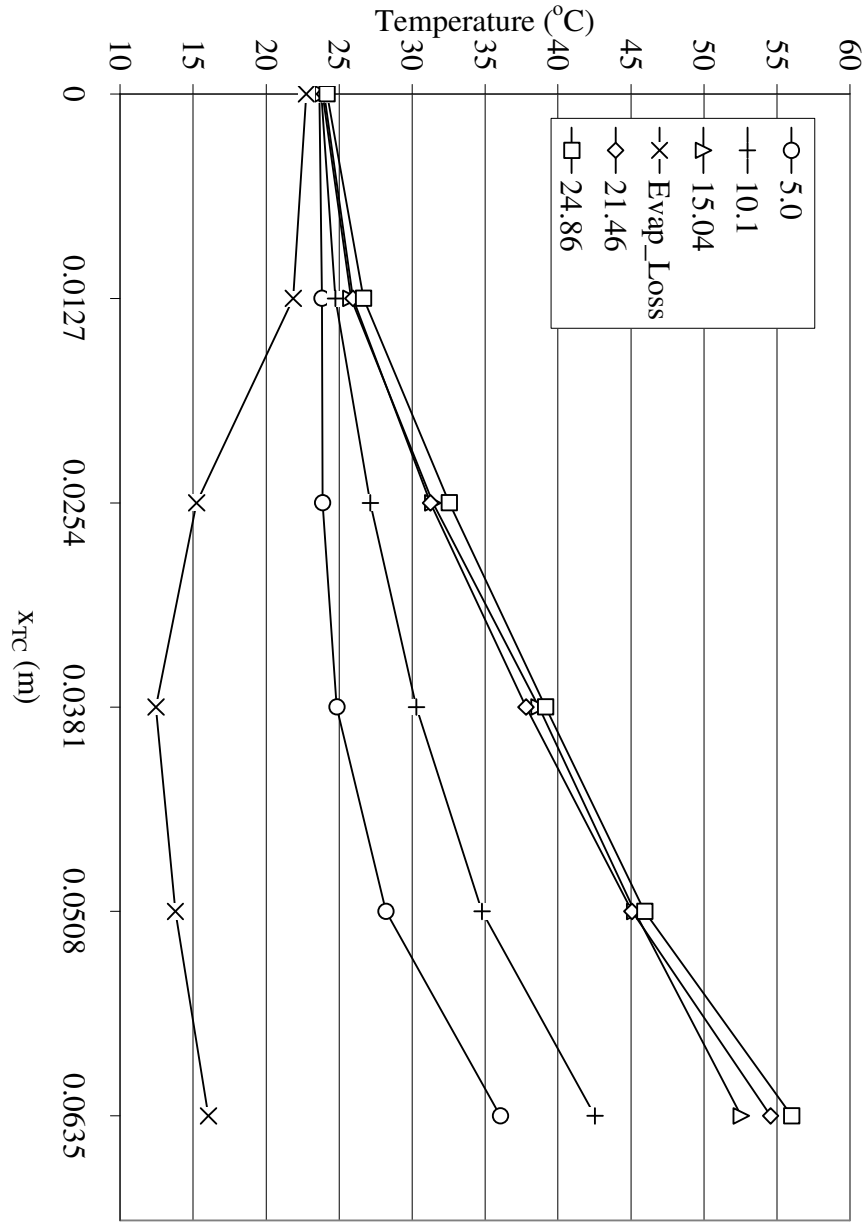

Figure D-1: S03 heat leak temperature profiles.

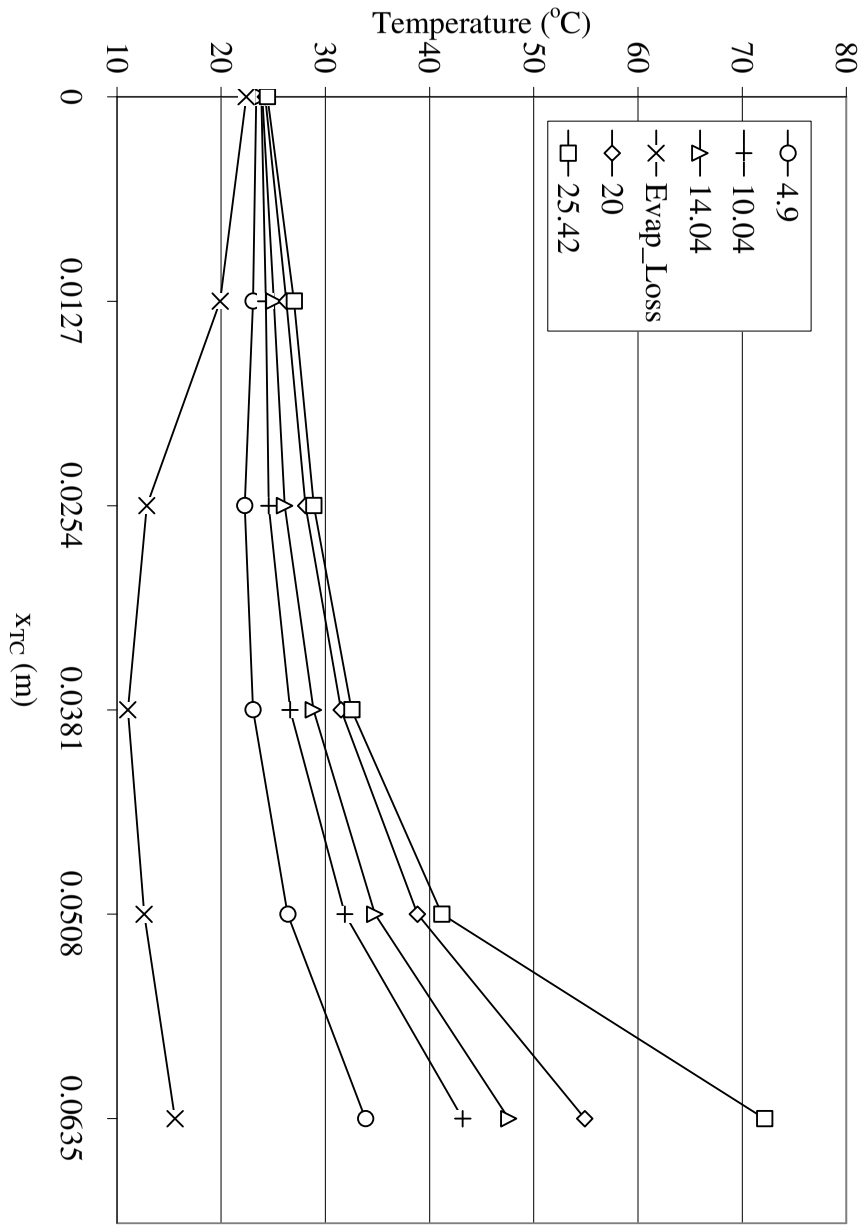

Figure D-2: S04 heat leak temperature profiles.

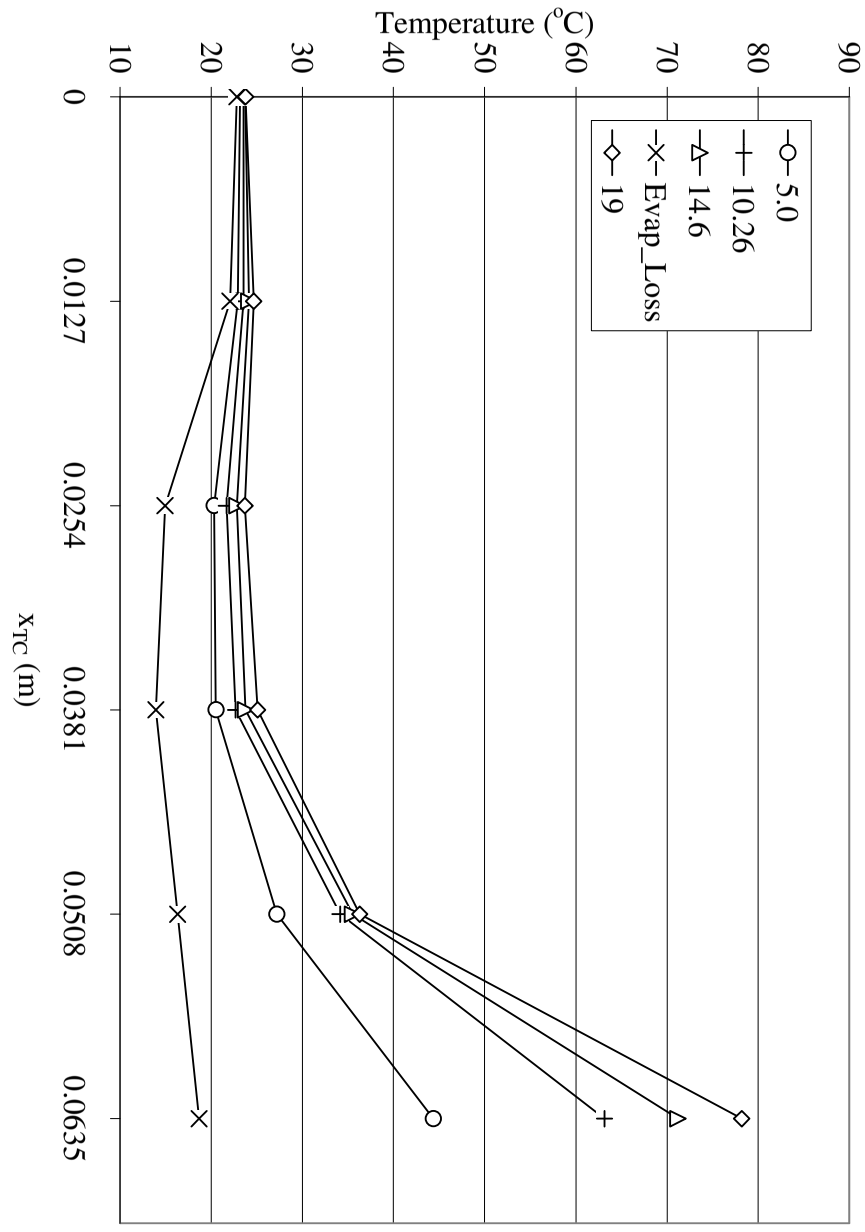

Figure D-3: S06 heat leak temperature profiles

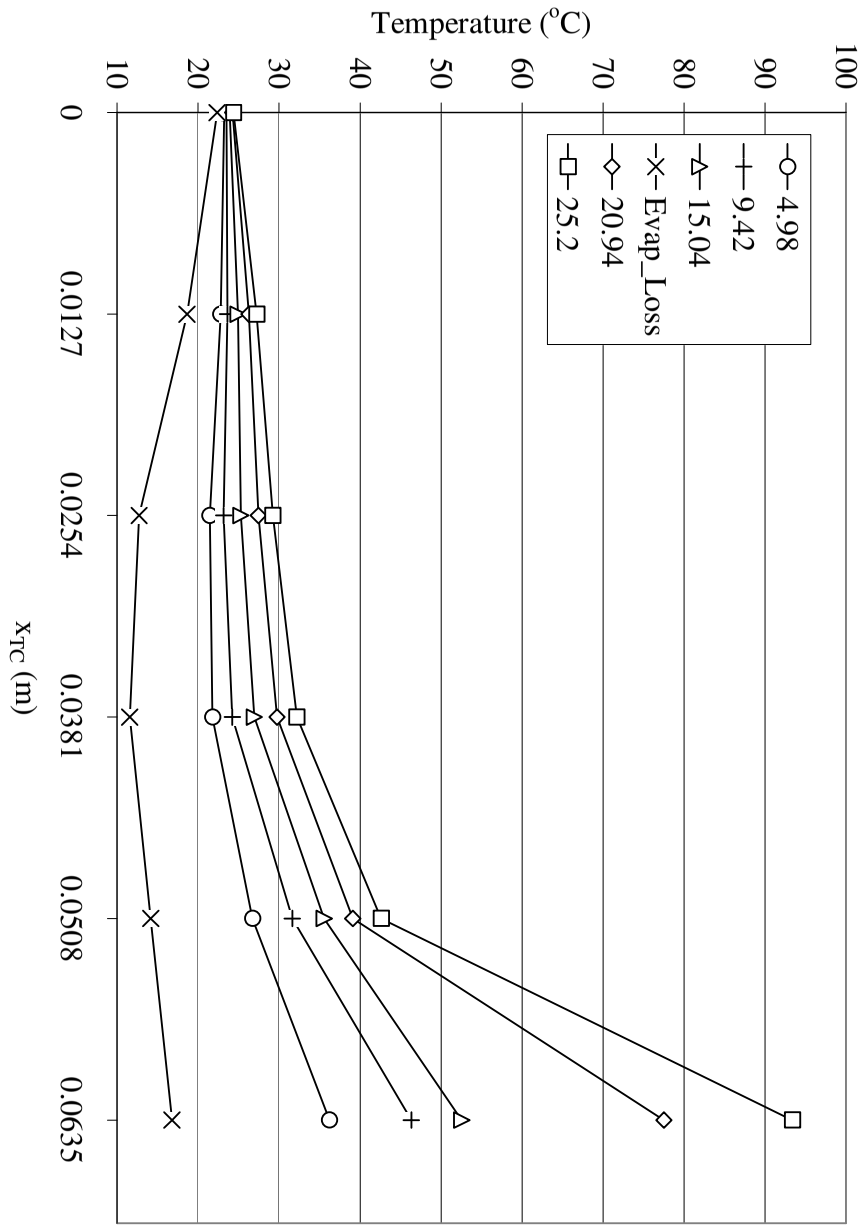

Figure D-4: S07 heat leak temperature profile.

Appendix E

Heat Leak Mass Flow Rate Data

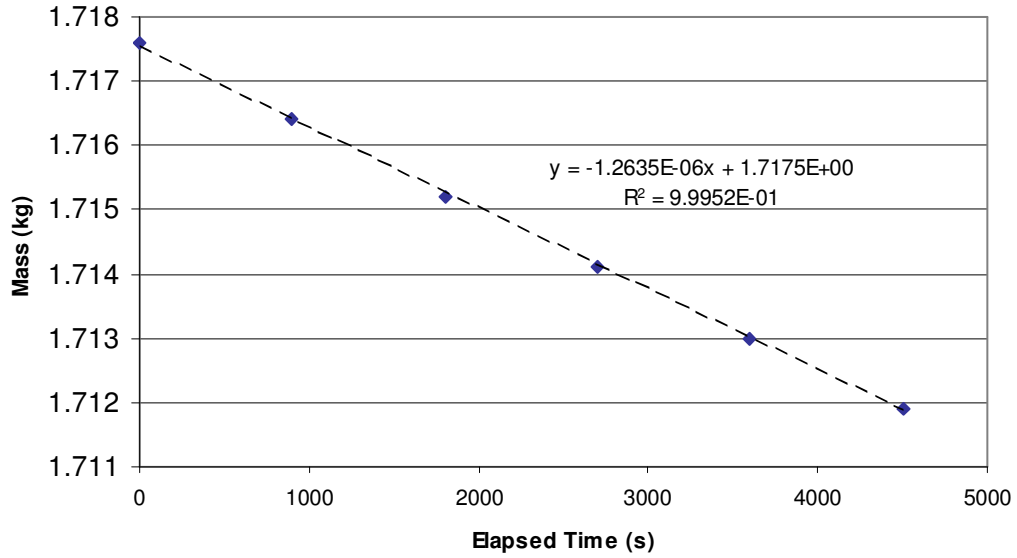

Figure E-1: S03 evaporative loss data.

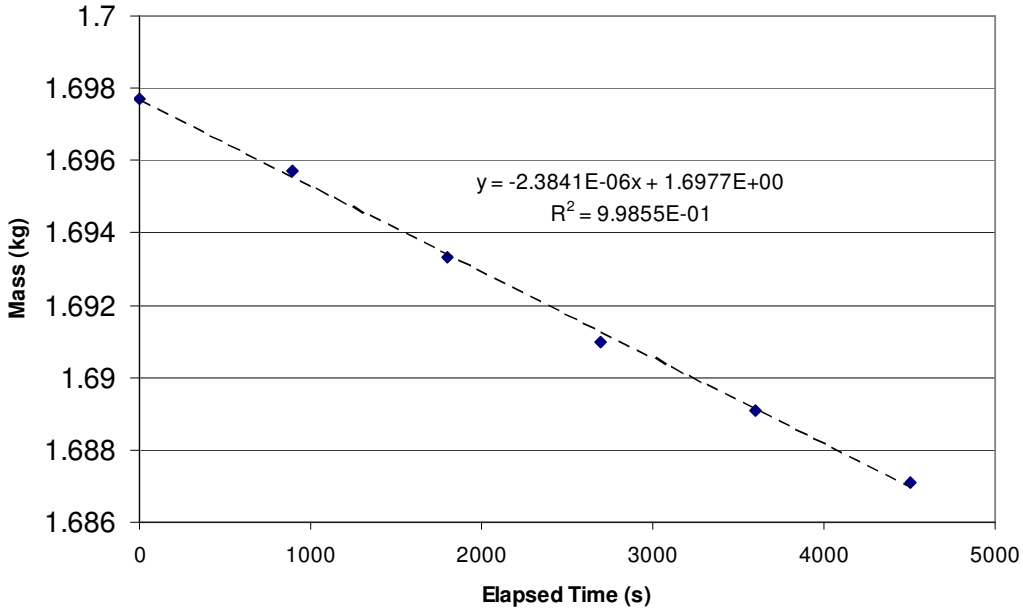

Figure E-2: S03 5.0W data.

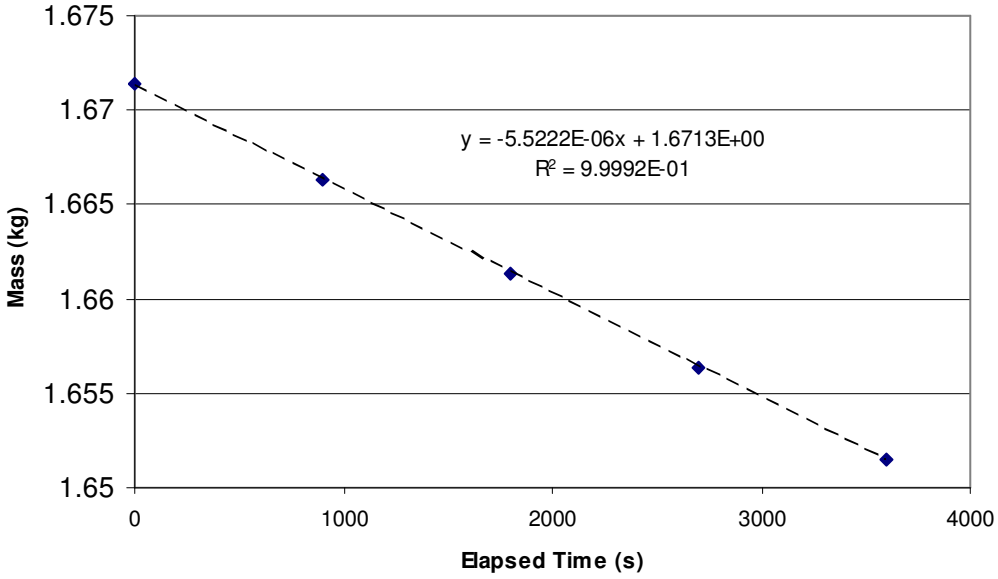

Figure E-3: S03 10.1W data.

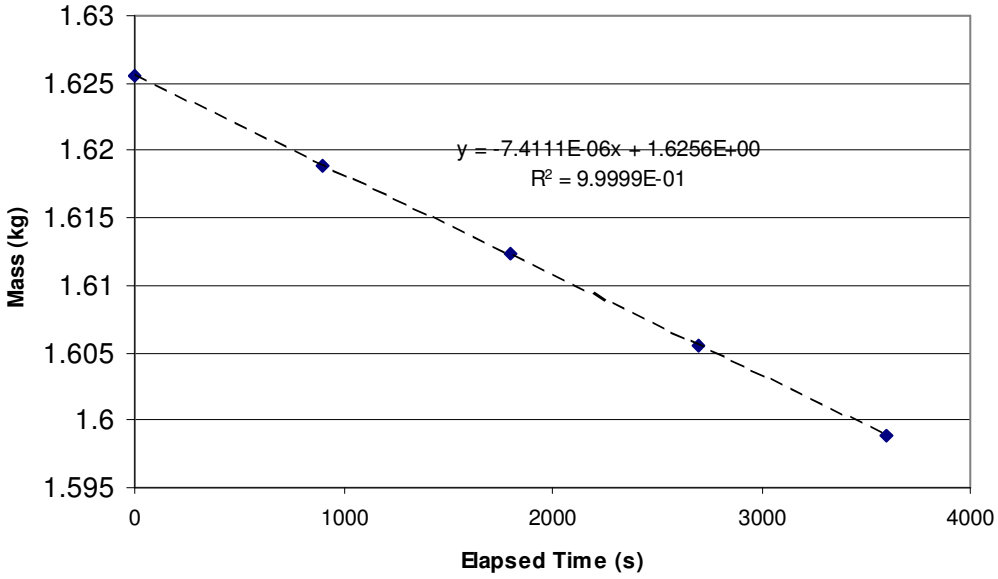

Figure E-4: S03 15.04W data.

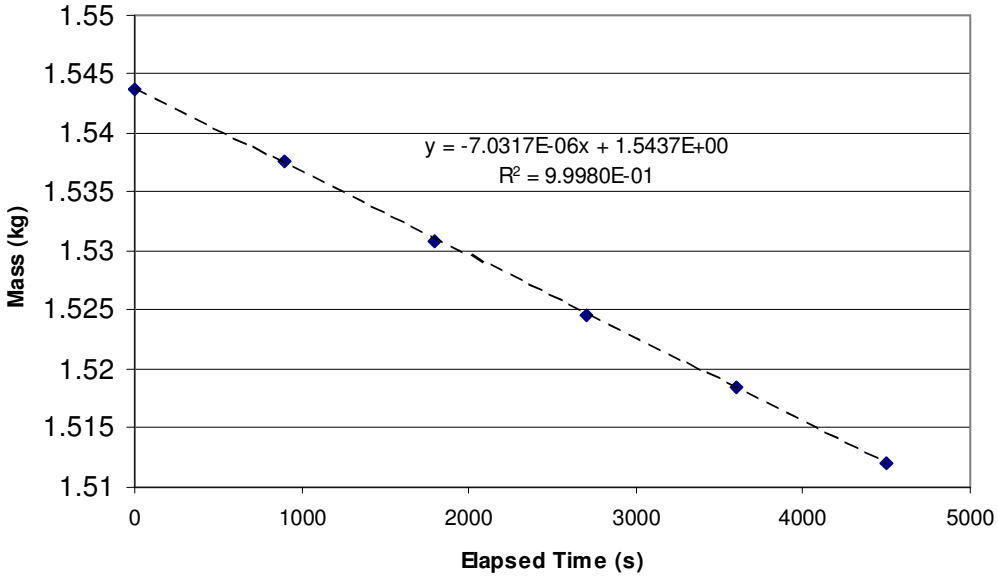

Figure E-5: S03 21.46W data.

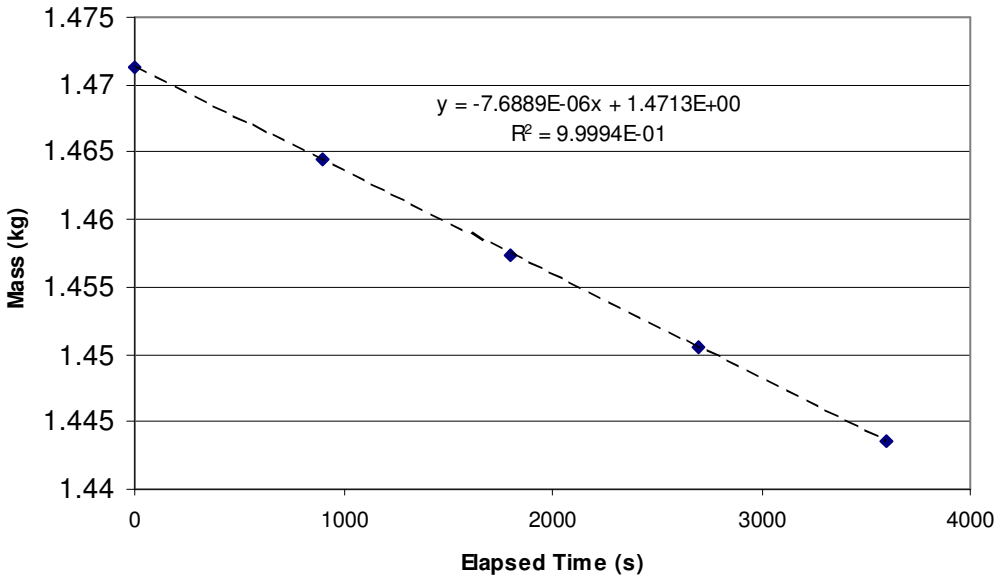

Figure E-6: S03 25.42W data.

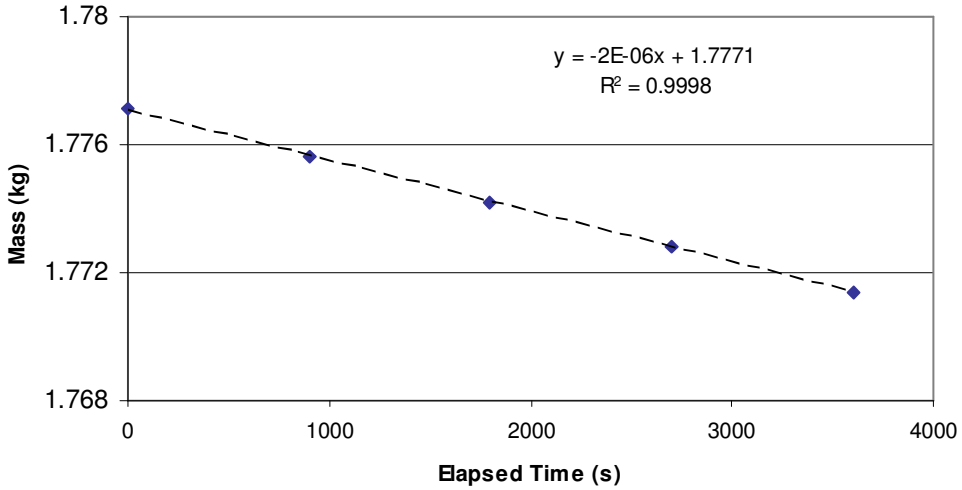

Figure E-7: S04 evaporative loss data.

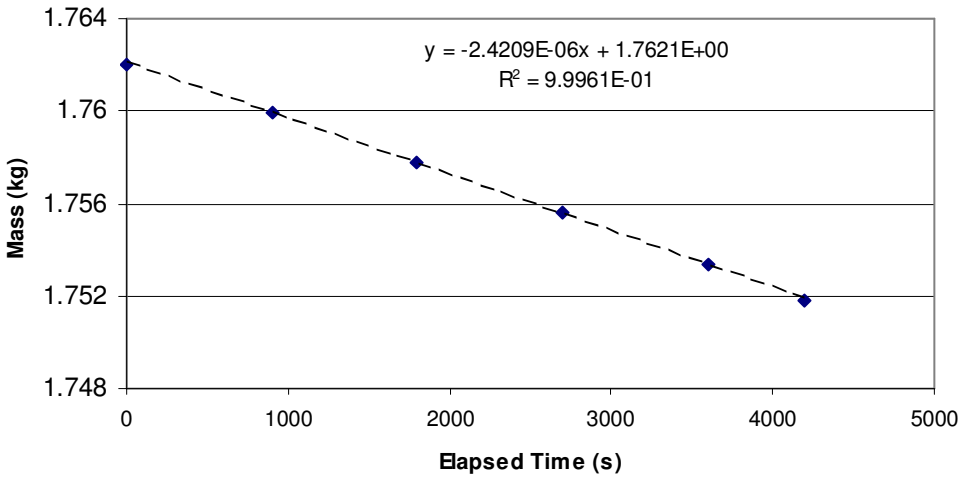

Figure E-8: S04 4.92W data.

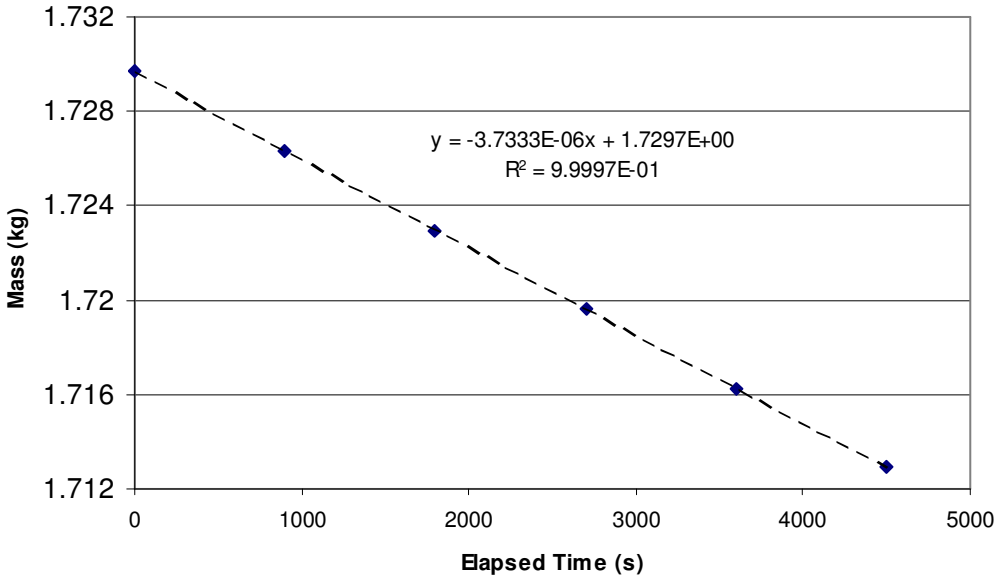

Figure E-9: S04 10.04W data.

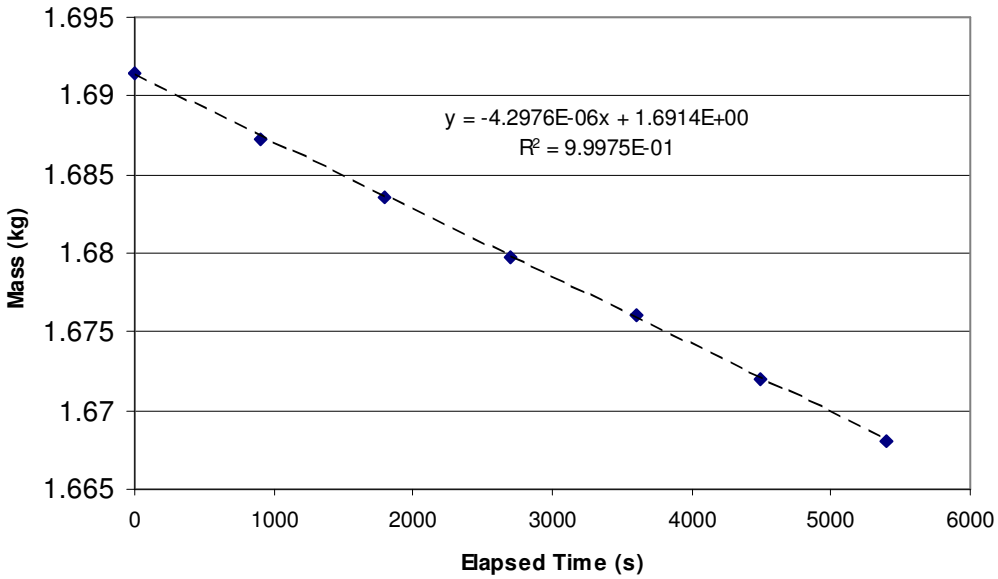

Figure E-10: S04 14.04W data.

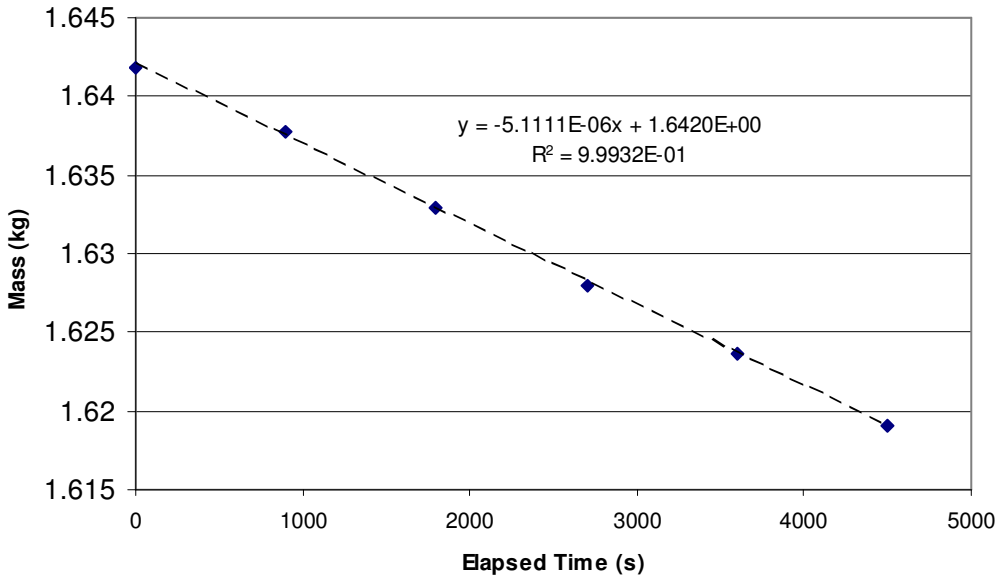

Figure E-11: S04 20.0W data.

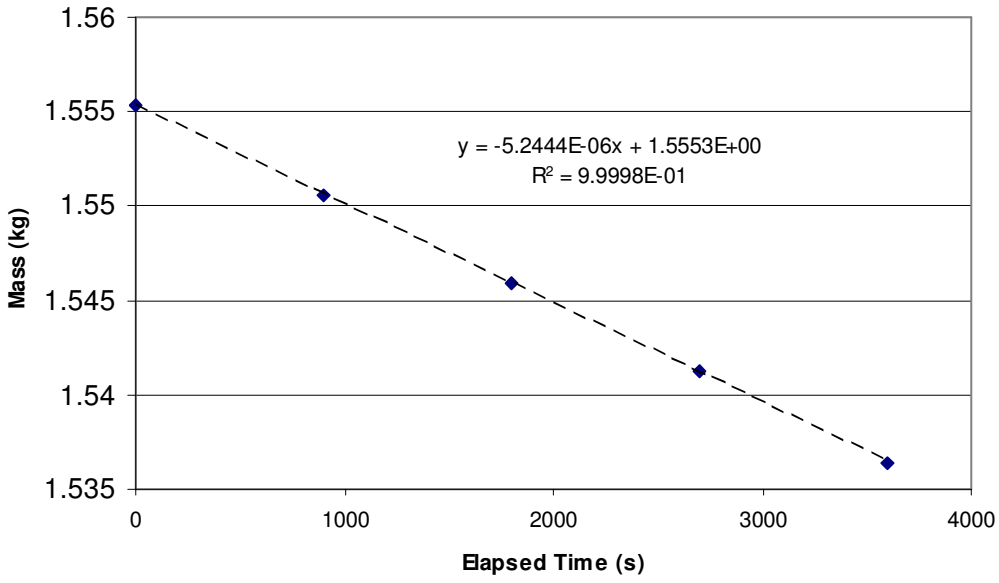

Figure E-12: S04 25.42W data.

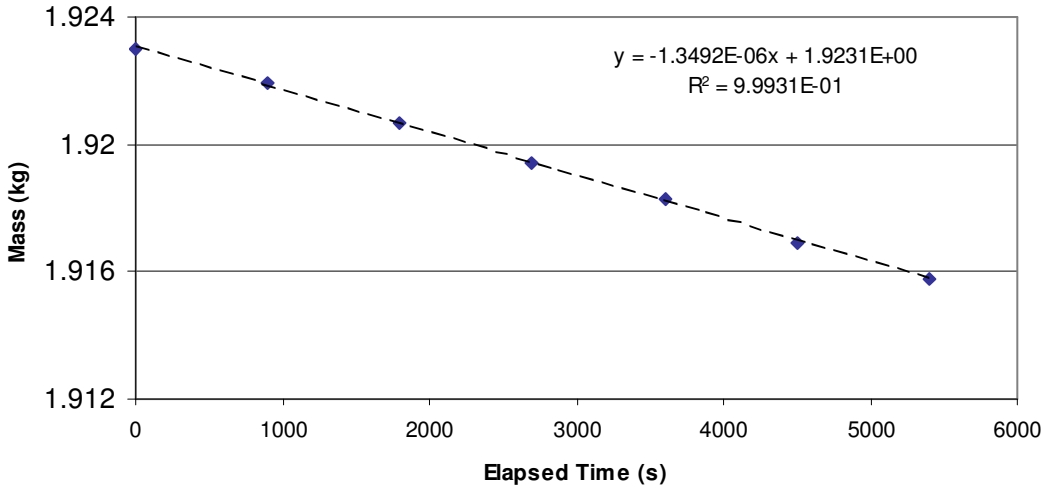

Figure E-13: S06 evaporative loss data.

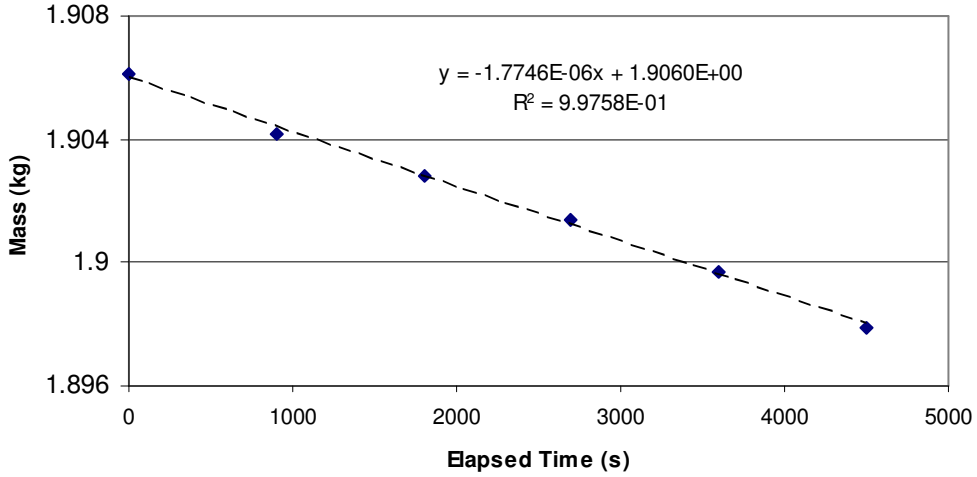

Figure E-14: S06 5.0W data.

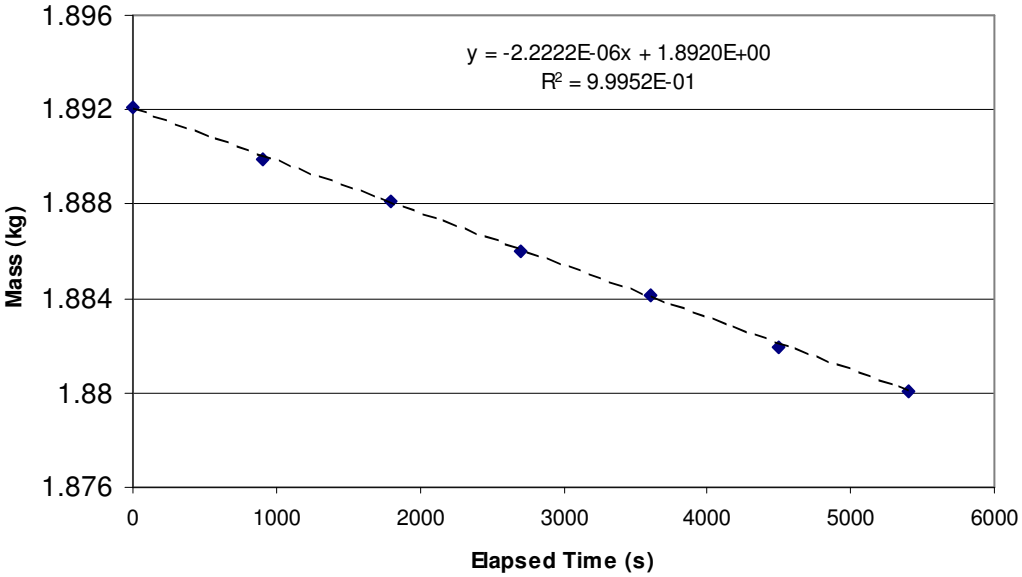

Figure E-15: S06 10.26W data.

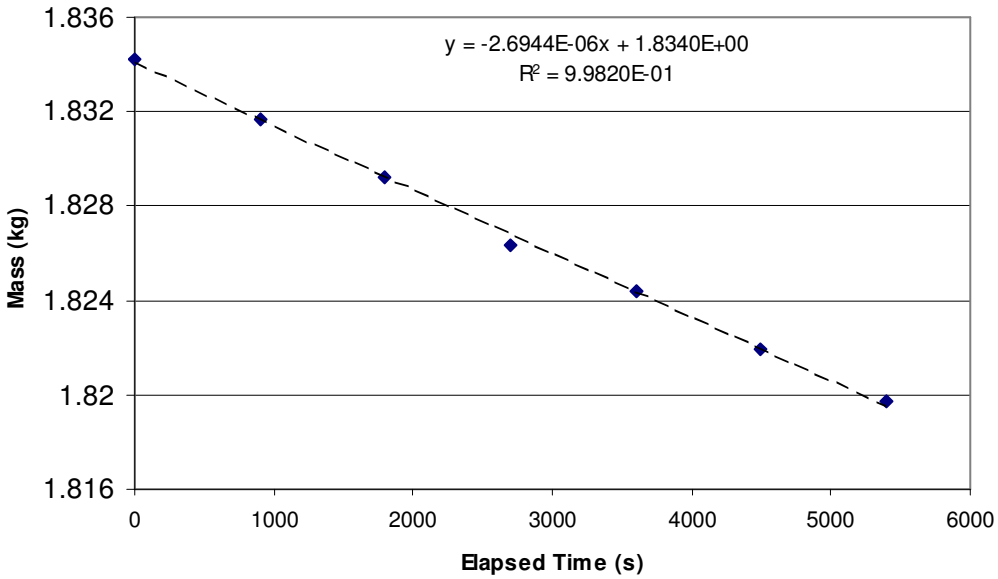

Figure E-16: S06 14.6W data.

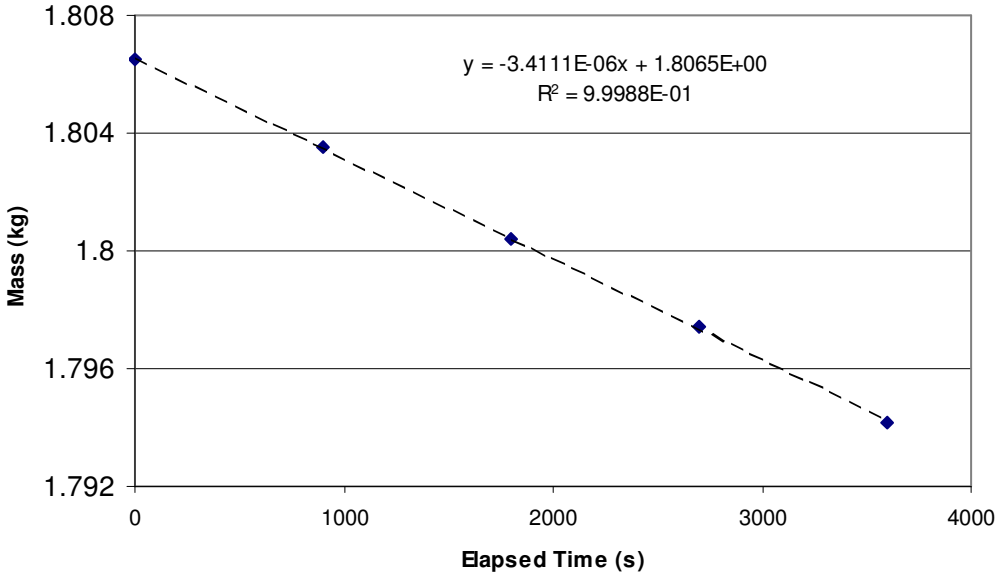

Figure E-17: S06 19.0W data.

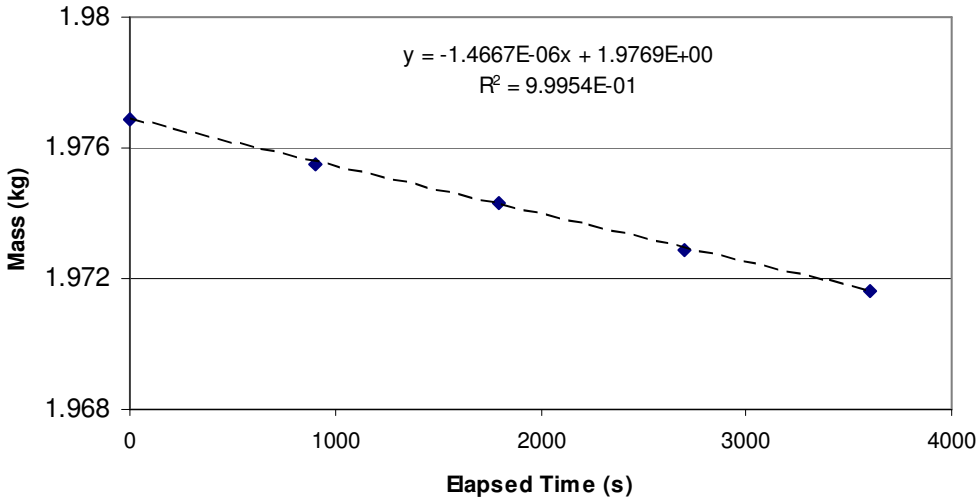

Figure E-18: S07 evaporative loss data.

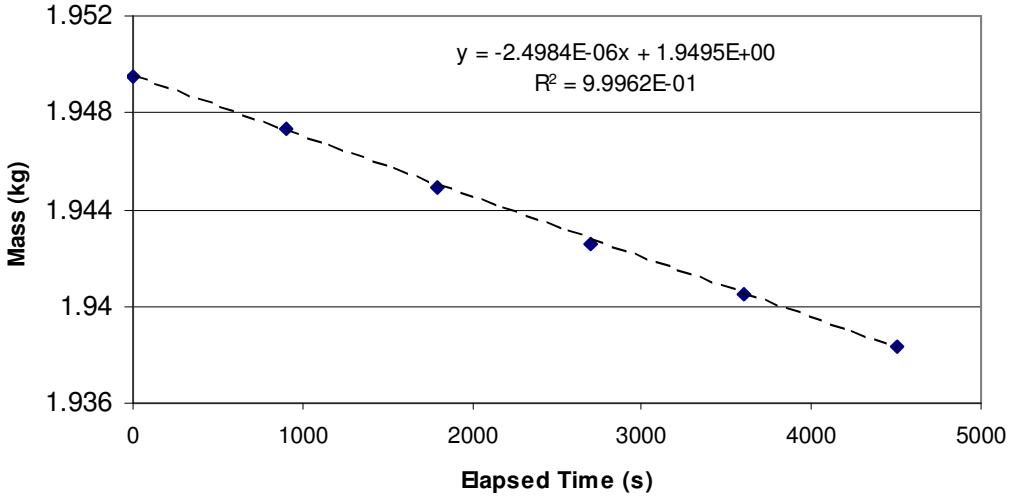

Figure E-19: S07 4.98W data.

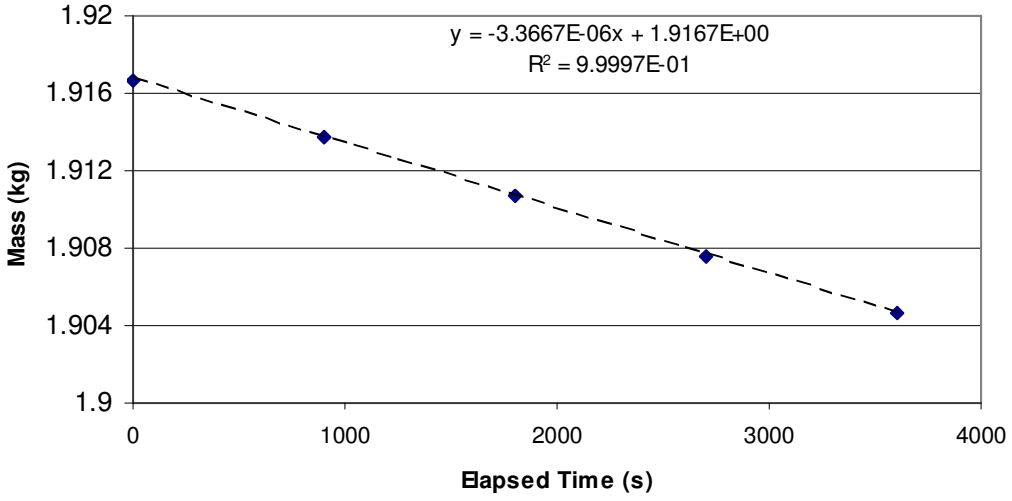

Figure E-20: S07 9.42W data.

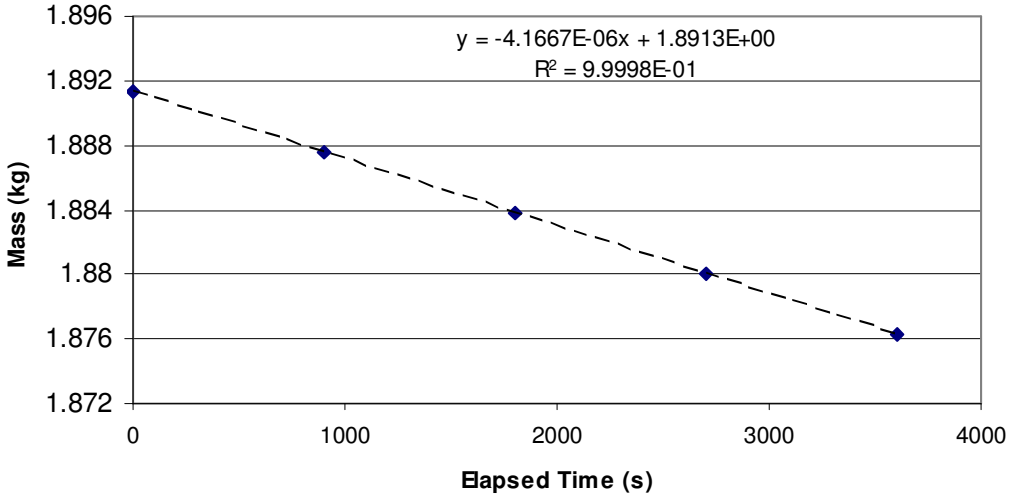

Figure E-21: S07 15.04W data.

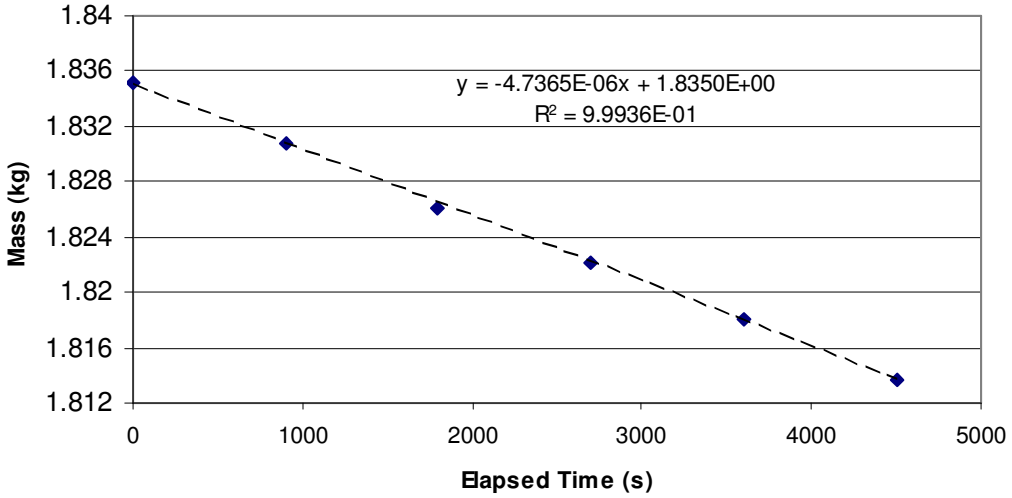

Figure E-22: S07 20.94W data.

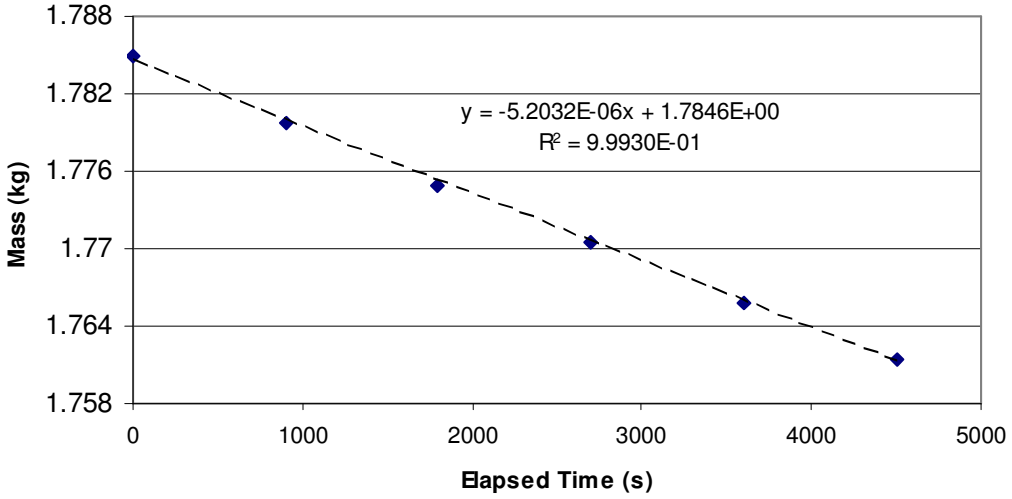

Figure E-23: S07 25.2W data.

Appendix F

Reference Stainless Steel Conductivity Data

Table C-1: Reference stainless steel conductivity data [19]

304 Stainless	
T (K)	k (W/m-K)
373.2	16.5
423.2	17.3
473.2	18
523.2	18.8
573.2	19.5

316 Stainless	
T (K)	k (W/m-K)
272.6	13.3
335.4	14.6
346.5	14.8
375.4	15.7
394.3	15.7
408.7	15.4
433.7	16.6
438.2	16
439.8	16.5

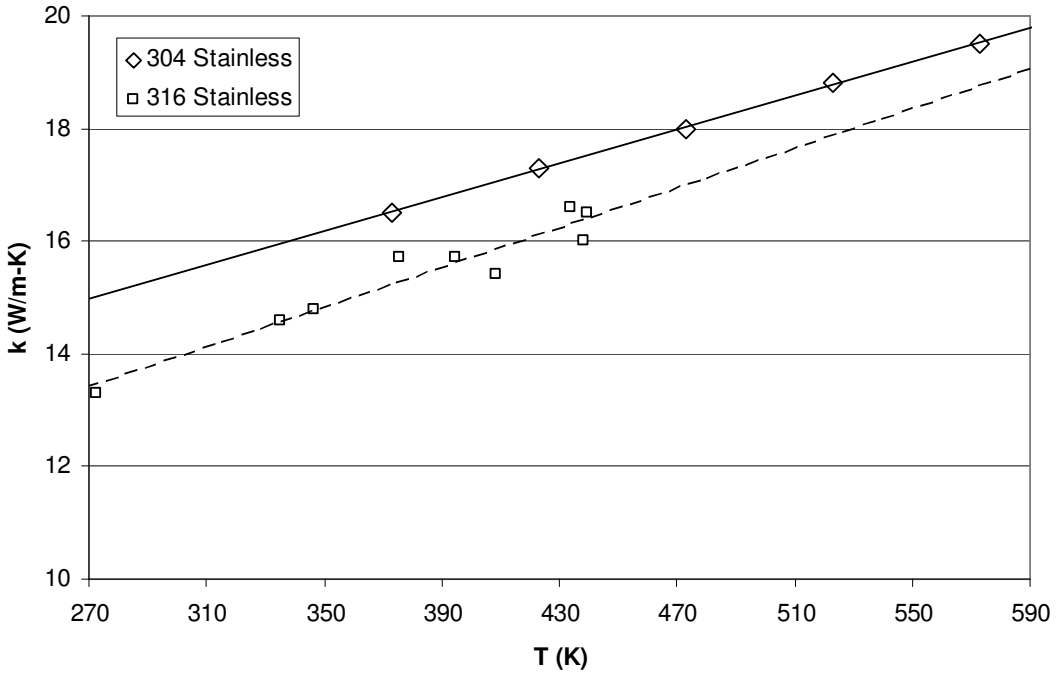

Figure C-1: Reference stainless steel conductivity data [19].

Appendix G

Reference Methanol Fluid Property Data

Table D-1: Reference methanol fluid property data [7, 21].

T (^{o}C)	P (Pa)	ρ (kg/m^{3})	h_{fg} (J/kg)	$C_{p,l}$ (J/kg-K)	k (W/m-K)	σ (N/m)
20	13032	790.93	1176570	2504.7	*0.204*	0.023
25	16981	786.24	1168970	2534.6	*0.203*	0.022
30	21914	781.55	1161218	2566.2	*0.203*	0.022
35	28021	776.83	1153200	2599.3	*0.203*	0.021
40	35518	772.1	1145011	2634	*0.203*	0.021
45	44649	767.33	1136544	2670.2	*0.202*	0.021
50	55684	762.53	1127890	2708	*0.202*	0.020
55	68928	757.69	1118943	2747.2	*0.202*	0.020
60	84713	752.79	1109694	2788	*0.202*	0.019
65	103410	747.84	1100035	2830.2	*0.201*	0.019
70	125410	742.83	1090160	2873.9	*0.201*	0.018

Appendix H

Uncertainty Analysis

An uncertainty analysis was carried out using methods outlined in Figliola and Beasley [23]. For all precision errors, the student-t distribution with a 95% confidence level was used. Individual uncertainties due to resolution, accuracy, and precision were combined using a root-sum-squares approach. For error propagation, a sequential perturbation approach was utilized. To determine uncertainty in temperature gradients and mass flow rates, the following method was employed.

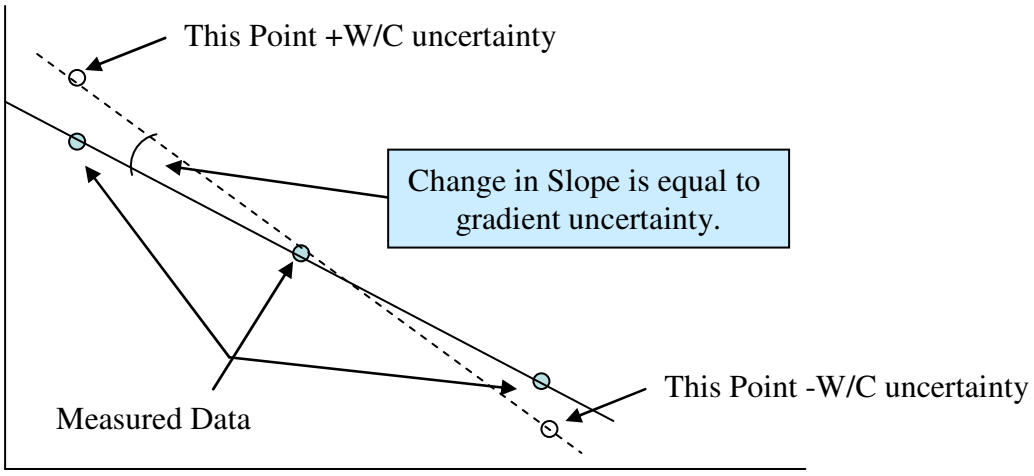

Figure E-1: Gradient uncertainty approach.

REFERENCES

[1] Y. F. Maydanik, "Loop Heat Pipes," *Applied Thermal Engineering*, Vol. 25, pp. 635-657, 2005.

[2] S. Launay, V. Sartre, J. Bonjour, "Parametric Analysis of Loop Heat Pipe Operation: A Literature Review," *International Journal of Thermal Sciences*, Vol. 46, pp. 621-636, 2007.

[3] S. V. Vershinin and Y. F. Maydanik, "Hysteresis Phenomena in Loop Heat Pipes," *Applied Thermal Engineering*, Vol. 27, pp. 962-968, 2007.

[4] J. Ku, "Operating Characteristics of Loop Heat Pipes," 29th International Conference on Environmental Systems, Denver, CO, July, 1999, SAE Paper 1999-01-2007.

[5] M. Bonnefoy and J. M. Ochterbeck, "Effective thermal conductivity of Saturated Sintered Nickel Loop Heat Pipe Wicks," *37th Thermophysics Conference*, American Institute of Aeronautics and Astronautics, Portland, Oregon, June 28-July 1, 2004, pp. 1-10.

[6] S.W. Chi, *Heat Pipe Theory and Practice: A Sourcebook*, Hemisphere Publishing Corp, New York, 1976.

[7] G.P. Peterson, *An Introduction to Heat Pipes: Modeling, Testing, and Applications*, Wiley-Interscience, New York, 1994.

[8] S. Mo, P. Hu, J. Cao, Z. Chen, H. Fan, and F. Yu, "Effective thermal conductivity of Moist Porous Sintered Nickel Material," *International Journal of Thermophysics*, Vol. 27, pp. 304-313, 2006.

[9] D.R. Chaudhary, R.C. Bhandari, "Heat Transfer Through a Three-Phase Porous Medium," *Journal of Physics D: Applied Physics*, Vol. 1, pp. 815-817, 1968.

[10] B. Holley and A. Faghri, "Permeability and Effective Pore Radius Measurements for Heat Pipe and Fuel Cell Applications," *Applied Thermal Engineering*, Vol. 26, pp. 448-462, 2006.

[11] R. R. Williams, and D. K. Harris, "Cross-plane and In-plane Porous Properties Measurements of Thin Metal Felts: Applications in Heat Pipes," *Experimental Thermal and Fluid Science*, Vol. 27, pp. 227-235, 2003.

[12] C. Ren and Q. Wu, "Heat Transfer in Loop Heat Pipes Capillary Wick: Effect Effective thermal conductivity," *Journal of Thermophysics and Heat Transfer*, Vol. 21, pp. 134-140, 2007.

[13] D. Khrustalev and A. Faghri, "Heat Transfer in the Inverted Meniscus Type Evaporator at High Heat Fluxes," *International Journal of Heat and Mass Transfer*, Vol. 38, pp. 3091-3101, 1995.

[14] T.S. Zhao, and Q. Liao, "On Capillary-Driven Flow and Phase Change Heat Transfer in a Porous Structure Heated by a Finned Surface: Measurements and Modeling," *International Journal of Heat and Mass Transfer*, Vol. 43, pp. 1141-1155, 2000.

[15] B. D. Iverson, T. W. Davis, S. V. Garimella, M. T. North, and S. S. Kang, "Heat and Mass Transport in Heat Pipe Wick Structures," *Journal of Thermophysics and Heat Transfer*, Vol. 21, pp. 392-404, 2007.

[16] M. Furukawa, "Model-Based Method of Theoretical Design Analysis of a Loop Heat Pipe," *Journal of Thermophysics and Heat Transfer*, Vol. 20, pp. 111-121, 2006.

[17] P.-Y.A. Chuang, *An Improved Steady-State Model of Loop Heat Pipes Based on Experimental and Theoretical Analyses*, PhD Thesis, The Pennsylvania State University, 2003.

[18] J.G. Hust, and A.B. Lankford, "Research Materials 8420 and 8421: Electrolytic Iron Effective thermal conductivity and Electrical Resistivity as a Function of Temperature from 2 to 1000K", National Bureau of Standards, U.S. Department of Commerce, Gaithersburg MD, May 1984.

[19] Y.S. Touloukian, *Thermophysical Properties of Matter-The TPRC Data Series: A Comprehensive Compilation of Data*, IFI/Plenum, New York, 1970.

[20] A. Jena, *Fundamentals of Extrusion Flow Porometry,* Porous Materials Inc., Ithaca, NY, 2004.

[21] E.W. Lemmon, M.O. McLinden, and D.G. Friend, "Thermophysical Properties of Fluid Systems" in *NIST Chemistry WebBook (http://webbook.nist.gov)*, NIST Standard Reference Database No. 69, Eds. P.J. Linstrom and W.G. Mallard, National Institute of Standards and Technology, Gaithersburg, MD, June 2005.

[22] T. Ahmed, *Reservoir Engineering Handbook 2nd Edition,* Butterworth-Heineman, Woburn, MA, 2001.

[23] R.S. Figliola, and D.E. Beasley, *Theory and Design for Mechanical Measurements 3rd Edition*, John Wiley & Sons, New York, NY, 2000.